

**FACULTY
OF MATHEMATICS
AND PHYSICS**
Charles University

MASTER THESIS

Bc. Kateryna Lutsai

**Page image classification for
content-specific data processing**

Institute of Formal and Applied Linguistics

Supervisor of the master thesis: Mgr. Pavel Straňák, Ph.D.

Study programme: Computer Science – Language
Technologies and Computational
Linguistics

Prague 2025

I declare that I carried out this master thesis on my own, and only with the cited sources, literature and other professional sources. I understand that my work relates to the rights and obligations under the Act No. 121/2000 Sb., the Copyright Act, as amended, in particular the fact that the Charles University has the right to conclude a license agreement on the use of this work as a school work pursuant to Section 60 subsection 1 of the Copyright Act.

In date

Author's signature

The project was managed by one of the data providers from Institute of Archaeology of the Czech Academy of Sciences in Prague (Archeologický ústav AV ČR Praha v. v. i. (ARÚP), IAP), Mgr. David Novák, Ph.D. Another data provider from the same institution, Ing. Dana Křivánková, helped with annotation approval and category enrichment. Thanks to her for both playing the role of the project beta tester and providing valuable feedback from the field-expert and end-user points of view.

On the Institute of Formal and Applied Linguistics (Ústav formální a aplikované lingvistiky (ÚFAL), IFAL) side, the project workflow was supervised by Mgr. Pavel Straňák, Ph.D., and the thesis writing was mentored by doc. RNDr. Pavel Pecina, Ph.D. Many thanks for their reading time, advice, and comments on the thesis manuscript.

This research received funding from the European Commission HORIZON Research and Innovation Actions under the grant agreement GAP-101132163 — ATRIUM — HORIZON-INFRA-2023-SERV-01-02 — **A**dvancing **F**ron**T**ier **R**esearch **I**n the Arts and **h**U**M**anities.

In particular, I am grateful to the Institute of Formal and Applied Linguistics for access to CPU (Central Processing Unit) and GPU (Graphics Processing Unit) nodes on their cluster, which made conversion from PDF (Portable Document File) to PNG (Portable Network Graphics), training, and evaluation procedures much faster. We also uploaded the annotated source dataset of pages to their LINDAT server as a repository [LK25], containing more than 35 GB of source pages complemented with an annotation table of more than 15,000 images.

Moreover, the developed software is publicly available under the MIT (Licensing policy created in Massachusetts Institute of Technology) license in the GitHub repository [Lut+25] (two branches: CLIP and ViT). Finetuned models were uploaded to the HuggingFace repositories (CLIP-based variants have a separate repository; ViT and EfficientNetV2 are combined in a ViT-based repository).

Title: Page image classification for content-specific data processing

Author: Bc. Kateryna Lutsai

Institute: Institute of Formal and Applied Linguistics

Supervisor: Mgr. Pavel Straňák, Ph.D., Institute of Formal and Applied Linguistics

Abstract: Digitization projects in the humanities, specifically within the archaeological domain, often generate vast quantities of page images from historical documents, presenting significant challenges for manual sorting and analysis. The primary goal of this project is to address this need by developing and evaluating an automated image classification system designed to categorize historical document pages based on their content, thereby enabling tailored downstream analysis pipelines. These archives contain diverse content, including various text types (handwritten, typed, printed), graphical elements (drawings, maps, photos), and layouts (plain text, tables, forms). By leveraging advancements in neural network architectures, this system facilitates content-specific workflows, such as separating pages requiring Optical Character Recognition (OCR) from those needing graphical analysis. The final models, datasets, and software are released under open-source licenses to support the broader digital humanities community.

Keywords: Image-based Document Processing, Archival Digitization, Page classification, Model finetuning, Layout elements detection

Contents

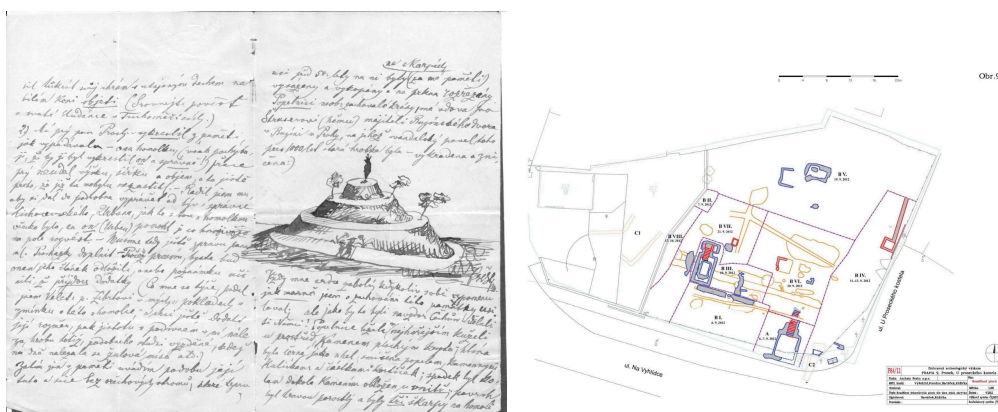
| | |
|---|-----------|
| Introduction | 8 |
| 1 Exploration of the raw data | 15 |
| 1.1 Characteristics of the source data | 15 |
| 1.1.1 Visual defects of the scanned pages | 15 |
| 1.1.2 Textual Variations and Annotations | 17 |
| 1.2 Application of the available DLA framework | 19 |
| 1.2.1 Optical Character Recognition (OCR) performance | 21 |
| 1.2.2 Structured data detection and extraction | 21 |
| 1.2.3 Graphic elements detection | 22 |
| 1.2.4 Human expert feedback | 22 |
| 1.3 Critical human expert feedback | 23 |
| 2 Dataset formation | 26 |
| 2.1 Image classification categories | 27 |
| 2.2 Representative subset selection | 28 |
| 2.2.1 Split procedure | 30 |
| 2.3 Datasets and annotation summary | 31 |
| 2.4 Data modifications in categories | 36 |
| 3 Image classification | 38 |
| 3.1 Low-compute approach | 38 |
| 3.1.1 Image feature extraction | 38 |
| 3.1.2 Random Forest Classifier (RFC) | 39 |
| 3.2 Typical Models for Image Classification Fine-Tuning | 39 |
| 3.2.1 EfficientNetV2 and RegNetY approaches | 40 |
| 3.2.2 Document Image Transformer (DiT) and ViT approaches | 41 |
| 3.2.3 Comparative Analysis and Error Patterns | 41 |
| 3.2.4 CLIP-based approach | 43 |
| 4 System architecture | 50 |
| 4.1 Interface | 52 |
| 4.1.1 Configuration file | 52 |
| 4.1.2 Command line entry point | 53 |
| 4.1.3 Streamlined Input Processing | 53 |
| 4.1.4 Web service interface | 53 |
| 4.2 Output formats | 55 |
| 4.3 Data preparation functionality | 55 |

| | | |
|----------|---|------------|
| 4.3.1 | PDF documents to page images | 56 |
| 4.3.2 | Annotated data sorting | 56 |
| 5 | Results | 58 |
| 5.1 | Accuracy of tested models | 58 |
| 5.2 | Picking the best model | 60 |
| 5.2.1 | Deployment and Usability | 60 |
| 5.2.2 | Agreement with field experts | 62 |
| 5.3 | Similarity of predictions in different models | 62 |
| 5.3.1 | Analysis of Common Mistakes | 64 |
| 5.4 | Labeled collections from Prague and Brno | 65 |
| | Conclusion | 67 |
| | LLM assisted copy editing | 69 |
| | Bibliography | 70 |
| | List of Figures | 73 |
| | List of Tables | 76 |
| | List of Abbreviations | 78 |
| A | Source data pages | 81 |
| B | Parsing attempts | 90 |
| C | Label examples | 95 |
| D | CLIP category descriptions | 107 |
| E | LLM prompts | 114 |
| F | System architecture | 117 |
| F.1 | Finetuning to downstream task functionality | 117 |
| F.1.1 | Transformation into model-friendly inputs | 117 |
| F.1.2 | Hyper-parameters | 118 |
| F.1.3 | Preprocessing of images | 119 |
| F.1.4 | Data split by category proportions | 119 |
| F.2 | Output | 119 |
| F.2.1 | Directory level parsing | 120 |
| F.2.2 | Confusion matrix plot generation | 120 |

Introduction

This thesis develops an automated system for classifying page images from historical archives based on visual content and layout. Such a tool is particularly relevant for institutions like Institute of Archaeology of the Czech Academy of Sciences in Prague (Archeologický ústav AV ČR Praha v. v. i. (ARÚP), IAP), which manage large digital collections and need scalable ways to organize and process them.

The goal is to enable targeted downstream processing on both historical and modern page scans (Figure 1), such as routing text-heavy pages to Optical Character Recognition (OCR) while sending pages with tables or graphics to specialized extraction pipelines. This leads to two central research questions. First, how can modern deep learning methods (e.g., CNN, CLIP, ViT) be adapted to a massive, heterogeneous archive of scanned archaeological reports? Second, how should this heterogeneity be represented through classification labels (e.g., which visual cues distinguish page classes)?



(a) Notebook with a freehand sketch & (b) Modern digital-born (printed and then scanned for some reason) map & tabular legend in the corner

Figure 1 One of the oldest and one of the newest pages in our collection. Both contain graphical objects of interest, but the modern page is annotated with a structured data format (table).

Nature of digitized archival collection

The dataset for this project consists of scanned pages from IAP (primary source) and Institute of Archaeology of the Czech Academy of Sciences in Brno (Archeologický ústav AV ČR Brno v. v. i. (ARÚB), IAB) (secondary source), initially

supplied as multi-page PDFs. These archives are marked by profound heterogeneity. A single collection can contain everything from handwritten manuscripts and typewritten correspondence to printed articles, technical drawings, maps, and annotated photographs.

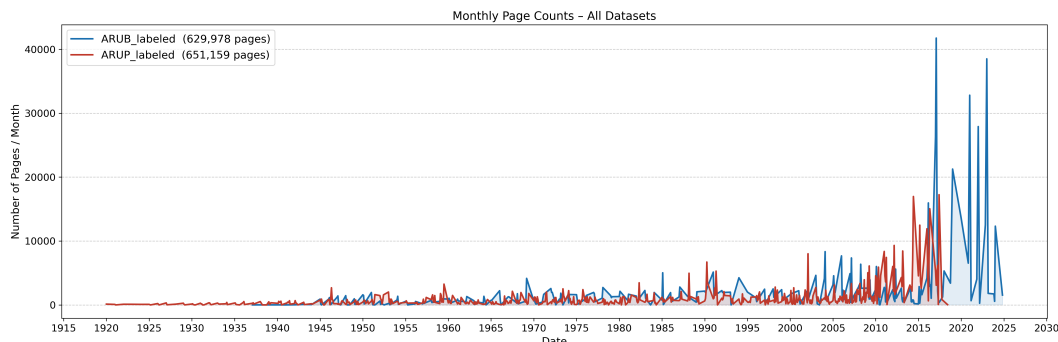


Figure 2 Prague and Brno data from IAP and IAB (unlabeled): Page-scan counts over time in the archives of scanned documents

Our collection spans more than a century, with document creation ranging from the early 20th century to the present day. The incoming data volume has increased substantially over time (Figure 2). In practice, the only consistently available metadata are the year and month recorded in filenames; scanning campaigns therefore appear as spikes in page counts along the timeline.

Because these collections were originally paper-based and digitized via scanning, they often lack descriptive metadata. Critical fields such as author, title, or document type are frequently missing, which complicates automated processing and retrieval.

At the same time, the archive contains many content types—often mixed within a single document—as demonstrated in Figures 1 and 3 to 5. High-resolution scans produce large files, and physical degradation (e.g., stains, skew, torn edges) introduces visual artifacts that complicate analysis and motivate robustness to common visual corruptions [HD19]. These properties make automated, content-aware page classification a practical prerequisite for scalable downstream processing.

A practical objective of this thesis is to evaluate whether existing open-source tools are sufficient for this task. When they are not, we define a domain-specific label scheme and train models that better match the needs of archaeologists.

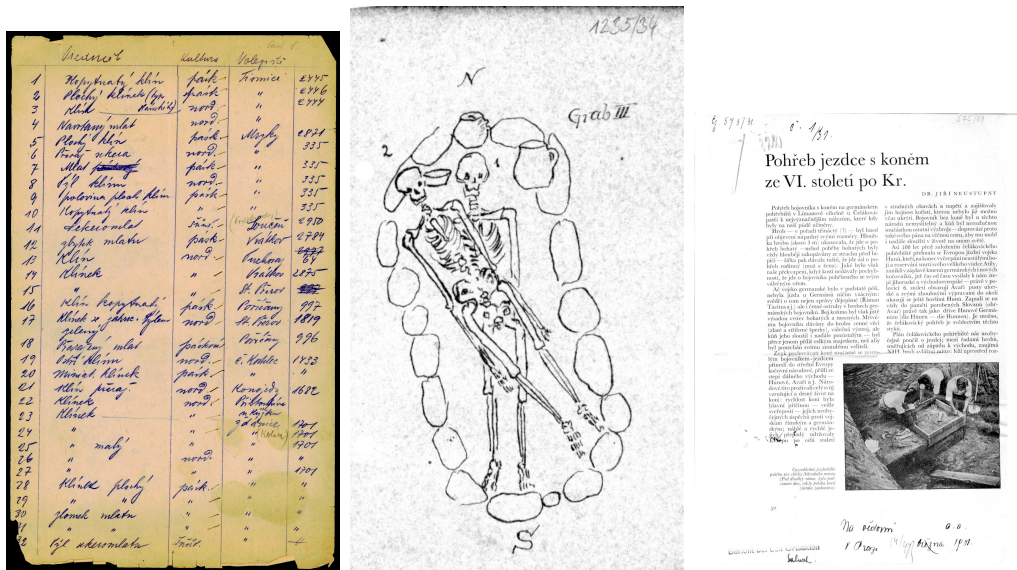
One basic system requirement addresses the challenge of processing large volumes of data: the system must accommodate different use cases by accepting multiple input types:

- Single image files for individual page classification (any standard image format, such as PNG, JPEG (Joint Photographic Experts Group), or TIFF (Tagged

Image File Format))

- Directories of image files for batch processing
- Directories with nested subdirectories of image files

The system should handle varying file structures, including those generated by recommended open-source PDF-to-PNG conversion tools for both Unix (pdftoppm) and Windows (ImageMagick), which differ in their page numbering conventions.



(a) Handwritten table on damaged paper (b) Tiny-scale drawing (c) Article scan with a photo & handwritten notes

Figure 3 Page examples derived from the same collection that differ substantially in size, content, and paper condition.

Challenges in management of scanned documents

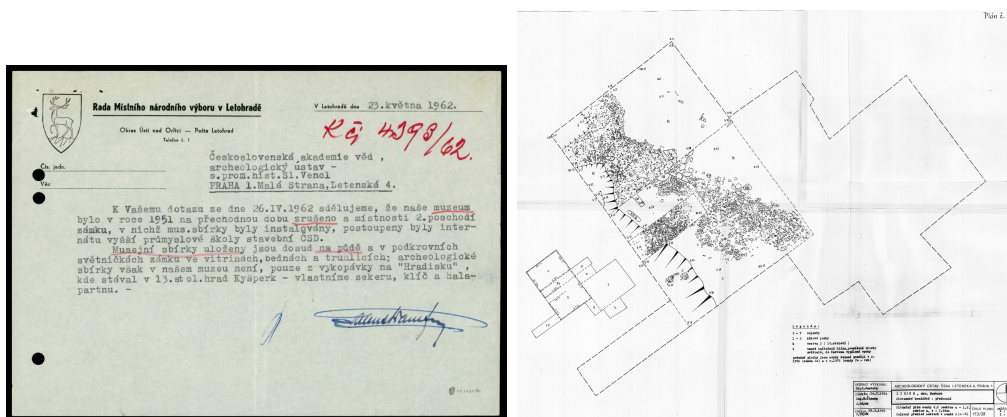
The characteristics outlined below create practical hurdles for archive management:

Manual collection organization: The volume and content diversity make manual sorting impractical. Scanning campaigns typically produce large batches, which increases the risk of human error and makes consistent organization difficult. Manually reviewing each page to determine its content category is prohibitively time-consuming.

File sorting without metadata: The lack of descriptive metadata—often a result of scanning with default equipment settings—prevents straightforward automated grouping and complicates database organization.

Need for content-specific processing: Different page types require different tools; for example, Optical Character Recognition (OCR) is appropriate for text, while layout analysis is needed for tables [ZTY19; Xu+20] and image analysis for photographs. Without an initial classification step, downstream pipelines (e.g., table parsing, image segmentation, text recognition) cannot be applied efficiently.

These challenges motivate automated methods that distinguish page types before specialized processing.



(a) Manually commented typewritten report with a small logo (b) Large-scale canvas with a map and a legend table

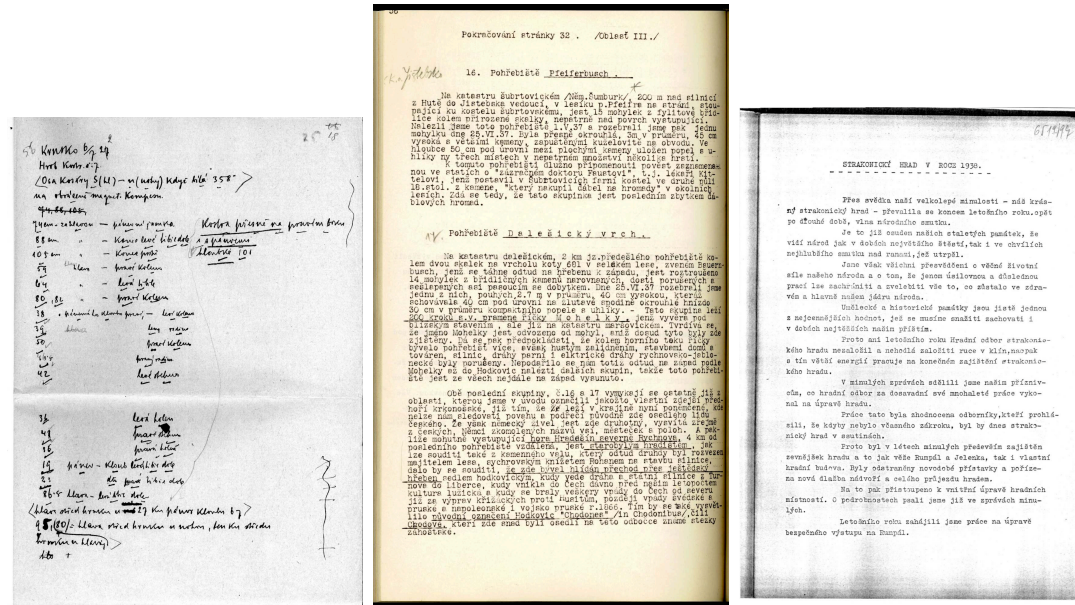
Figure 4 Examples of scans with different physical sizes from our annotated subset

Related work

Prior research in document analysis has typically addressed cleaner, more uniform printed documents; for instance, open-source OCR engines like Tesseract [Smi07b] perform well on standard printed text but struggle with the noisy, handwritten, or structurally complex pages common in historical archives (see Figure 5). The limitations of traditional feature-based classifiers on such heterogeneous data have prompted a shift toward more robust methods.

The combination of diversity and poor documentation is a well-known characteristic of large-scale digitization efforts [Nik+22]. Initial consultations with our data providers from IAP and IAB confirmed that our collection was perceived as

highly disorganized, reflecting a common reality in digitization projects where the scale of data acquisition outstrips the resources available for curation.



(a) Handwritten text on a gray paper (b) Page from a large volume journal (c) Scanned copy with printing defects

Figure 5 Pages with background artifacts that degrade OCR performance

Furthermore, the burden of manual curation is a widely recognized challenge in digital humanities and archival sciences [Nik+22]. For a large-scale project, this manual process becomes a repetitive pattern-recognition task that is inefficient at scale, directly impeding progress towards a fully analyzed collection.

Recent surveys highlight the success of deep learning models, particularly Transformer-based architectures, in document image analysis [Liu+21; Dos+20; Tou+21]. Adopting these advanced models, this work develops a page image classification system specifically tailored to the complexities of historical archives.

Methodology

The practical goal of this project was to implement an annotation scheme of classification labels in collaboration with end users and then fine-tune a model on the labeled dataset. The result is intended to be published as an open-source toolset consisting of annotated data, model weights, and source code for content-aware page classification of archival materials.

The development process consisted of several stages of design and implementation:

1. First, we designed experiments with freely available Document Layout Analysis (DLA) tools to justify annotating a new dataset for supervised image classification based on statistics of images' visual features, rather than recognized text and graphical elements pre-extracted from pages. This phase included studying raw data samples and defining the visual elements considered in the analysis.
2. Next, we designed a set of classification labels to be recognized by the system. We conducted experiments with classic image classification algorithms (e.g., RFC, k-NN, SVM) on a preliminary label set to determine a division of pages into categories that matched end-user needs and the technical capabilities of the applied models. Visual elements that fit into low-resolution patches used by the models (handwriting, table layout, drawings) were structured into distinguishing groups. The resulting annotation scheme was then used to compose a dataset of manually classified pages for fine-tuning more advanced models.
3. We then fine-tuned state-of-the-art image classification models on the annotated data (several cross-validation folds) and evaluated them on a test set for comparison. This stage included defining model selection criteria to compare fine-tuned models across architectures and select the best models based on accuracy and size-efficiency trade-offs across CNNs [TL21; Rad+20], Transformers [Dos+20; Li+22], and multimodal CLIP models [Rad+21].
4. Selecting a representative data subset for accuracy evaluation was a separate task. Because filenames refer only to the year & month of creation, and more than a third of pages in our archive originate from the 21st century, the subset selection algorithm must account for chronological order while allowing randomization for cross-validation model fine-tuning.

Overall, end users' impressions of model usage were considered a major factor in the final model selection. Beyond accuracy scores, model size parameters, and common model-specific mistakes across categories, there were no other indicators we could compute automatically.

One possible mitigation for fine-tuned model errors was to run several models per input image and return multiple labels. End users expected models to make consistent mistakes in some categories; comparing outputs from multiple models could help balance these errors.

The intended end users required that the open-source system run efficiently on local infrastructure (e.g., office desktop computers) and offer a user-friendly interface. Because archaeologists are often tied to Windows-specific software in their work, a relatively lightweight and fast tool (models with fewer parameters) that remains accurate and is supported on both Windows and Unix systems was a key objective.

Finally, the project should be reusable from raw data through to a working image classification model. The user-friendly interface should support dataset development and model management and be reusable as the label scheme evolves.

Expected contributions include:

1. annotated dataset of almost 50,000 pages
2. data-aware subset selection algorithm
3. model architecture comparison based on test-set accuracy
4. practical deployment guidelines

1 Exploration of the raw data

The IAP archive available for this thesis totals approximately 400–420 GB (more than 60,000 PDFs and almost 650,000 pages). All PDFs were converted into individual PNG image files and organized into directories corresponding to the source documents. This structure formed the basis for exploratory analysis and for manually annotating a representative subset of the collection.

This chapter summarizes the key characteristics of the collection identified during initial exploration and explains how they informed the annotation scheme for manual page classification.

1.1 Characteristics of the source data

The total collection contains 29,590 document-level folders holding 649,723 image files, with a mean of ≈ 23 files per folder (median: 4). In total, 35,978 documents are single-page samples. Most folders are small (75% contain 15 or fewer pages; 90% contain 50 or fewer), but a long tail of large documents exists (99th percentile: 240 pages per document).

In practice, this means that most inputs are short (one to several pages), while a small number of very large documents dominate storage and variance. We therefore treat the dataset as many small documents with rare large outliers. Downstream pipelines were designed to process data folder-by-folder and, for large outlier directories, in chunks of 1,000 pages.

The 100 largest images range from 61 to 169 MB, which is typical for maps digitized with specialized canvas-size scanning equipment. To handle these large files, we increased the cache memory limit of the Python image-reading library based on observed failures.

Finally, we implemented safeguards for truncated files so that damaged images can be filtered out before creating data loaders (which operate on scaled images represented as numerical vectors).

1.1.1 Visual defects of the scanned pages

The scanned pages frequently exhibit visual defects caused by both the physical condition of the source documents and the scanning process. These defects make naive document processing unreliable and motivate classifiers that are robust to visual noise.

Artifacts range from minor blemishes (e.g., stains) to severe degradation that complicates automated content extraction and helps explain why general-purpose

document analysis pipelines often perform poorly on historical scans. The primary defect types are summarized below.

- Background Artifacts and Low Contrast:** A common issue is the presence of aged, yellowed, or gray paper backgrounds, which diminishes the contrast between text and page (Figures A.2, A.3, A.11, C.1b, C.1c, C.1e, C.1g, C.2e, C.2f, C.3g, C.4e, C.5b, C.5c, C.5f, C.5g, C.6c, C.7f, C.8c, C.8g, C.9b, C.9c, C.11b and C.11i). This degradation is directly caused by paper aging and the quality of the original materials.

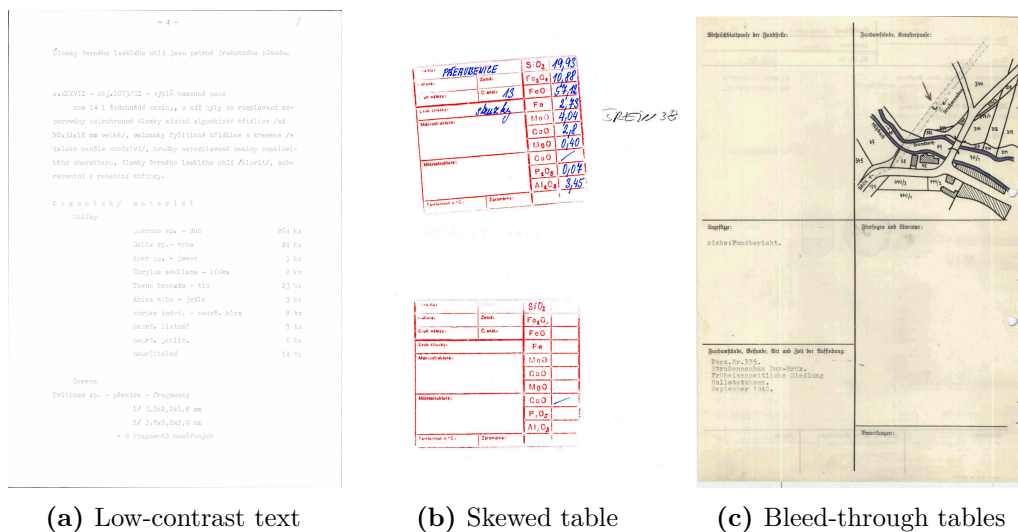
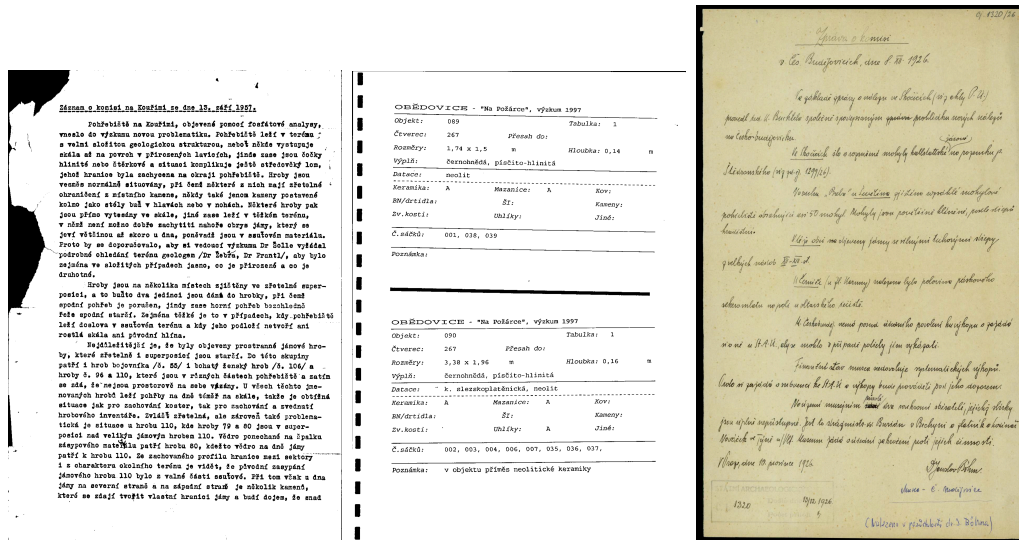


Figure 1.1 Examples of content defects that reduce readability.

- Page Skew and Alignment Issues:** Many pages suffer from skew, where content is not aligned horizontally (Figures A.6, C.1g, C.3c, C.4c, C.4g, C.5d, C.5f, C.6a, C.8d, C.8e, C.11c, C.11g and C.11i). This is a well-documented [BBC23] problem in OCR literature that can arise from improper paper feeding during scanning or the document’s original state and often requires specialized preprocessing to correct.
- Text Bleed-Through:** On documents printed on thin paper, ink on the reverse side is often visible, creating superimposed text that interferes with primary content (Figures A.5 and C.9b). This phenomenon, known as bleed-through, is a significant challenge for OCR systems, as it introduces noise that can be difficult to segment from the foreground text.
- Water Damage:** Some documents show clear signs of water damage, resulting in blurred ink, stains, and overlapping text (Figures A.1 and C.9g).

This type of degradation is particularly severe in documents that have been exposed to events such as floods.

- **Physical Damage:** Prevalent physical damage includes tears, holes, and worn edges (Figures A.2, A.7, C.5f, C.6a, C.8g, C.11d, C.11f and C.11g). This ranges from simple corner tears to more significant edge damage and punch holes from binding.



(a) Torn page corner (b) Large volume bound & (c) Corrections & filled-in stamp

Figure 1.2 Defects and physical page features transferred to digitized scans as transparent or black fragments.

- **Scanning artifacts from Bound Volumes:** Scanning pages from thick, bound journals that cannot lie flat often introduces page curl and a dark gradient near the inner margin (Figures A.9 and C.11b).

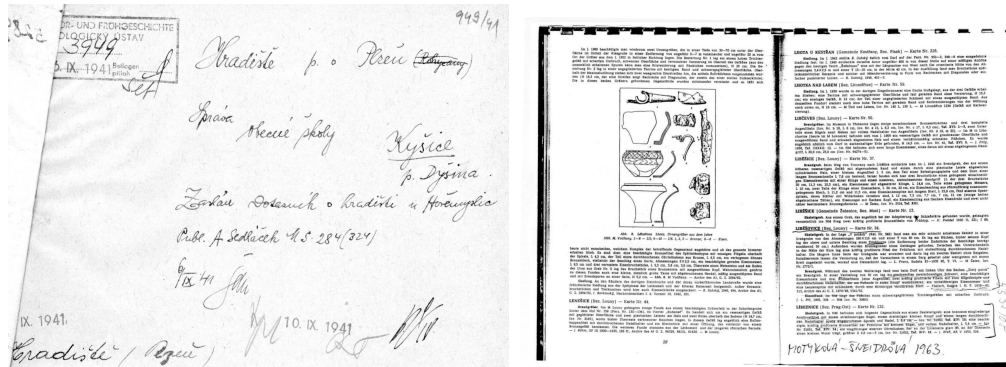
1.1.2 Textual Variations and Annotations

The documents also show substantial variation in textual presentation and annotation. Our objective is therefore to capture visual features that computer vision models can detect reliably and use as signals for page classification.

The diversity of page layouts—complicated by stamps (often small, fillable forms) placed at arbitrary locations—motivated an approach that is largely independent of heavy preprocessing. The model must generalize across visual features and capture differences in textual elements, including mixtures of printed, typewritten, and handwritten text within a single image.

In addition, the model must recognize sketches and handwritten content on grainy paper and distinguish graphical elements of interest from the visual noise described in Subsection 1.1.1.

- **Stamps:** Official stamps and other preformatted ink annotations are frequently found on the documents, sometimes appearing as faint graphical elements. Figures A.4, C.5a, C.5b, C.6c, C.8a, C.8e, C.8f, C.9f and C.9g illustrate various pages with stamp impressions.



(a) Wet paper, Czech writing & a German (b) Commented book scan with a drawing stamp

Figure 1.3 Variability of handwritten font sizes based on the format of physical pages

- **Manual Corrections:** Handwritten modifications were common, ranging from simple strikeouts of characters and words to the removal of entire paragraphs (see Figures A.10, C.3c, C.5b, C.7a, C.8c, C.9c and C.9g) to interlinear notes on typewritten documents (Figures A.10a, C.3e, C.3f, C.5b and C.8c).
- **Scribbles and annotations:** Beyond formal corrections, pages frequently contained scribbles, underlines, and other margin notes, as shown in Figures A.11a, C.1f, C.5a and C.6a. These marginal annotations are often ambiguous, making it difficult to determine their relevance or relationship to the primary content.
- **Mixed Text Styles:** Pages often combined multiple text formats. For instance, typewritten documents frequently had handwritten page numbers or comments (Figures A.6a and C.8a to C.8c). Front pages might mix printed letterheads, stamps (Figures A.4b, C.5a, C.5b, C.6c, C.8a, C.8e, C.8f, C.9f and C.9g), and handwritten notations, followed by typewritten text, drawings, or forms filled in by hand. Figures A.3 and C.8 illustrate such mixed-content pages.

- **Text within Graphics:** Finally, textual elements were commonly embedded within graphical content. Maps and technical drawings included labels and captions (Figures A.8a, A.8b, C.1 and C.2), while photographs were often accompanied by typewritten or handwritten descriptions (Figures A.12b, A.12c, C.6d and C.6e). Consequently, purely graphical pages devoid of any text were relatively rare.

The range of text styles that can be distinguished is limited by the models’ input resolution (i.e., the degree of downsampling), leaving mainly handwritten, typewritten, and printed genres of textual content. In contrast, layout (whether mixed in style or not) is expected to be captured more easily at typical model input sizes of 200–400 pixels in width.

These varied annotations and mixtures of typewritten and handwritten text mean that any classification system must be robust to diverse, combined content types on a single page.

All samples in Figures 1.1 to 1.3 and additional examples are provided in Appendices A and C.

In summary, the visual characteristics of the source pages vary too much for a one-size-fits-all preprocessing strategy (e.g., globally increasing contrast or sharpening edges). Instead, an effective system must be robust to page color, paper grain, and low contrast between text and background, and it should tolerate pencil drawings and informal annotations.

1.2 Application of the available DLA framework

Document Layout Analysis aims to identify and categorize components within a document image, such as text blocks, images, and tables. We evaluated DLA tools as a potential “off-the-shelf” solution and as a way to understand which visual signals are realistically detectable in our data.

The primary purpose of these experiments was to justify the need for a problem-specific labeled dataset and to inform the label scheme used later for supervised model training. To establish a baseline, we applied the DeepDoctection framework to detect structural elements (examples in Figures B.1 to B.3 and B.6). In parallel, we used the Tesseract OCR engine [Smi07b] to assess text extraction quality.

These experiments did not rely on manual ground-truth labels. Instead, they used automatically detected elements (tables, figures, text blocks) to infer page layout and to estimate whether rule-based categories could support reliable sorting.

Table 1.1 shows our initial, rule-based label set, derived from detected layout elements and counts of long/short horizontal and vertical lines.

End users reviewed the proposed labels and the per-page element counts produced by these handcrafted rules (e.g., text lines, headers, tables, images).

| Category | Description |
|--------------|--|
| Form | Pages characterized by horizontal lines (<code>H_line</code>) but lacking the high vector line counts associated with technical drawings. Also includes pages where detected table content outweighs text content (<code>TXT < TAB</code>), implying a structured layout without a strict grid. |
| Form-figure | A hybrid category where pages contain both horizontal lines and moderate vector line complexity (<code>maybe_picture</code>), or where both Table and Image detectors return positive values. |
| Table | Pages strictly defined by the presence of vertical or horizontal separators (<code>V_line</code> , <code>H_line</code>) where text content is negligible or non-existent, representing clean grids. |
| Text-body | Pages dominated by recognized text blocks (<code>TXT > 0.9</code>) or explicitly flagged as <code>Manuscript</code> (handwritten content). This category also applies when headers exist but make up a smaller portion of the page than the body text. |
| Gallery | Pages identified primarily by high counts of “long” or “short” vector lines (exceeding 1000–3000 lines), indicating technical drawings, maps, or blueprints. Also includes pages where image content occupies the majority of the page area (<code>IMG > 0.9</code>). |
| Figure-text | Pages containing a mixture of text and visual elements where the image content is present but does not dominate the page (<code>TXT > IMG</code>), or where text is present but significantly less than the image area (<code>TXT < IMG</code>). |
| Table-text | Mixed-content pages where a table is detected but is smaller in proportion to the accompanying text block (<code>TAB < TXT</code>). |
| Headers-text | Pages where text is detected, but the header regions are calculated to be larger or more significant than the remaining text body (<code>TXT < HDR</code>). |
| Mixed | A fallback category for pages containing a combination of Images, Headers, Text, and Tables, where no single element meets the dominance threshold to trigger a specific category. |
| Neither | A default state for pages that do not trigger any specific detection rules. |
| Empty-text | Pages with very low content scores and vector line counts below the threshold (e.g., < 100 lines), representing (nearly) blank pages. |

Table 1.1 Classification categories based on detected content features and line complexity. No ground-truth labels existed for this scheme.

These trials indicated that off-the-shelf tools could not meet the project’s content-specific classification goals (Figure 1.4), motivating a tailored solution.

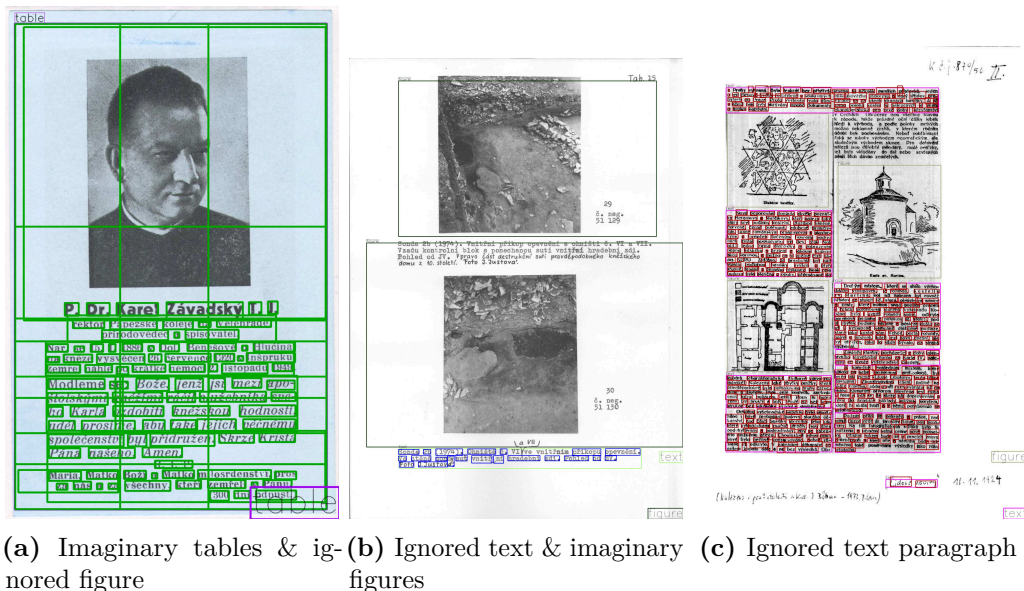


Figure 1.4 DLA application samples

1.2.1 OCR performance

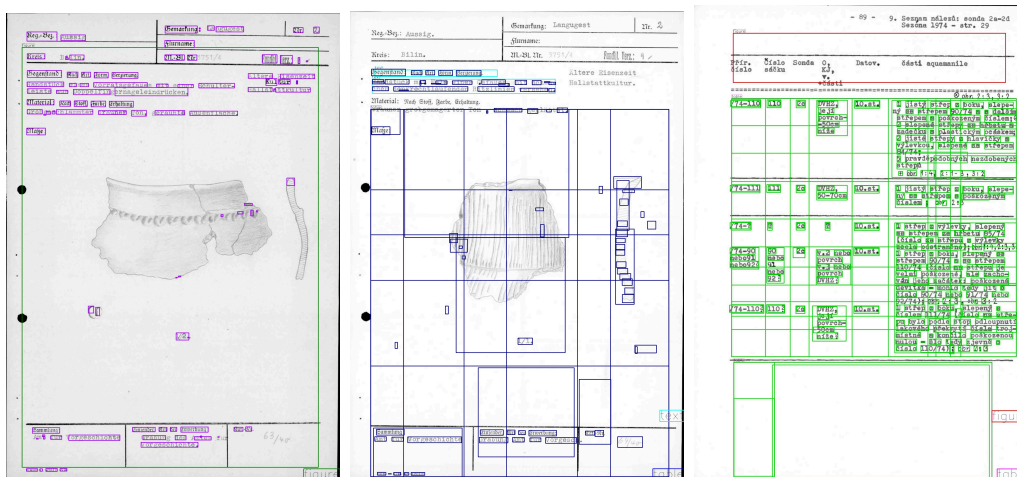
Optical Character Recognition (OCR) converts images of text into machine-readable text, enabling search and downstream analysis.

We applied the Tesseract [Smi07a; Smi07b] OCR engine (via the DLA framework) to a sample of pages. Recognition was accurate on clean, high-contrast scans (Figure B.3) but degraded on dark or noisy backgrounds, often producing incomplete or garbled output (Figure B.8).

1.2.2 Structured data detection and extraction

For general DLA and table recognition, we used Detectron2 (Facebook AI Research), which also serves as the table-recognition module in DeepDoctection.

Table detection and structure extraction were unreliable: DD merged rows or missed cells when borders were faint, incomplete, or skewed (Figures B.2 and B.7), and it sometimes confused tables with other page elements. A recurring failure case involved tables placed near page corners, which were often ignored.



(a) Table as a figure (b) Drawing as a table (c) Header as a figure

Figure 1.5 DeepDoctection (DD) mistakes on pages with tables and figures

1.2.3 Graphic elements detection

Detection of graphical elements (maps, drawings, photographs) was often inaccurate: items were missed or misclassified (e.g., maps labeled as tables; Figures B.1, B.4 and B.6), and handwritten annotations further confused the detector. Overall, the tested tools did not reliably capture the archive’s graphical diversity.

1.2.4 Human expert feedback

A domain expert from IAP reviewed the DLA outputs as an intended end user, focusing on whether the results were inspectable and trustworthy.

Given the heterogeneity described in Sections 1.1.1 and 1.1.2, the expert expected layout predictions from open-source models to be an unreliable basis for content classification.

The handcrafted label set (Table 1.1) showed inconsistent assignments for visually similar pages, motivating clearer category definitions in the next scheme (Tables 1.2 and 1.3).

Feedback emphasized misclassification of high-priority content, particularly full-page tables (e.g., Figure B.2) and large drawings (e.g., Figure B.4); DLA sometimes swapped these classes (Figure 1.5).

While preprocessing (e.g., binarization, thresholding) may improve some cases, manual validation at archive scale is impractical; meaningful evaluation therefore required a manually annotated dataset, which motivated provider involvement in annotation review.

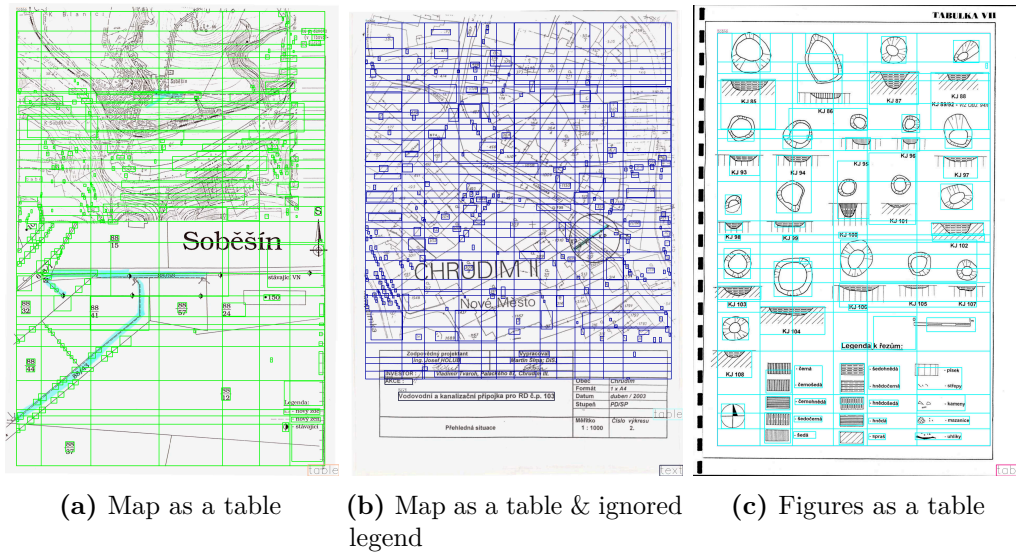


Figure 1.6 DD mistakes on pages with maps and drawings

1.3 Critical human expert feedback

Further collaboration with the domain expert clarified the classification criteria. Evaluation on a held-out set highlighted systematic limitations of the automated approach and helped refine the project goals and final categories.

The DLA test set was relatively small (fewer than 2,000 pages) and intentionally contained difficult samples (e.g., water damage, copy scans), allowing worst-case scenarios to be identified early.

The data providers summarized their conclusions about the applied DLA tool as follows:

- **Classification consistency:** Pages with similar content must be assigned to the same category. Consistency was prioritized over isolated instances of correctness.
- **Primacy of structured data:** Pages containing tabular or form-like data must be classified as such, even when substantial plain text is present (e.g., Figure 1.5). Only fillable stamps are of interest (as structured data), although they may be ignored if values are barely legible or the page contains clearer mixed content.
- **Priority of graphical content:** A significant graphical element (e.g., photograph, map, drawing) should take precedence over text. The definition of “significant” was refined from an initial one-third-of-page threshold to a smaller, stamp-sized element, reflecting the actual archive content.

- **Handling of handwritten annotations:** A consistent policy is needed: minor peripheral notes (e.g., page numbers) can be ignored, while prominent handwritten elements should influence classification.
- **Robustness to defects:** The system must tolerate background noise and degradation, which caused the DLA framework to hallucinate tables and figures (e.g., Figures 1.6, B.5 and B.7).

This expert input clarified the annotation guidelines and established an initial six-label scheme proposed by the data providers (Table 1.2). This scheme was a pragmatic starting point aligned with downstream tools for table/graphics extraction and text recognition, rather than a final taxonomy.

| Category | Description |
|------------|---|
| REST | Mixture of printed, handwritten, and/or typewritten text, potentially with minor graphical elements (contained all ambiguous cases, including drawings considered insignificant at that time), as illustrated in Figure C.8b. |
| TEXT_LINE | Pages primarily consisting of typewritten, printed, or handwritten text organized in a tabular or form-like structure, illustrated in Figures C.2c and C.3 to C.5. |
| PHOTO | Pages dominated by photographs or photographic cutouts (maybe maps, paintings, schematics), with few text captions. Illustrated in Figures C.1a, C.1b and C.7b. |
| PHOTO_TEXT | Similar to PHOTO, but the visual content is presented along with a text block(s) of any style (Figures C.2 and C.6). |
| TEXT | Pages containing plain corpora of almost pure printed, or handwritten, or typewritten text, as illustrated in Figures C.5b and C.9 to C.11. |
| TEXT_OTHER | Pages containing mixtures of printed, handwritten, and/or typewritten text, potentially with minor graphical elements. Demonstrated in Figure C.8a. |

Table 1.2 Category definitions initially designed by the data provider, inspired by the previously observed DLA attempts

The six categories were the minimum granularity the providers considered feasible to annotate. For supervised learning, we then split visually heterogeneous classes and redefined labels to better match what computer vision models can distinguish.

The revised definitions (Table 1.3) supported an initial training set and a comparison between a seven-label variant and the original six labels. The confusion

matrices in Figure 2.1 suggest that separating handwritten from typewritten text improves performance (Figure 2.1b, `HW`) and that contour-heavy drawings are distinct from photographs (Figure 2.1b, `DRAW-TXT`), motivating the refined categories.

| Category | Description |
|-------------------------|---|
| <code>DRAW_TEXT</code> | Pages dominated by drawings, maps, paintings, schematics, or graphics that include text labels or captions (Figures C.1 and C.2). |
| <code>TEXT_LINE</code> | Pages consisting primarily of typewritten, printed, or handwritten text organized in a tabular or form-like structure (Figures C.3 to C.5). |
| <code>PHOTO</code> | Pages dominated by photographs or photographic cutouts (and related graphics), with few text captions (Figures C.6c and C.7b). |
| <code>PHOTO_TEXT</code> | Similar to <code>PHOTO</code> , but the visual content is accompanied by a substantial text block (Figures C.6a, C.6b, C.7a and C.7c). |
| <code>TEXT</code> | Pages containing plain corpora of almost pure printed or typewritten text (Figures C.10 and C.11). |
| <code>HW</code> | Pages consisting purely of handwritten text in paragraph or block form (non-tabular) (Figure C.9). |
| <code>TEXT_HW</code> | Pages containing mixtures of handwritten and typewritten text, potentially with minor graphical elements (Figures C.5b and C.8c). |

Table 1.3 Overview of the revised intermediate category definitions derived from the initial provider’s proposal

Early low-compute experiments and expert feedback motivated finer label granularity. We refined the scheme to reflect (i) dominant text style, (ii) structured layouts, and (iii) graphical content (photos versus drawings); for example, `PHOTO_TEXT` was split into `PHOTO_L` and `DRAW_L`, and `TEXT/TEXT_LINES` were subdivided into handwritten (`_HW`), typewritten (`_T`), and printed (`_P`) variants. Further details are given in Section 2.1. We then finalized the eleven-label training scheme (Table 2.1); Tables 1.1 to 1.3 reflect intermediate steps toward this taxonomy.

2 Dataset formation

The collection required a tailored approach to annotation and dataset splitting into training, development, and performance test subsets. Pages are alphabetically ordered by filename and therefore only approximately chronological, because filenames encode scan dates rather than document creation dates.

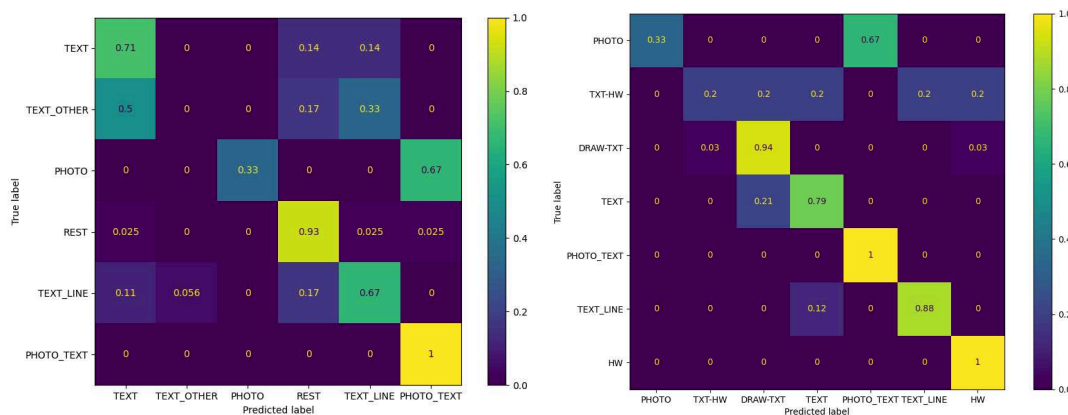
Because the collection is heterogeneous (Section 1.1) and pages cluster by scanning campaign or document type, we avoided random shuffling and instead used deterministic periodic sampling with a small randomized offset (select every S -th page) to preserve category proportions while maintaining coverage across the archive’s 100-year span.

This chapter describes the split algorithm (Section 2.2), the annotation scheme development (Section 2.1), and dataset modifications based on development-set mistakes (Section 2.4).

The following abbreviations used in category names refer to page content genres:

- *_L — filled-in form lines; linear outer frame of a table (tabular legend)
- *_T — typewritten; typed on a machine with a monospaced font
- *_P — printed; printed using a laser or ink printer
- *_HW — handwritten; manual writing

These subcategories capture visual features that we expect the fine-tuned models to distinguish.



(a) Annotation proposed by our data provider (b) Annotation variant proposed by us

Figure 2.1 RFC (Section 3.1.2) confusion matrices of early annotation schemes (fewer than 3,000 samples in total)

2.1 Image classification categories

The initial category scheme followed the structure of the tested DLA framework, distinguishing figures, tables, and text (Table 1.2). This DLA-based division was expanded with an ambiguous category, and the mixed content category was considered sufficient from the data provider’s perspective. The scheme was subsequently adjusted to better align with the capabilities of statistical models. Based on the observation in Figure 2.1 that distinguishing handwritten from typewritten text was beneficial (Figure 2.1b, category HW), and that drawings with contour lines appeared visually distinct from photographs (Figure 2.1b, category DRAW-TXT), we proposed a refined set of categories (Table 1.3).

| Category | Description |
|----------|--|
| DRAW | Pages dominated by drawings, maps, paintings, schematics, or graphics, potentially containing text labels or captions, as illustrated in Figure C.1. |
| DRAW_L | Similar to DRAW, but presented within a table-like layout or including a legend formatted as a table (Figure C.2). |
| LINE_HW | Handwritten text organized in a tabular or form-like structure (Figure C.3). |
| LINE_P | Printed text organized in a tabular or form-like structure (Figure C.4). |
| LINE_T | Typewritten text organized in a tabular or form-like structure (Figure C.5). |
| PHOTO | Pages dominated by photographs or photographic cutouts, potentially with text captions (Figure C.6). |
| PHOTO_L | Similar to PHOTO, but presented within a table-like layout or accompanied by tabular annotations (Figure C.7). |
| TEXT | Mixtures of printed, handwritten, and/or typewritten text, potentially with minor graphical elements (Figure C.8). |
| TEXT_HW | Handwritten text in paragraph or block form (non-tabular), as demonstrated in Figure C.9. |
| TEXT_P | Printed text in paragraph or block form (non-tabular), as demonstrated in Figure C.10. |
| TEXT_T | Typewritten text in paragraph or block form (non-tabular), as demonstrated in Figure C.11. |

Table 2.1 Overview of categories used in the fine-tuned models; unless otherwise specified, each category includes pages primarily dominated by the described content type.

After demonstrating initial results with these categories on low-compute models, the data providers agreed to expand the set of target categories. Subsequent expert feedback led to finer granularity. For instance, the `PHOTO_TEXT` category was eventually replaced by `PHOTO_L` and `DRAW_L` to better distinguish the type of graphical content in tabular layouts. Likewise, the `TEXT` and `TEXT_LINES` categories were subdivided into handwritten (`_HW`), typewritten (`_T`), and printed (`_P`) variants.

This collaborative process ultimately produced a final set of eleven distinct categories designed to capture relevant variations for downstream processing pipelines. These eleven target classes are defined in Table 2.1, which covers almost half of all content type combinations shown in Table 2.2.

A priority order was established to handle pages that could fit multiple categories, prioritizing visually distinct or structured content requiring specific processing:

1. PHOTOS (`PHOTO`, `PHOTO_L`): highest priority during graphic extraction.
2. DRAWS (`DRAW`, `DRAW_L`): second priority for graphic extraction.
3. LINES (`LINE_HW`, `LINE_P`, `LINE_T`): third priority for structured data extraction (e.g., fields as keys and contents as values).
4. TEXTs (`TEXT`, `TEXT_HW`, `TEXT_P`, `TEXT_T`): lowest priority, targeting font-specific OCR.

This hierarchy ensures that visually dominant or structured content is prioritized during subsequent pipeline processing.

Importantly, the priority order above was established as common ground for data annotators. Data annotation was carried out by me and Dana from IAP, a domain expert and end-user representative.

Multiple labels per page were disallowed because categories were defined as mutually exclusive. The data provider decided that a single label would be sufficient for further page aggregation.

To capture the full variability of the data, we created an expanded label scheme of 24 distinct types by separating each core category into printed, typewritten, and handwritten variants (Table 2.3). This comprehensive set was used for analysis, while the 11-category set was used for training and fine-tuning the final models.

2.2 Representative subset selection

The primary goal of subset selection was to preserve the proportional size of each category across the training, validation, and test sets. We therefore selected samples independently within each category. However, matching category proportions alone

| | Printed | Typewritten | HandWritten | Mixed |
|------------------|---------------|---------------|----------------|----------------|
| Photos | | | | PHOTO |
| Drawings etc. | | | | DRAW |
| Photo in table | | | | PHOTO_L |
| Drawing in table | | | | DRAW_L |
| Tables & Forms | LINE_P | LINE_T | | LINE_HW |
| Plain texts | TEXT_P | TEXT_T | TEXT_HW | TEXT |

Table 2.2 Coverage of data feature variability, summarizing the mapping between content type and writing mode.

| | Printed | Typewritten | Handwritten | Mixed |
|-------------------|---------------|---------------|----------------|----------------|
| Photos | P_P | P_T | P_HW | PHOTO |
| Drawings | D_P | D_T | D_HW | DRAW |
| Photos in table | P_L_P | P_L_T | P_L_HW | PHOTO_L |
| Drawings in table | D_L_P | D_L_T | D_L_HW | DRAW_L |
| Tables & Forms | LINE_P | LINE_T | LINE_HW | LINE |
| Plain texts | TEXT_P | TEXT_T | TEXT_HW | TEXT |

Table 2.3 Expanded label scheme illustrating coverage of data variability (analytical only).

does not guarantee representativeness: each category contains substantial internal variability, and many page types are clustered by scanning campaign.

To reduce bias toward specific templates or time periods, we designed a time-aware selection procedure based on the alphabetic filename order (which is approximately chronological because filenames encode scan dates). The key motivations were:

Clustering in the source data Pages are often clustered by scanning campaign or document type. A naive random shuffle can place too many near-duplicate pages from the same source into the development or test sets, inflating or destabilizing evaluation.

Long-term variability The collection spans 100 years and includes systematic changes in scan appearance (e.g., black-and-white vs. color scans, yellowed paper, and common defects like damage from floods). These factors are not uniformly distributed over time.

Evolving document features Fonts, tabular templates, and annotation practices change over time (from early typewritten pages to modern printed

layouts). Preserving chronological coverage helps the model generalize across these shifts.

Deterministic periodic sampling Selecting every S -th element (with a bounded random offset) provides controlled randomness while ensuring that each subset receives samples across the full timeline.

Concretely, the selection procedure must balance several varying factors, including color scheme, font, content type clustering, form templates, graphical objects, defects, and the prevalence of annotations.

These interacting sources of variability—combined with clustering—make a simple random shuffle inadequate. A shuffle can easily create a development or test set dominated by a single scanning campaign, template, or era, skewing the estimated performance. We therefore use the structured splitting procedure below.

2.2.1 Split procedure

Instead of a simple random shuffle, we employ deterministic periodic sampling with a randomized offset. To keep the training set as large as possible, the development and test subsets are selected first, and the training subset contains the remaining pages. For each category, we proceed as follows:

1. Compute the desired subset size k as a fixed proportion of the category N .
2. Compute the selection step S as $S \approx \frac{N}{k}$.
3. Select every S -th element from the alphabetically ordered sequence, but perturb each selected index with a small bounded random offset (e.g., within $\pm \frac{S}{4}$) to avoid strict periodicity.
4. Apply boundary checks to handle out-of-range indices.

This procedure (a) respects the original ordering and local clustering, (b) preserves category proportions, and (c) adds controlled randomness so that selected samples are not perfectly periodic. Crucially, it maintains coverage of the full chronological and structural variability of the collection.

We used random seeds 420–424. Document-level grouping was not preserved. For each fold, the final subset counts were 38,625 / 4,823 / 4,823 for train / development / test. Overall, 43,050 images were used across the five training subsets; the remaining 5,449 images (Figure 2.4) formed the final performance test subset used for results visualization.

To preserve historical and structural variability, we leverage chronological ordering despite its weak correlation with exact document creation dates. Deterministic

Category Proportions Over Time by Fold and Subset

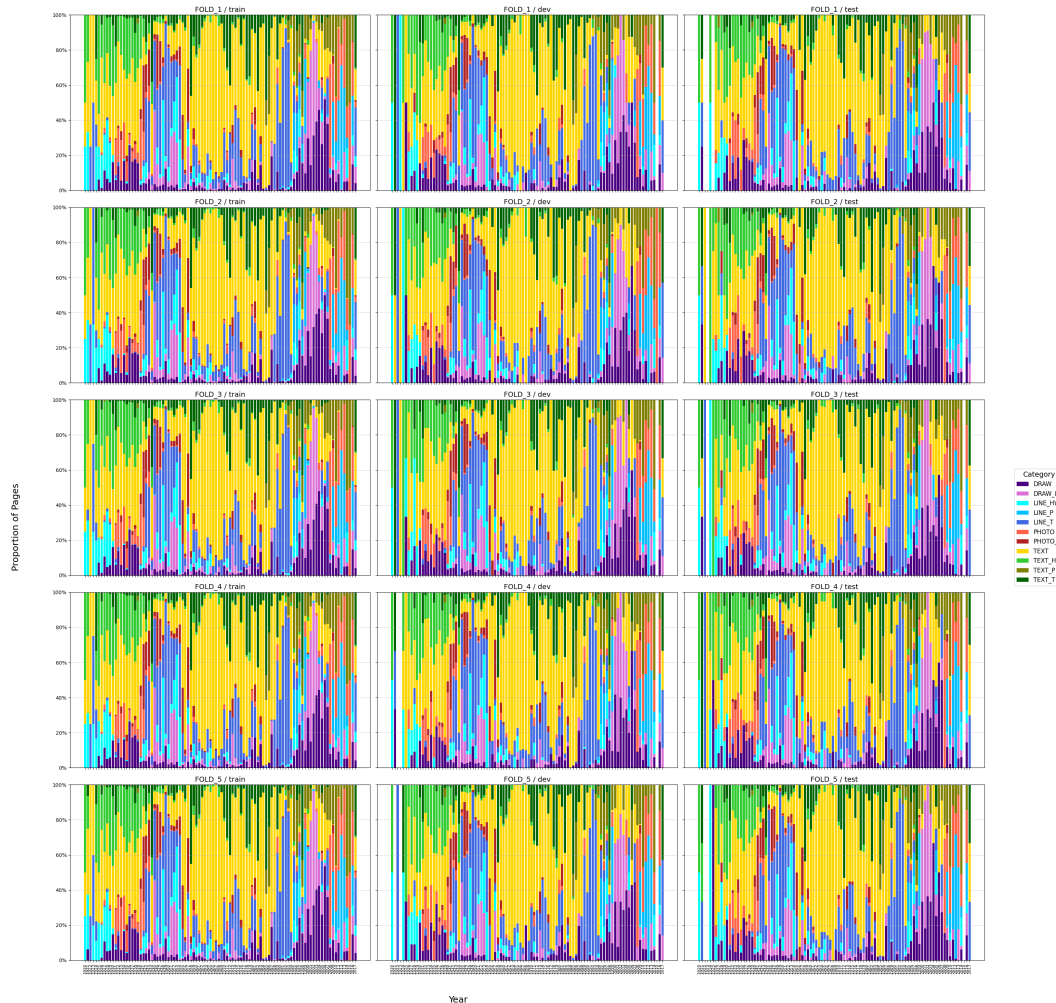


Figure 2.2 Proportions of categories in train, development, and test subsets (columns) across five folds (rows) on a timescale of document creation dates.

periodic sampling (with a bounded random offset) maintains local clustering while ensuring that all subsets cover the full chronological spectrum. This reduces bias toward any single time period and enables evaluation against long-term shifts in document appearance.

2.3 Datasets and annotation summary

This section details the dataset composition and annotation metadata used for training (fine-tuning the pretrained models) and evaluating the image classification

models.

Training sets The iterative development of the models relied on four progressively larger training sets:

- **8950** images for initial **vX.0**.
- **10745** images for poor selection **vX.1**.
- **14565** images for refined **vX.2**.
- **38625** images for the final (largest) **vX.3**.

Evaluation (test) sets Model performance was assessed using distinct evaluation sets corresponding to development stages:

- **1290** images (taken from **vX.2** annotations and used for all older models).
- **4823** images for every **vX.3** model.
- **5449** images for the final cross-validation of **vX.3** models, including the 227 excluded **TEXT** samples (see Table 2.4).

The manual annotation process was time-intensive, drawing from a diverse collection of archival documents spanning 1920–2020. While the specific textual content and language of the source data are irrelevant given the model’s visual-only resolution, the data source itself introduces potential bias. All samples were sourced from *archaeological reports*, which frequently contain freehand sketches and digitized illustrations of common object forms (e.g., ceramic pieces, arrowheads, rocks). This provenance may bias the model toward drawing detection.

Table 2.4 summarizes category distributions for successive versions of the annotated dataset (columns are ordered chronologically). The final column, **Dataset 3**, represents the full partition used for the **vX.3** models. The table reports the total number of available samples per category in each version; the main exception is **TEXT**, which was capped at 14,000 pages in practice, leaving 227 **TEXT** samples without a subset marker (e.g., train, development, or test).

For the latest models (**Dataset 3**), we used an **80%/10%/10%** train/development/test split. Earlier model versions used a **90%** training split, with the remaining **10%** shared between development and test. This earlier approach was a pragmatic choice when annotations were scarce and was later abandoned; models fine-tuned on **Dataset 2** also proved insufficiently representative of the full collection.

| Category | Dataset 0 | Dataset 1 | Dataset 2 | Dataset 3 |
|--------------------|-------------|--------------|--------------|---------------|
| DRAW | 1090 (9.1%) | 1368 (8.8%) | 1472 (9.3%) | 2709 (5.6%) |
| DRAW_L | 1091 (9.1%) | 1383 (8.9%) | 1402 (8.8%) | 2921 (6.0%) |
| LINE_HW | 1055 (8.8%) | 1113 (7.2%) | 1115 (7.0%) | 2514 (5.2%) |
| LINE_P | 1092 (9.1%) | 1540 (9.9%) | 1580 (10.0%) | 2439 (5.0%) |
| LINE_T | 1098 (9.2%) | 1664 (10.7%) | 1668 (10.5%) | 9883 (20.4%) |
| PHOTO | 1081 (9.1%) | 1632 (10.5%) | 1730 (10.9%) | 2691 (5.5%) |
| PHOTO_L | 1087 (9.1%) | 1087 (7.0%) | 1088 (6.9%) | 2830 (5.8%) |
| TEXT | 1091 (9.1%) | 1587 (10.3%) | 1592 (10.0%) | 14227 (29.3%) |
| TEXT_HW | 1091 (9.1%) | 1092 (7.1%) | 1092 (6.9%) | 2008 (4.1%) |
| TEXT_P | 1083 (9.1%) | 1540 (9.9%) | 1633 (10.3%) | 2312 (4.8%) |
| TEXT_T | 1081 (9.1%) | 1476 (9.5%) | 1482 (9.3%) | 3965 (8.2%) |
| Unique PDFs | 5001 | 5694 | 5729 | 37328 |
| Total Pages | 11,940 | 15,482 | 15,854 | 48,499 |

Table 2.4 Category distribution across the models’ dataset partitions. The set of eleven categories tabulated here refers to the final labels scheme described in Section 2.1

The category imbalance in **Dataset 3** is not a design choice; it reflects the natural composition of the archive. The increase in short documents in the final dataset is largely due to a deliberate effort to process and manually correct all single-page PDFs.

Figures 2.3 to 2.5 visualize how the annotations vary over time. In these plots, labeled pages are sorted by document creation year and colored by category.

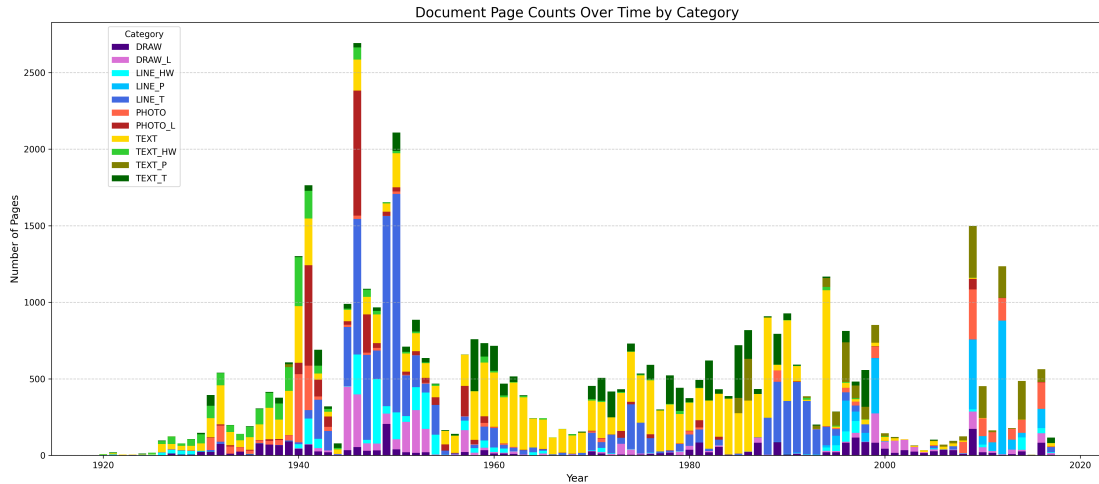


Figure 2.3 Distribution of categories in the final annotated dataset (**Dataset 3**) based on the document creation year

Figure 2.3 illustrates the temporal distribution of the final annotated data, while Figure 2.4 shows the same for the final performance test set (a subset of the full annotations). This test subset includes all annotated samples not used in the training subset of any cross-validation fold.

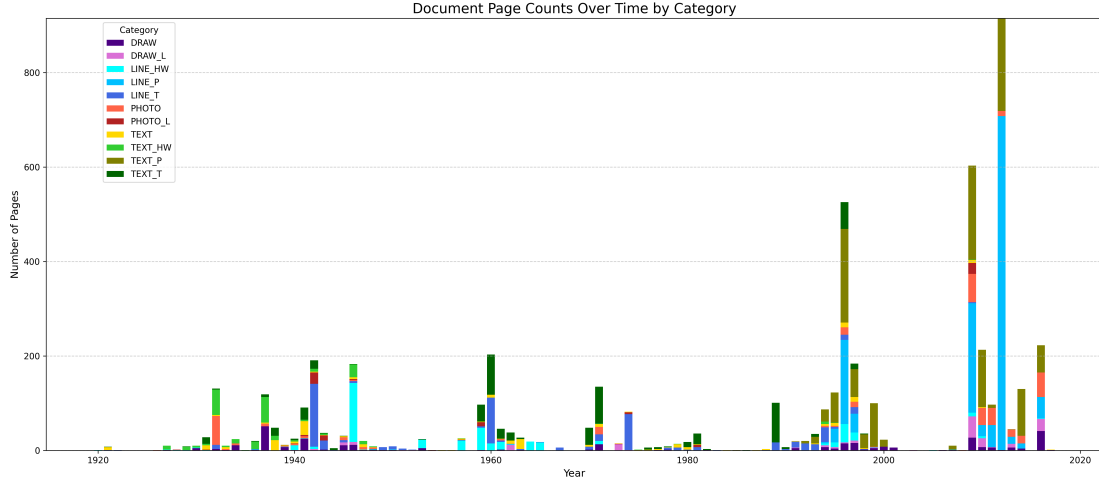


Figure 2.4 Distribution of categories in the performance test subset (samples not included in training subsets of the five cross-validation folds), based on the document creation year.

Figure 2.5 compares the temporal category distributions across annotation stages: the initial (Dataset 0), refined (Dataset 2), and final (Dataset 3) versions. The intermediate *poor selection* version (Dataset 1) is omitted.

Samples were selected manually, largely influenced by the page count of the source PDFs. As a result, many samples were drawn from the same multi-page documents, and pages from a single document could be assigned to either the same or different categories.

All three temporal plots reveal a gap in the 1990s. Documents from this period were difficult to classify because printed text often used monospaced fonts that resemble typewritten text. We intentionally excluded these ambiguous pages from the so-called ground-truth collection, forcing the models to learn and infer the distinction.

Finally, the prominent spikes in early-year samples (Figure 2.3 and the bottom graph of Figure 2.5) are a direct result of the single-page document enrichment step. This initiative substantially increased the proportion of short documents in the final annotated collection compared to earlier versions (Dataset 0–Dataset 2).

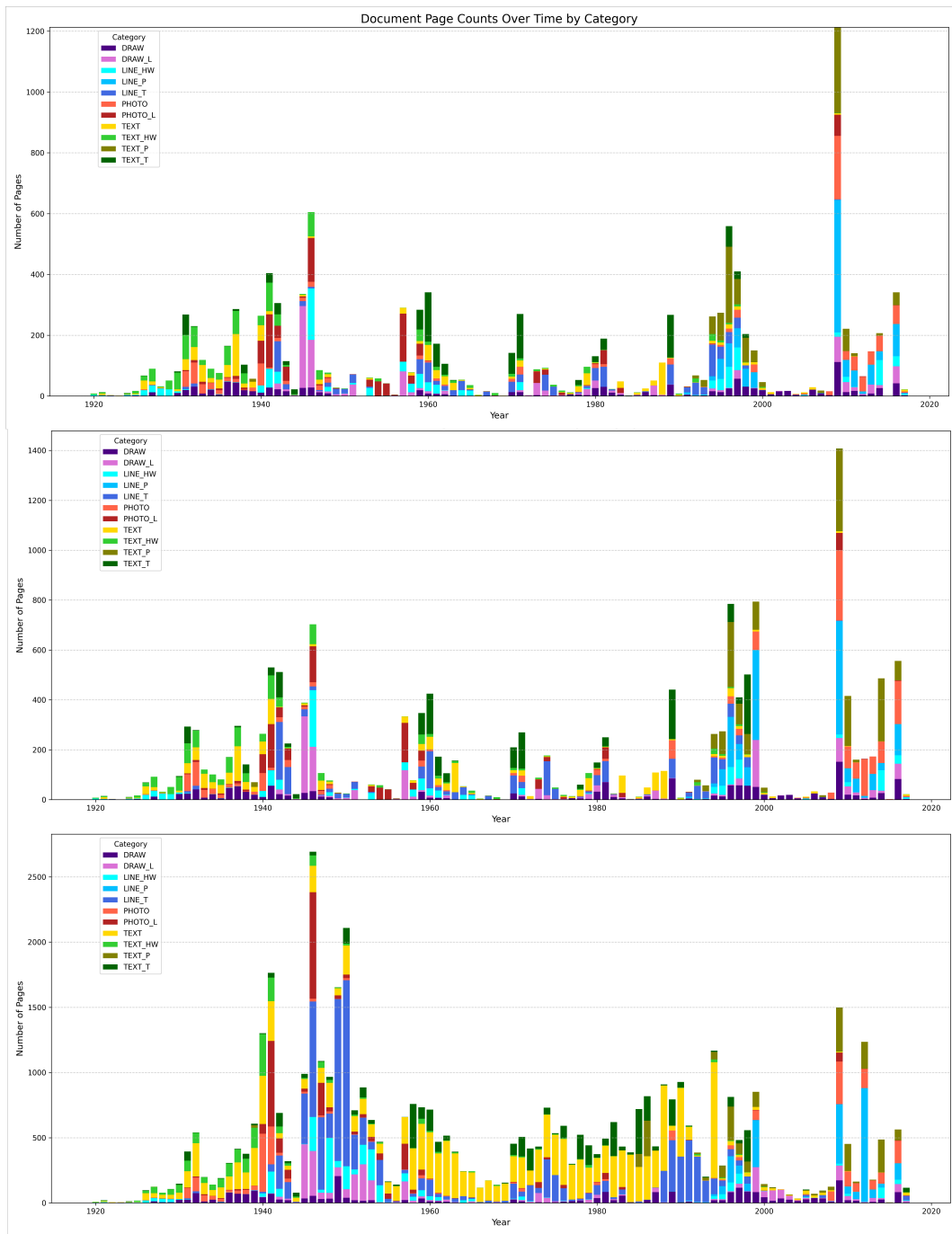


Figure 2.5 Temporal distributions of categories across annotation versions (Datasets 0, 2, and 3), based on the document creation year

2.4 Data modifications in categories

Achieving high accuracy was not only a matter of model selection but also of careful dataset curation. The training data evolved through successive stages of annotation and refinement. We measured the impact of these changes by evaluating a baseline ViT model (ViT-B/16-224) fine-tuned for each dataset version using the evaluation subset of the refined (Dataset 2 in Table 2.4) annotation version.

Initially, our *initial* annotation set had limited document variety. We expanded samples within each category, corrected misclassifications, and reclassified ambiguous items such as pages containing stamps. One iteration, referred to as *poor selection*, involved removing samples that seemed too noisy or redundant from the data provider’s perspective; however, evaluation revealed that removing these semi-repetitive but distinct examples was detrimental to performance.

Consequently, the *refined* annotation phase involved restoring many removed pages to ensure sufficient sample diversity, particularly for the PHOTO, TEXT_P, and TEXT_T categories. This iterative cycle of training, evaluation, expert review, and dataset refinement was critical to achieving the final high-performing models.

Figure 2.6 shows the Top-1 prediction confusion matrices for the ViT-Base (224px) model fine-tuned on the *initial*, so-called *poor selection* (Dataset 1), and *refined* (but not *final*) versions of the dataset, illustrating the category-specific performance improvements gained through careful data curation.

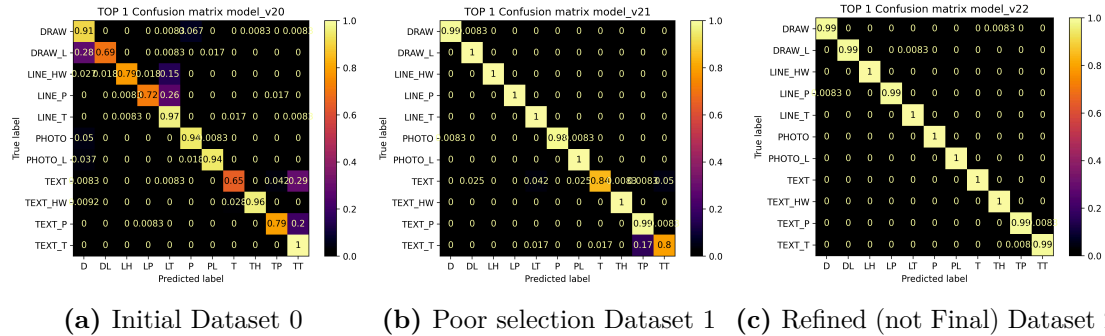


Figure 2.6 Confusion matrices of Top-1 predictions for ViT-Base at 224×224 resolution, fine-tuned on successive dataset versions and evaluated on the refined test set (before the final test set was created). Accuracy scores are not included. Dataset numbers refer to the versions in Table 2.4.

Key takeaways from developing the annotated dataset of digitized pages:

- Transformer models such as ViT, DiT, and CLIP tokenize images into 16×16 or 32×32 patches. Because we did not use rotation or flip augmentations, it was important to include diverse page layouts so that the model learned to

attend to the whole page (not only the most likely location of a photograph or the borders of a form).

- Distinguishing typewritten from printed text remains challenging at common input resolutions (224×224 to 384×384). As a result, pairs such as `TEXT_T`–`TEXT_P` and `LINE_T`–`LINE_P` are likely separated using subtle cues (e.g., whitespace between lines and page margins).
- Freehand sketches are highly variable; it is unlikely that a finite dataset captures all relevant drawing styles.
- Mixed-content pages (`TEXT`) often contain stamps or small graphics (e.g., newspaper logos), which can resemble `LINE_T` or `DRAW`.

A direct mitigation is to expand the dataset with more examples per category. Given time constraints and the number of pages already labeled by hand, we stopped expansion before reaching 50,000 records. The smallest category size reached slightly above 2,000 pages, while the largest exceeded 14,000 pages.

The category-size imbalance reflects the source data and the addition of single-page documents during refined annotation. To reduce the impact of imbalance during training, we used a batch sampler that fixes the batch size to the number of categories (i.e., one sample per category per batch; Section F.1). During each epoch, the sampler revisits already-seen samples in a randomized order, similar to the CLIP few-shot fine-tuning example.

3 Image classification

Given the limitations of unsupervised Document Layout Analysis (DLA) methods on heterogeneous historical document data (Section 1.3), we shifted to supervised image classification. This chapter presents (i) a low-compute baseline, (ii) a comparison of state-of-the-art deep learning architectures, and (iii) the iterative data refinement process that enabled high accuracy.

3.1 Low-compute approach

As a computationally efficient baseline, we first implemented a traditional computer vision pipeline using handcrafted features and a RFC. This initial system was designed for resource efficiency, requiring no specialized GPUs and making it suitable for standard CPU-based hardware.

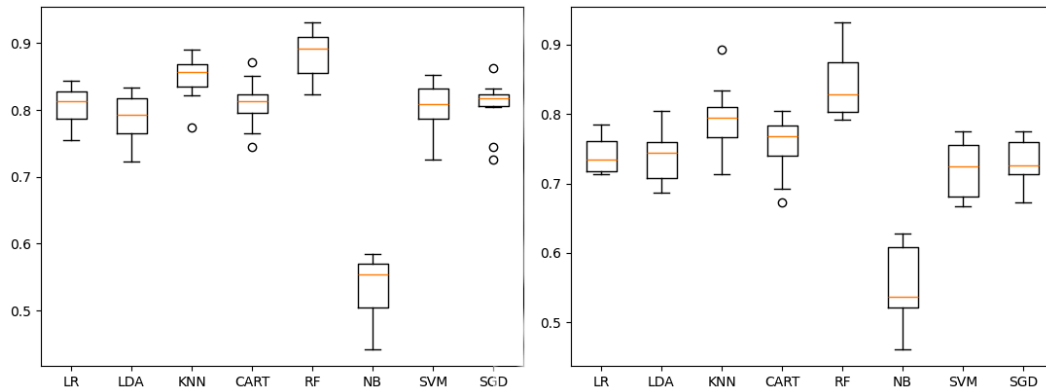


Figure 3.1 Low-compute models compared on the same data in cross-fold validation. Left: data-provider annotation. Right: our proposed annotation scheme.

3.1.1 Image feature extraction

The feature extraction step transforms each raw page image into a numerical feature vector. We engineered this vector by combining descriptors computed from both the grayscale image and a binarized version produced by Otsu thresholding:

- **Preprocessing:** Grayscale conversion, Otsu thresholding [You11], and basic image properties (dimensions, pixel ratios).
- **Hu moments [Hu62]:** Seven invariant moments capturing shape information robust to translation, scale, and rotation.

- **Haralick texture features [HSD73]:** Statistics derived from gray-level co-occurrence matrices (GLCM), including contrast, correlation, and homogeneity.
- **Histogram features:** Pixel-intensity distributions (256 bins for grayscale; two bins for binary).

The resulting representation is low-dimensional (298 floats), enabling efficient processing on modest hardware. However, it is less expressive than deep features, especially for visually subtle distinctions beyond coarse categories such as photographs or handwriting.

3.1.2 RFC

A Random Forest Classifier (RFC) [Bre01] is an ensemble learning method that aggregates the predictions of multiple decision trees. Each tree is trained on a random subset of the training data and features, and the final prediction is obtained by combining the trees’ outputs.

We chose RFC due to its effectiveness, interpretability, and efficiency on modest hardware. While we also evaluated other low-compute models (Latent Dirichlet Analysis (LDA), k-NN, Naive Bayes, SVM, logistic regression), RFC achieved the best preliminary accuracy (Figure 3.1).

Our implementation included class weighting to mitigate imbalance, optional hierarchical classification, and Top- N confidence outputs.

To evaluate the impact of the evolving label scheme, we trained RFC on two early annotation variants: the data-provider proposal (Table 1.2) and our refined proposal (Table 1.3). Development-set results are shown in Figure 2.1.

Overall accuracy was about 75%, which is insufficient for reliable automated sorting in production. Nevertheless, the baseline performed well on some categories, confirming that image-based classification is viable and motivating the transition to deep learning models trained on larger datasets using the final annotation scheme (Table 2.1).

3.2 Typical Models for Image Classification Fine-Tuning

Given the performance limitations of the classical approach, we turned to deep neural network architectures, which are highly effective for complex image recognition tasks. We evaluated several architectures by fine-tuning them on our dataset, initializing each with ImageNet-pretrained weights. We experimented with CNNs

(EfficientNetV2 [TL21; TL19], RegNetY [Rad+20]) and Transformer-based models (DiT [Li+22], ViT [Dos+20], CLIP [Rad+21]).

All models used a consistent set of data augmentations (Section F.1.3). Hyperparameters such as the learning rate and scheduler were kept at default values (chosen by the training code) across models. All image-based models were fine-tuned for three epochs, while hybrid (CLIP) models were fine-tuned for seven epochs.

For image-based models, the cross-validation training procedure involved five folds of randomized data selection (Subsection 2.2.1). For models with the same base architecture, the resulting weights were averaged, as described in Section 2.1. Hybrid models were fine-tuned using the split generated from the first cross-validation seed. Finally, we composed a performance test subset consisting of images not included in any fold’s training subset and used it to evaluate each final model.

3.2.1 EfficientNetV2 and RegNetY approaches

EfficientNetV2 is a convolutional neural network family optimized for faster training and improved parameter efficiency [TL21] and is related to the original EfficientNet compound-scaling formulation [TL19], pretrained on ImageNet-21k [Rid+21]. RegNetY is a family of ResNet-like architectures that defines a parameterized design space optimizing depth and width [Rad+20].

Model specifications are provided in Table 3.1, and evaluation results are summarized in Table 3.3.

EfficientNetV2 and RegNetY are CNN architectures that achieve strong performance on image classification benchmarks. We fine-tuned several variants of each family, ranging in size and input resolution. For all CNN models, we replaced the final classification layer to match the eleven classes and trained using cross-entropy loss. These models achieved high accuracies: the large variants exceeded 98%, and the best (RegNetY-16GF) surpassed 99%.

| Model | Resolution | Pretraining dataset | Params (M) |
|-------------------|------------------|----------------------------|------------|
| EfficientNet-v2-S | 300×300 | ImageNet-21k | 48.2 |
| EfficientNet-v2-M | 384×384 | ImageNet-21k & ImageNet-1k | 54.1 |
| EfficientNet-v2-L | 384×384 | ImageNet-21k & ImageNet-1k | 118.5 |
| RegNetY-12GF | 224×224 | ImageNet-12k & ImageNet-1k | 51.8 |
| RegNetY-16GF | 224×224 | ImageNet-12k | 83.6 |
| RegNetY-64GF | 384×384 | SEER & ImageNet-1k | 281.4 |

Table 3.1 Specifications of EfficientNetV2 and RegNetY Models

3.2.2 DiT and ViT approaches

Document Image Transformer (DiT) builds upon BEiT-style masked visual token prediction but was specifically pretrained on large-scale document images. The DiT-base and DiT-large models [Li+22] were self-supervised on 42M pages from IIT-CDIP (Lewis et al. [Lew+06]) and optionally fine-tuned on RVL-CDIP [HUD15] (400K grayscale images across 16 document types). Input images were resized to 224×224 , patchified into 16×16 tokens, and augmented via the standard image transform.

Similarly, ViT applies Transformers directly to image patches [Dos+20] and was pretrained on ImageNet-21k [Rid+21] and ImageNet-1k [BZK22].

| Model | Resolution | Pretraining dataset | Params (M) |
|-------------------|------------------|----------------------------|------------|
| dit-base-rvlcdip | 224×224 | IIT-CDIP (42M) & RVL-CDIP | 86 |
| dit-large | 224×224 | IIT-CDIP (42M) | 304 |
| dit-large-rvlcdip | 224×224 | IIT-CDIP (42M) & RVL-CDIP | 304 |
| vit-base-patch16 | 224×224 | ImageNet-21k & ImageNet-1k | 86.6 |
| vit-base-patch16 | 384×384 | ImageNet-21k & ImageNet-1k | 86.9 |
| vit-large-patch16 | 384×384 | ImageNet-21k & ImageNet-1k | 304.7 |

Table 3.2 Specifications of DiT and ViT models

Model specifications are provided in Table 3.2, and evaluation results are shown in Figures G.4 and G.3.

DiT and ViT apply the Transformer mechanism directly to image patches, in contrast to traditional CNNs. Because DiT was pretrained on large-scale document images, it is a strong candidate for our task. We fine-tuned several variants of both DiT and ViT.

All variants consistently achieved accuracies above 98%, performing on par with CNNs, but typically at the cost of 3–4 times more parameters for transformers.

ViT yielded one of the highest accuracies among image-based models. We therefore used a ViT-based model as the default classifier for annotation refinements (Section 2.4). However, the best-performing Transformer model was much larger than the best CNN model; thus, we evaluated a hybrid approach next.

3.2.3 Comparative Analysis and Error Patterns

While all deep learning architectures achieved high performance, their trade-offs differ in accuracy, parameter efficiency, and error patterns. Table 3.3 summarizes the top-performing models.

| Rank | Model | Type | Resolution | Params (M) | Accuracy |
|------|---------------------|-------------|------------|-------------|---------------|
| 1 | RegNetY-16GF | CNN | 224 × 224 | 83.6 | 99.21% |
| 2 | ViT-Large-384 | Transformer | 384 × 384 | 304.7 | 99.12% |
| 3 | ViT-Base-384 | Transformer | 384 × 384 | 86.9 | 98.92% |
| 4 | EfficientNet-V2-M | CNN | 384 × 384 | 54.1 | 98.90% |
| 5 | RegNetY-64GF | CNN | 384 × 384 | 281.4 | 98.79% |
| 6 | EfficientNet-V2-L | CNN | 384 × 384 | 118.5 | 98.77% |
| 7 | DiT-Base-RVL | Transformer | 224 × 224 | 86.0 | 98.72% |

Table 3.3 Consolidated model performance ranking (Top-1 accuracy)

RegNetY-16GF is the most efficient performer: despite having far fewer parameters (83.6M) than large Transformer models (304M), it achieves the highest overall accuracy. To understand this gap, we inspected the main confusion patterns (see Appendix G).

The TEXT ambiguity The largest error source across models is distinguishing generic TEXT from typeset/transcribed text (TEXT_T).

- **CNN scaling:** EfficientNet-V2-S struggles most, misclassifying 13% of TEXT. Increasing resolution (EfficientNet-V2-L) reduces this error to 5.6%.
- **Architecture efficiency:** RegNetY-16GF handles this ambiguity best, reaching 94% accuracy on TEXT with 5.1% confusion.
- **Transformer limitations:** Even domain-specific Transformers such as DiT-Large achieve slightly lower accuracy on this distinction (91%) than the best CNNs.

Structural detection (drawings) A secondary pattern appears when separating DRAW (freehand) from LINE (technical/line drawings). CNNs tend to be sharper on this edge-driven distinction: RegNetY-16GF reaches 99% accuracy on DRAW. Transformers show slightly fuzzier boundaries; for example, DiT-Base-RVL reaches 95% accuracy and confuses a small fraction with other line-based categories.

Based on these results, RegNetY-16GF is the preferred deployment model: it combines the highest accuracy (99.21%) with lower computational cost than the ViT-Large alternatives, and it performs best on the dataset’s hardest distinction (TEXT vs. TEXT_T).

3.2.4 CLIP-based approach

Finally, we investigated a multimodal approach using CLIP [Rad+21], pretrained on WebImageText [Xu+23]. CLIP supports zero-shot classification by comparing image features to the features of textual category descriptions. In our domain, however, zero-shot performance was limited (below $\approx 50\%$ accuracy; Figure 3.4), highlighting the difficulty of applying general models to specialized archival data without adaptation.

| Model | Resolution | Pretraining dataset | Params (M) |
|---------------------|------------------|---------------------|------------|
| CLIP-ViT-B/32 | 224×224 | WebImageText (400M) | 151 |
| CLIP-ViT-B/16 | 224×224 | WebImageText (400M) | 150 |
| CLIP-ViT-L/14 | 224×224 | WebImageText (400M) | 428 |
| CLIP-ViT-L/14@336px | 336×336 | WebImageText (400M) | 428 |

Table 3.4 Specifications of OpenAI’s CLIP-ViT models

After fine-tuning for seven epochs on our annotated dataset, CLIP achieved results comparable to the image-only CNN and Transformer baselines. Accuracy was typically above 98.0%, but only ViT-B/16 among the CLIP-based models exceeded 99.0%.

The smaller of the two ViT-B variants reached 99.0% accuracy (Figure 3.5), while the larger ViT-B and both ViT-L models scored in the 98–99% range (Figure G.5). Overall, these results show that targeted few-shot-style fine-tuning can make CLIP competitive for archival page classification.

Description of Categories

We evaluated CLIP using multiple sets of category descriptions, where each set defines the text features used at inference time. The goal was to assess how sensitive CLIP is to linguistic variations in the category prompts. Table 3.5 summarizes the tested description sets (details in Tables D.1 and D.8).

Most description sets were written manually and ranged from brief to highly detailed. To broaden the linguistic variation, we also tested two sets proposed by GPT-4 Deep Research and Gemini 2.5 Deep Research (Tables D.4 and D.6). These prompts were based on the manual descriptions (Tables D.1 to D.3) and included a request to follow best practices for CLIP prompting (Appendix E).

Early experiments showed that isolated prompt variants can yield inconsistent error rates. We therefore also evaluated an averaging strategy (“Average” in Figures 3.2 and 3.3 and Figure 3.7), where the text feature for each category is computed

| Rev. | Label set | Characteristics of category descriptions |
|------|--------------------------|--|
| vX.1 | init is in Table D.1 | Provides the full, initial set of classification categories with detailed distinctions between drawings, photos, and text, and further separates content by handwritten, printed, and typewritten forms both inside and outside tables or forms. |
| vX.2 | detailed in Table D.8 | Delivers the most detailed annotation-driven version, augmenting each label with notes on layout (legends, tables), annotation styles, and use-case examples. |
| vX.3 | extra in Table D.7 | Presents a balanced yet thorough taxonomy enriched with illustrative examples, combining clarity and completeness with real-world document-type scenarios. |
| vX.4 | gemini in Table D.6 | Expands upon the page-based description with verbose, researcher-oriented vocabulary, adding examples and elaborations per category. |
| vX.5 | gpt’s from Table D.4 | Reframes the classification around page-level context, explicitly noting that each label applies to an entire page containing the specified content, thereby shifting focus from isolated elements to page composition. |
| vX.6 | large from Table D.9 | Like <i>gpt</i> ’s, but page mentions are moved to the end, and it also provides an extension that includes specific composite labels for graphics combined with tables or legends. |
| vX.7 | mid from Table D.2 | Offers a more concise restatement of the <i>init</i> taxonomy, trimming phrasing while preserving the same category distinctions, emphasizing brevity - shortness & minimalism - in the labels’ descriptions. |
| vX.8 | min from Table D.3 | Distills the taxonomy to its bare essentials, reducing each description to the minimal wording needed to convey whether an element is a drawing, table, photo, or text and its modality, completely eliminating any redundancies in phrasings. |
| vX.9 | short from Table D.5 | Adapts the minimal set by omitting the word “page” and refining descriptions to emphasize cropped or cell-level occurrences of drawings, tables, photos, or text without referencing full pages. |

Table 3.5 Summary of CLIP category description sets. “Rev.” denotes the revision (model version) fine-tuned to a specific label set of text features.

as the mean of features from multiple description sets. This was intended to reduce prompt sensitivity and stabilize predictions.

Zero-shot model inference

The zero-shot inference process involves using an off-the-shelf pretrained CLIP model to classify images based on their similarity to the provided textual descriptions

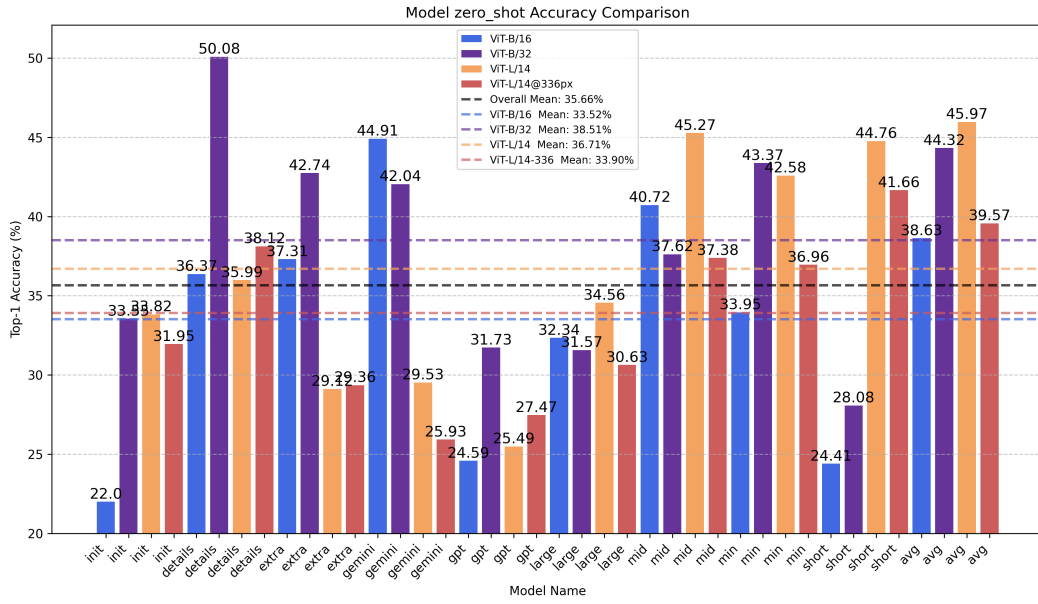


Figure 3.2 Zero-shot CLIP models comparison of classification accuracy per category descriptions set plus averaged text features variants of all four base models

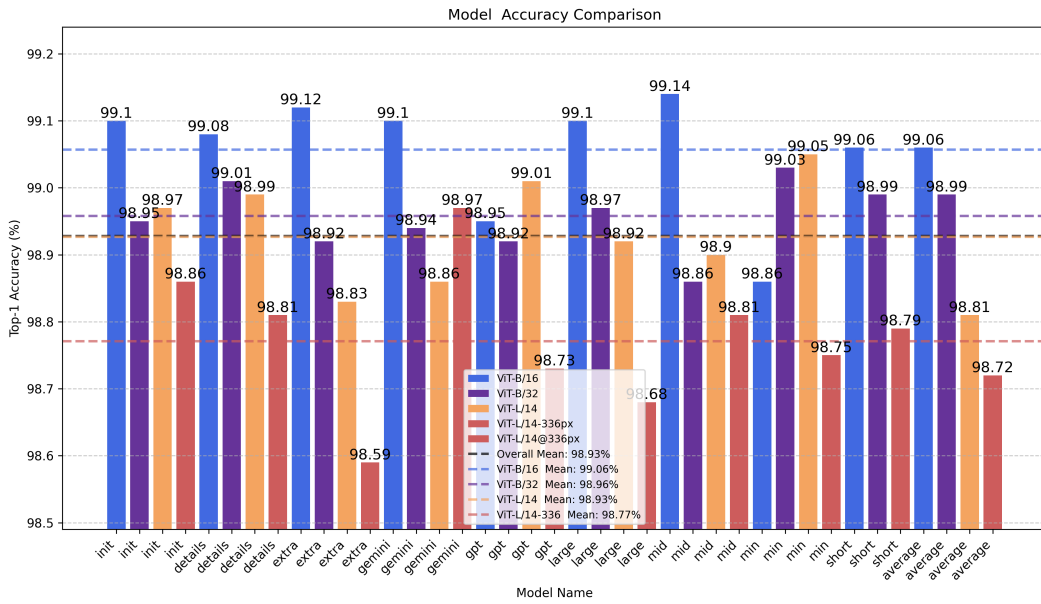
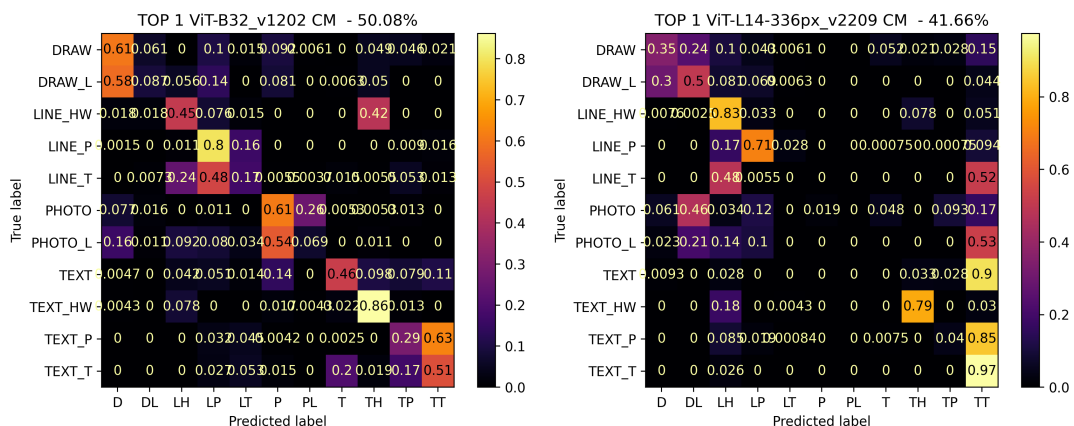
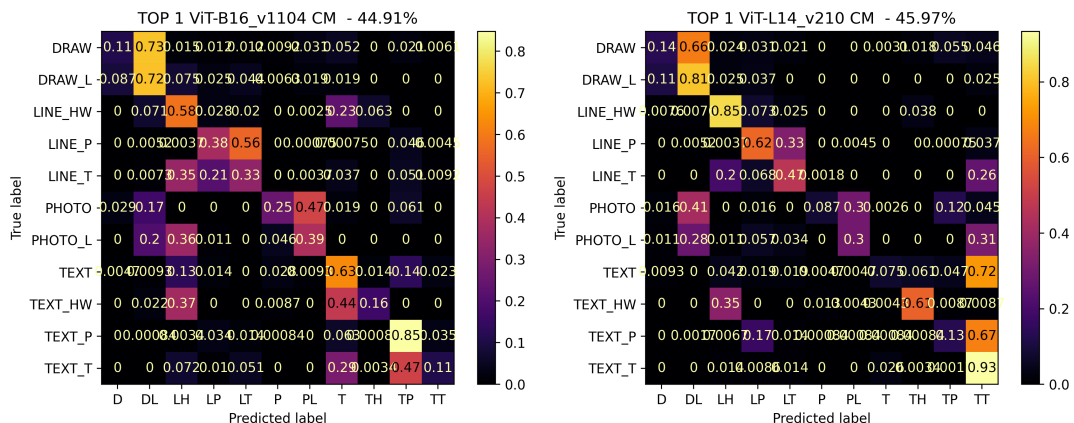


Figure 3.3 Comparison of fine-tuned CLIP models by classification accuracy across category description sets (label set names in alphabetical order). “Average” denotes averaged text features.

of the image categories.



(a) ViT-B/32 (detailed; Table D.8): 50.08% (b) ViT-L/14-336 (short; Table D.5): 41.66%



(c) ViT-B/16 (Gemini; Table D.6): 44.91% (d) ViT-L/14 (averaged): 45.97%

Figure 3.4 CLIP zero-shot confusion matrices (averaged text features)

While CLIP can separate broad visual concepts, its domain-specific zero-shot performance was limited: the mean accuracy across all label sets in Table 3.5 (including averaged-feature variants) was 35.69%. The ambiguity of natural-language prompts and the presence of domain-specific page types led to many errors across model setups (Figure 3.2). The best variant of each base model family is illustrated with confusion matrices in Figure 3.4.

In zero-shot settings, accuracy variations do not correlate clearly with either the base model type or the description set. Moving to few-shot fine-tuning, we found that zero-shot averaged models and models using the *mid* description set (Table D.2) consistently outperform the overall mean score. We therefore used

these text feature sets as reliable defaults in subsequent experiments.

Fine-tuned model inference

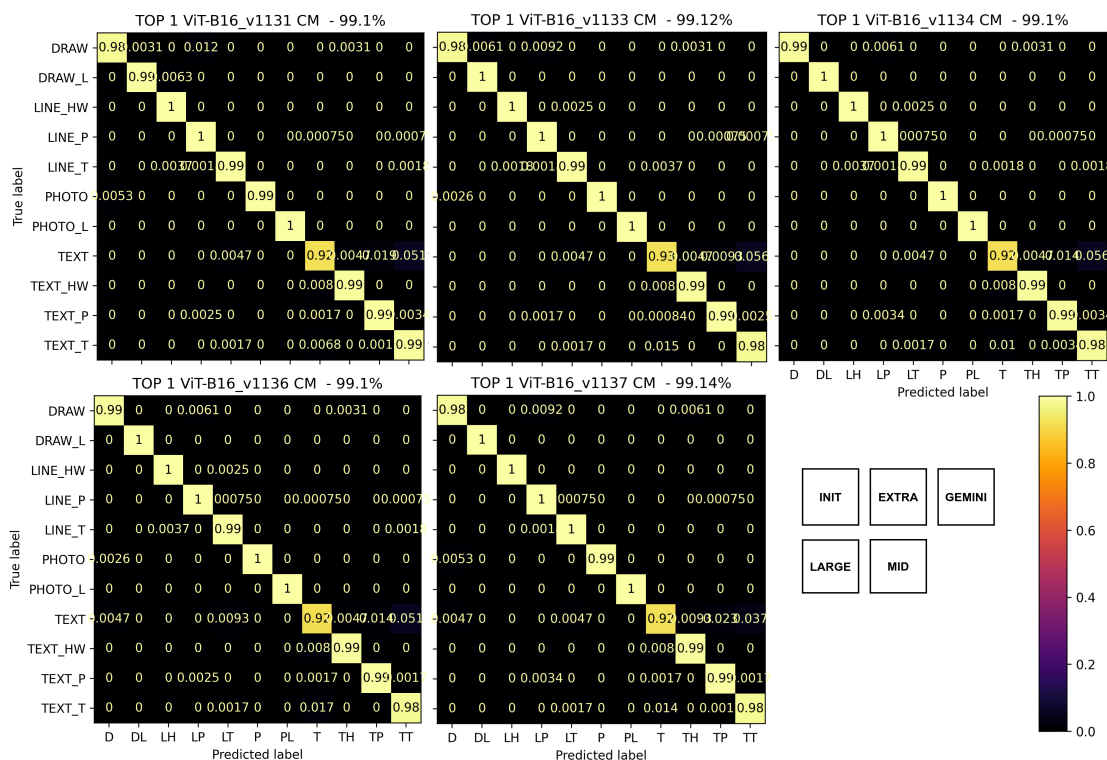


Figure 3.5 CLIP best models (ViT-B/16 variations) confusion matrices, seven epochs

We explored versions of CLIP through few-shot fine-tuning for seven epochs on the first fold (of five cross-validation runs) of the data split, in addition to testing its inherent zero-shot capabilities. Differences in predictions among the same base models are attributed to the category-specific text features used during fine-tuning and inference.

Figures 3.3 and 3.7 present a comprehensive analysis of classification accuracy among models tailored to different category description sets, highlighting the modest benefit of the averaging strategy observed in the zero-shot setting. In few-shot fine-tuning experiments, only the ViT-B/32 averaged model consistently outperformed its non-averaged counterparts. The *mid* set of category descriptions (Table D.2), used for ViT-B/16 fine-tuning and also scoring above the global average in all four zero-shot models (Figure 3.2), achieved the highest score among all fine-tuned CLIP models (99.14%), as shown in Figure 3.5.

Unexpectedly, the largest, highest-resolution model (ViT-L/14 at 336px) struggled with the mixed-content category `TEXT`, which it often misclassified as pure typewritten pages (Figure G.5). The other base models showed similar behavior, which is expected given the visual similarity between `TEXT` and `TEXT_*`, `LINE_T`, or `DRAW`.

We also observed a dataset effect (Figures 3.7 and 3.8). Average accuracy per base model dropped by 3–4%, and some label sets changed rank, likely because the expanded test dataset contains a wider variety of samples in the smaller categories. Among the fine-tuned CLIP models, B/16 and B/32 scored 99.06% and 98.96% on average on the standard performance test set, but on the expanded test dataset (Figure 3.6), only B/16 kept pace with the larger L/14 and L/14-336px variants.

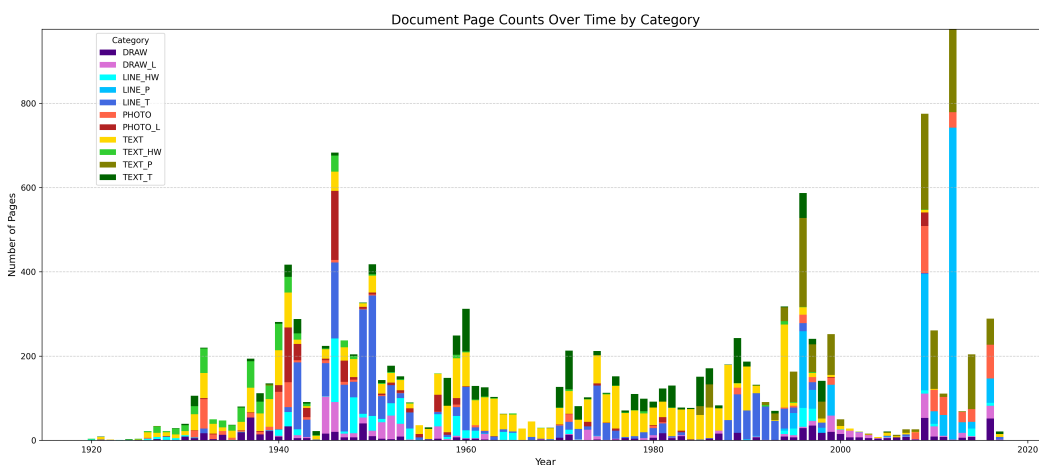


Figure 3.6 Category distribution in the expanded test dataset (all non-training samples from the first-fold split, random seed 420; 14,162 pages).

Accuracy varied across both label sets and base models. For example, L/14-336px improved, whereas B/32 decreased relative to other models. A likely reason is that the expanded test dataset includes a wider variety of samples in the smaller categories. As shown in Figures 2.4 and 3.6, the pool of available non-training annotations differs substantially across folds: the expanded test dataset includes development and test subsets from the first fold, plus additional pages labeled `TEXT` that were not filtered out from the training subsets of folds 2–5.

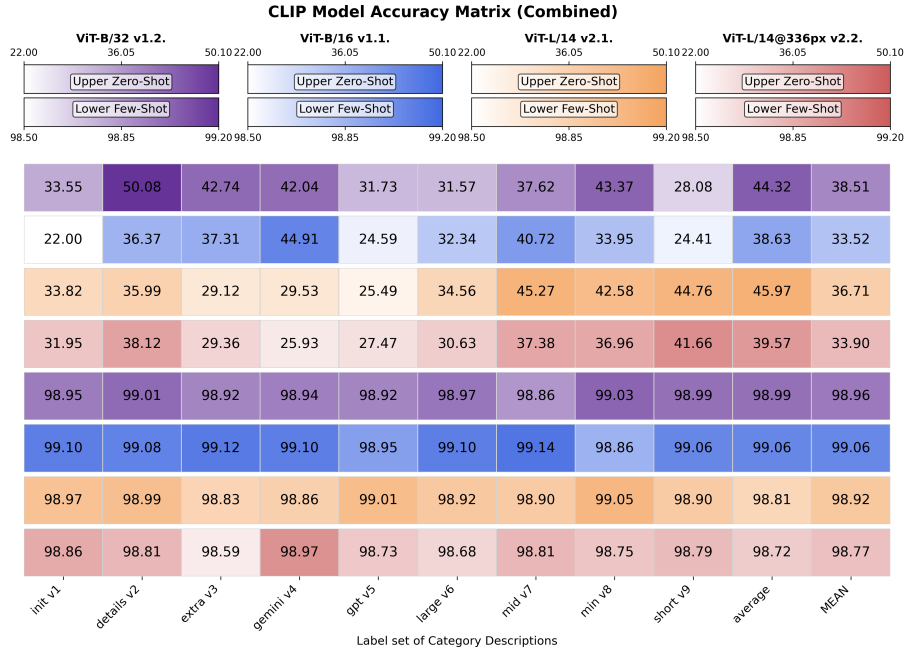


Figure 3.7 Combined zero-shot and fine-tuned CLIP models: comparison of classification accuracy across category description sets on the standard test dataset (5,449 pages).

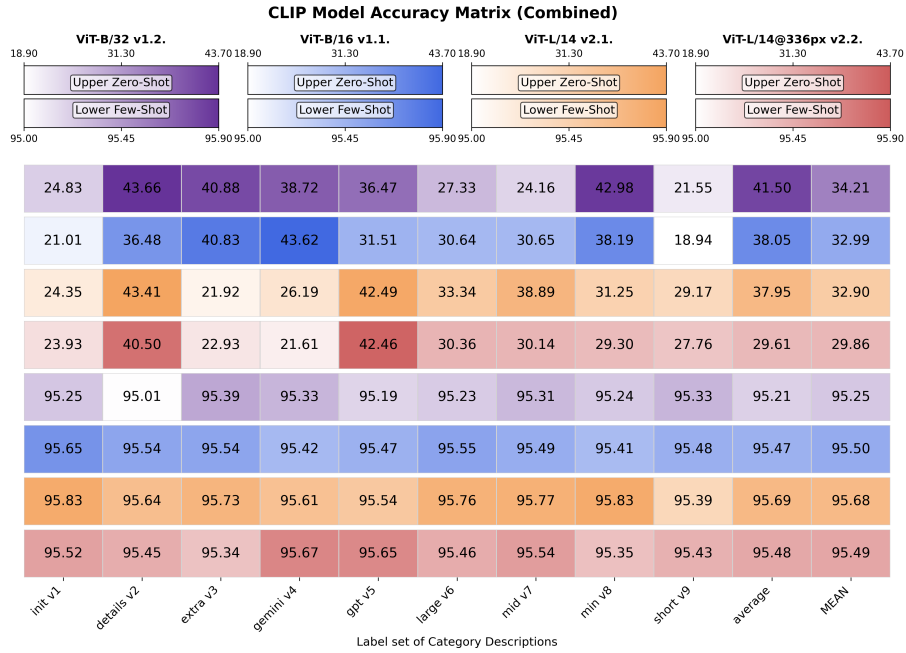


Figure 3.8 Combined zero-shot and fine-tuned CLIP models: comparison of classification accuracy across category description sets on an expanded test dataset (all non-training samples from the first-fold split, random seed 420; 14,162 pages).

4 System architecture

The classification system is implemented as a modular pipeline that transforms raw, disorganized archival documents into a categorized, searchable repository. It is designed to be platform-agnostic, supporting both the Unix environments common in research and the Windows systems typically used in archival offices.

At its core, the pipeline applies fine-tuned image classification models—CNNs (e.g., EfficientNetV2 [TL21], RegNetY [Rad+20]), Transformers (DiT [Li+22], ViT [Dos+20]), and hybrid multimodal models (CLIP [Rad+21])—to sort historical page scans (Figures 4.1 and 4.2).

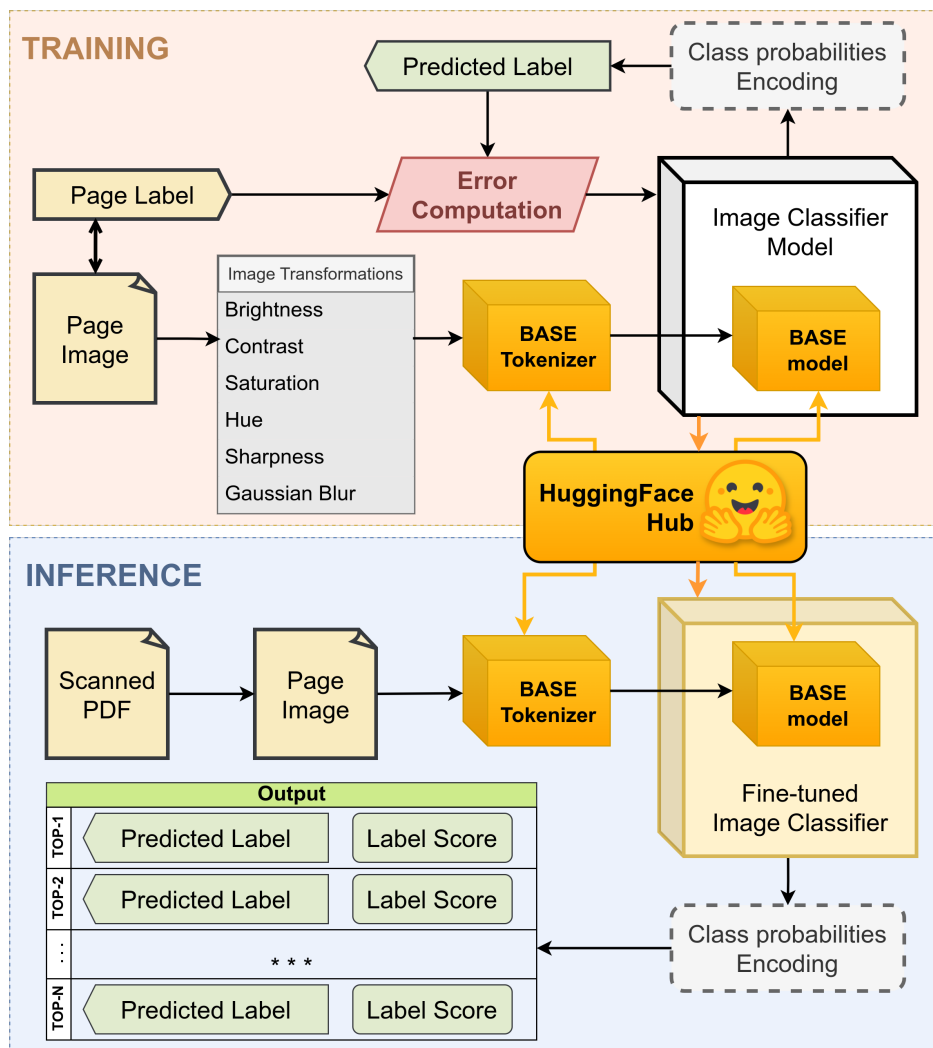


Figure 4.1 System overview for the image-only (CNNs and Transformer) variants

The architecture consists of (i) configuration and interfaces (Section 4.1), (ii) input processing (Section 4.1.3), (iii) model training (fine-tuning; Section F.1), (iv) evaluation and output generation (Section F.2), and (v) data preparation utilities (Section 4.3). The system is implemented in Python, with helper scripts for input/output processing on both Windows and Unix platforms.

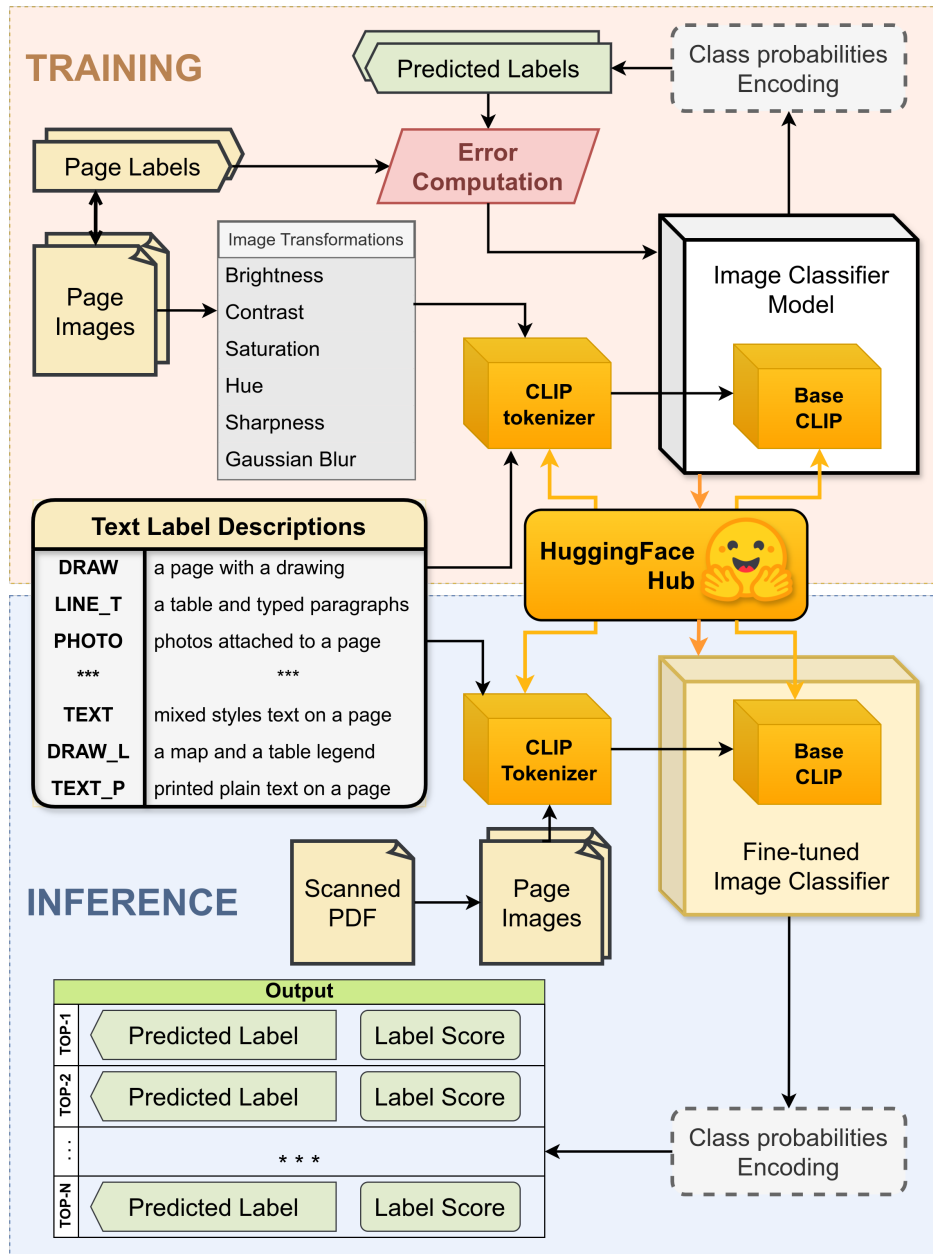


Figure 4.2 Model overview for the hybrid CLIP variant

The system is built in Python using PyTorch [Pas19] and HuggingFace Transformers [Wol+19] to manage model loading and input processing across model types. The complete codebase (including both ViT and CLIP branches) is available in a public GitHub repository [Lut+25].

Recognizing the sensitivity of many archival collections, the architecture is strictly on-premises: processing occurs entirely on local hardware, ensuring that restricted or unpublished data never leaves the institution’s secure network.

Additional implementation details are provided in Appendix F, including hyperparameters, image preprocessing, dataset splitting, and output options.

4.1 Interface

To accommodate both end users and developers, the system provides a configuration file for persistent settings, a Command-line Interface (CLI) for direct operation, and utility scripts for data preparation. To reduce the required programming expertise, the two primary interaction modes are an editable text configuration file and a command-line interface for automation.

4.1.1 Configuration file

The `config.txt` file serves as the central repository for user-adjustable parameters, allowing users to modify the system’s behavior without changing the source code. The settings are organized into the sections summarized in Table 4.1.

| Section | Description of variables in section |
|----------|--|
| [INPUT] | Specifies the default input directory and chunk size; controls whether processing is chunked or results are recorded at the end. |
| [OUTPUT] | Sets paths for result CSV (Comma-separated Values) files, model checkpoints, and visualization outputs. |
| [SETUP] | Contains operational parameters: batch size, input file format, top- N value, base model architecture, and random seed. |
| [TRAIN] | Stores training settings such as dataset path, number of epochs, learning rate, validation split, and logging frequency. |
| [EVAL] | Sets the evaluation directory layout (category subdirectories with files named {document_name}-{page_number}). |
| [HF] | Stores HuggingFace integration settings and defines a global model revision. |

Table 4.1 Summary of configuration settings in `config.txt` sections

All system behaviors (e.g., input discovery, chunk size, and model choice) are managed through `config.txt`. Users can toggle settings (e.g., “safe mode” for corrupted files) without editing the Python code.

4.1.2 Command line entry point

The system’s primary entry point is `run.py`, which exposes a CLI for fine-grained control.

For large-scale processing, a single command can process an entire directory (`-dir`) and optionally include nested folders (`-inner`). The framework is also designed to support rapid adaptation: launching fine-tuning on a new annotated dataset does not require code changes and can be done via a single flag (`-train`).

| Option | Purpose |
|---------------------|--|
| <code>-file</code> | Classify a single image file (one page). |
| <code>-dir</code> | Classify all supported images in a directory. |
| <code>-inner</code> | Recursively include nested subdirectories under <code>-dir</code> . |
| <code>-chunk</code> | Enable chunked processing for large folders (memory-efficient batching). |
| <code>-b</code> | Set batch size (overrides <code>config.txt</code>). |
| <code>-train</code> | Run fine-tuning on an annotated dataset specified in <code>config.txt</code> . |

Table 4.2 Selected CLI options in `run.py` (representative subset)

4.1.3 Streamlined Input Processing

The system bridges the gap between raw scans and model-ready inputs through a robust input layer. For large archives, chunked processing improves memory efficiency by loading and predicting on small batches of images; this can be enabled via the `-chunk` flag.

While the system can run on a CPU for small batches, it is optimized for NVIDIA GPUs to increase throughput on large collections. Batch size can be configured in `config.txt` or via the `-b` command-line flag.

4.1.4 Web service interface

To support interactive testing and integration with downstream applications, the system additionally exposes a lightweight Representational State Transfer (REST)

Application Programming Interface (API) built with FastAPI, served from the `service/` subdirectory of the main project repository. The service provides three Hypertext Transfer Protocol (HTTP) endpoints summarized in Table 4.3.

| Method | Path | Description |
|--------|----------|--|
| GET | / | Serves the static HyperText Markup Language (HTML) frontend for manual image upload and testing. |
| GET | /info | Returns metadata about available model versions and the active computation device (<code>cpu</code> or <code>cuda</code>). |
| POST | /predict | Performs inference on a single uploaded image and returns structured JavaScript Object Notation (JSON) predictions. |

Table 4.3 REST API endpoints exposed by the web service

The primary `/predict` endpoint accepts a multipart form-data request with three parameters: `file` (a JPEG or PNG image), `version` (the model version string, e.g., `v5.3`, or `all` to invoke a five-model ensemble), and the optional integer `topn` controlling the number of returned predictions (default: 3). The JSON response includes the best predicted category, its confidence score, and the full ranked Top-*N* list, as illustrated in Listing 4.3.

```
{
  "model_version": "google/vit-large-patch16-384 (v5.3)",
  "best_category": "TEXT",
  "score": 0.985,
  "requested_topn": 3,
  "predictions": [
    {"label": "TEXT", "score": 0.985},
    {"label": "TEXT_P", "score": 0.010},
    {"label": "LINE_P", "score": 0.002}
  ]
}
```

Figure 4.3 Example JSON response from the `/predict` endpoint (model `v5.3`, Top-3 predictions)

The service supports all model architectures listed in Section 3.2 and automatically detects available Compute Unified Device Architecture (CUDA) devices to accelerate inference. A static HTML/JavaScript frontend (`service/frontend/`) is

bundled for immediate browser-based testing without additional tooling. Full client integration should be maintained separately in the LINDAT Service repository.

4.2 Output formats

The system provides several output formats to support different analysis and workflow needs:

1. **Console output:** For single-file classification, the system prints the Top- N predictions with confidence scores.
2. **Top- N tables:** CSV files sorted by file and page number, with columns `CLASS-N` and `SCORE-N` for each of the Top- N predictions.
3. **Averaged Top- N tables:** CSV files sorted by file and page number, with columns for Top-1 model guesses from `v1.3` to `v5.3`, then, `CLASS-N` and `SCORE-N` for each of the Top- N predictions computed as average of five models' scores per category.
4. **Raw probability tables:** CSV files containing the model's raw probabilities for all categories, enabling detailed analysis of normalized logits.
5. **Confusion matrix plots:** Visualizations of model performance on annotated data, showing the relationship between predicted and true categories.

Results are saved to locations specified in `config.txt`, with filenames that include timestamps and model identifiers for traceability.

For archival management, the outputs are designed to be immediately actionable: the system can generate tables listing each file and its predicted category (e.g., `LINE_P`, `PHOTO_L`, `TEXT_HW`) with a confidence score. It can also copy or move images into category-specific subfolders based on predictions, allowing an archivist to open a folder such as `DRAW` or `PHOTO_L` and quickly verify results or begin targeted processing.

4.3 Data preparation functionality

The system includes a suite of utilities to help users prepare document data for both fine-tuning and classification, starting from raw PDF files. Figure 4.4 illustrates the end-to-end workflow for a typical model inference use case.

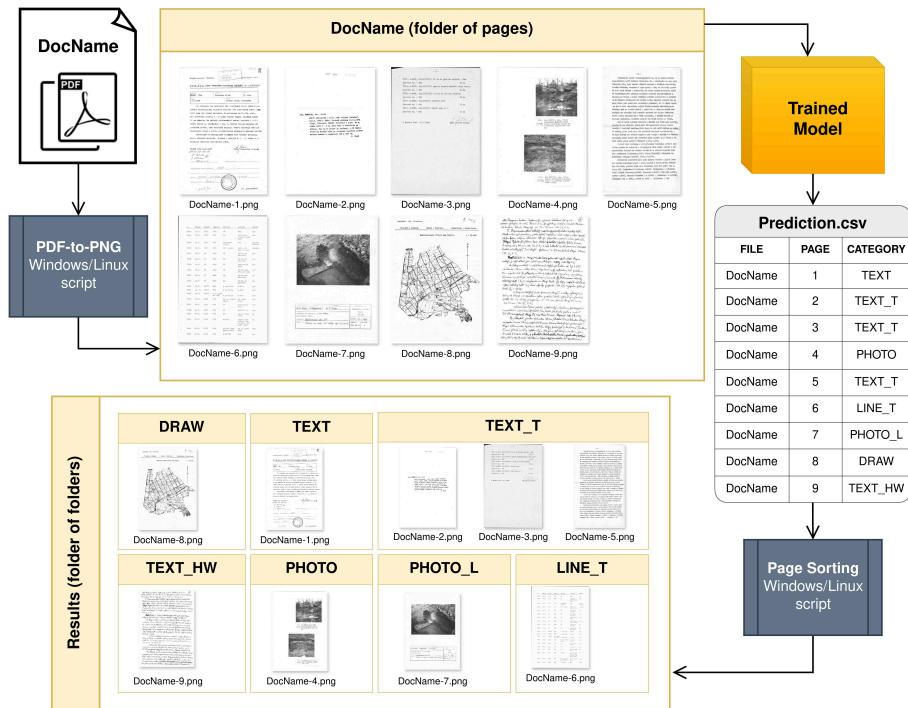


Figure 4.4 Model inference use-case: input PDF is parsed into a folder of pages, then sorted into category-specific subdirectories

4.3.1 PDF documents to page images

The data preparation pipeline includes cross-platform scripts to convert PDF documents into PNG images:

- **Unix script** (`pdf2png.sh`): uses `pdftoppm` for conversion with zero-padded page numbers
- **Windows script** (`pdf2png.bat`): uses ImageMagick and Ghostscript with sequential page numbers

These scripts create a directory structure where each PDF is converted into a subdirectory of page-specific images. Additional utilities facilitate the organization of single-page documents (any subdirectories containing a single file) for more efficient annotation.

4.3.2 Annotated data sorting

To facilitate model training (and fine-tuning of pretrained models), the system provides tools for organizing annotated data into a structured format:

1. **Annotation process:** Users create CSV files with three required columns: `FILE`, `PAGE`, and `CLASS`.
2. **Data sorting:** The provided scripts (`sort.sh/sort.bat`) parse the annotation files and copy the corresponding image files into category-specific subdirectories. These scripts also support quick visual verification of annotations and model outputs.
3. **Category balancing:** The `max_categ` parameter in the configuration file can be used to limit the number of samples in overrepresented categories, helping to address class imbalance that could otherwise bias model performance during fine-tuning.

This structured workflow ensures that training data is properly organized according to the model's expected input format.

5 Results

This chapter evaluates the best fine-tuned models and discusses how the resulting classifiers can be used in archival workflows.

We report Top-1 accuracy and relate it to model size (efficiency). We also analyze agreement between model predictions on unlabeled pages.

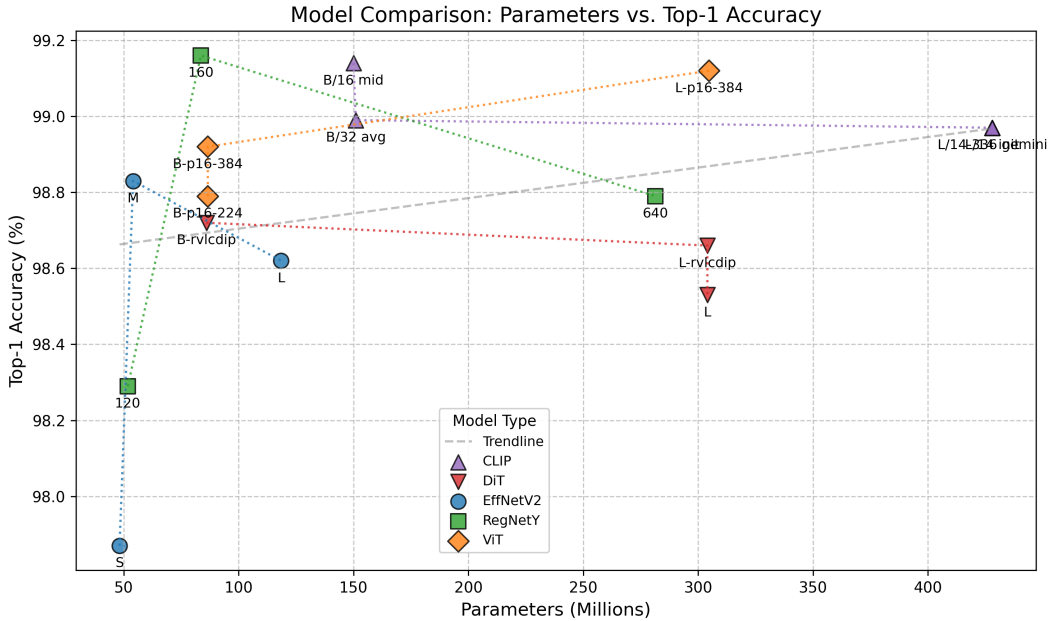


Figure 5.1 Accuracy vs. parameter count across evaluated models. Models above the trendline deliver superior efficiency.

Figure 5.1 shows that CNNs, ViT models, and fine-tuned hybrid (text+image) CLIP models exceed $\approx 98.5\%$ accuracy with parameter budgets below 200M. In comparison, similarly sized DiT variants perform acceptably but below the top-performing architectures.

5.1 Accuracy of tested models

We compared CNNs (EfficientNetV2 [TL21], RegNetY [Rad+20]), Transformers (ViT [Dos+20], DiT [Li+22]), and hybrid CLIP models [Rad+21] (Sections 3.2.1, 3.2.2, 3.2.4). Models were fine-tuned and evaluated on the archival dataset using Top-1 accuracy.

The test set contains 5,449 images that were not used in any training subset, enabling fair evaluation of all cross-validation folds (and their averaged variants).

Figure 2.4 illustrates the category distribution over time. Table 5.1 summarizes model size, input resolution, and performance.

| Base model | Parameters (M) | Resolution | Accuracy Top-1 (%) |
|--------------------------|----------------|------------------|--------------------|
| RFC baseline | 333 trees | 298×1 | 75.34 |
| EfficientNetV2-S | 48.2 | 300×300 | 97.87 |
| EfficientNetV2-M | 54.1 | 384×384 | 98.83 |
| EfficientNetV2-L | 118.5 | 384×384 | 98.62 |
| RegNetY-12GF | 51.8 | 224×224 | 98.29 |
| RegNetY-16GF | 83.6 | 224×224 | 99.16 |
| RegNetY-64GF | 281.4 | 384×384 | 98.79 |
| DiT-base-RVL | 86 | 224×224 | 98.72 |
| DiT-large | 304 | 224×224 | 98.53 |
| DiT-large-RVL | 304 | 224×224 | 98.66 |
| <i>ViT-base-patch16</i> | <i>86.6</i> | 224×224 | <i>98.79</i> |
| ViT-base-patch16 | 86.9 | 384×384 | 98.92 |
| ViT-large-patch16 | 304.7 | 384×384 | 99.12 |
| CLIP-ViT-B/16 | 150 | 224×224 | 99.14 |
| CLIP-ViT-B/32 | 151 | 224×224 | 98.99 |
| CLIP-ViT-L/14 | 428 | 224×224 | 98.97 |
| CLIP-ViT-L/14 | 428 | 336×336 | 98.97 |

Table 5.1 Top-1 accuracy and model complexity for all evaluated architectures. *Italic*: most efficient; **bold**: most accurate (and most efficient) per model type.

Table 5.1 and Figure 5.1 summarize the main results:

- **RegNetY (CNN)**: RegNetY-16GF achieves $\approx 99.16\%$ accuracy with a relatively small parameter count (83.6M) at 224×224 resolution [Rad+20]. RegNetY-64GF (281.4M parameters) falls below the global efficiency trendline, but was published (v6.3) for comparison.
- **EfficientNetV2 (CNN)**: EfficientNetV2-M reaches $\approx 98.83\%$ accuracy at 54.1M parameters with 384×384 inputs [TL21], making it a reasonable option for lower-resource machines (subject to throughput constraints).
- **Vision Transformers (ViT)**: ViT-large reaches $\approx 99.12\%$ Top-1 accuracy [Dos+20] but requires substantially more parameters (304.7M) than the best-performing CNNs.

- **Document image Transformers (DiT):** DiT variants achieve 98–99% Top-1 accuracy [Li+22] but do not outperform the best CNNs and ViT models at comparable sizes.
- **CLIP:** Zero-shot performance is inadequate for this domain ($\leq 50\%$), highlighting the need for fine-tuning and carefully designed text features [Rad+21]. After fine-tuning (seven epochs on 80% of annotated pages), all tested CLIP variants exceed $\approx 98.97\%$ accuracy; the best result is achieved by CLIP-ViT-B/16 ($\approx 99.14\%$) with the *mid* label descriptions (Table D.2).

5.2 Picking the best model

The primary objective of this research was to develop a classification system that combines accuracy with practical applicability within existing archival processes. This section outlines the deployment specifications and the expert-defined criteria the system is designed to meet.

5.2.1 Deployment and Usability

Comprehensive installation and usage instructions are provided in the project’s public repository (e.g., via the GitHub README). To facilitate adoption by archival institutions, the system is packaged for local deployment under the MIT license.

| Specification | A30 | A40 | L40 | RTX 3090 |
|---------------------|-------------------|-------------------|-------------------------|-------------------|
| Architecture | Ampere (GA100) | Ampere (GA102) | Ada Lovelace (AD102) | Ampere (GA102) |
| Comp. Cap. | 8.0 | 8.6 | 8.9 | 8.6 |
| Mem. Size | 24 GB | 48 GB | 48 GB | 24 GB |
| Mem. Type | HBM2 | GDDR6-ECC | GDDR6-ECC | GDDR6X |
| Mem. Interf. | 3072-bit | 384-bit | 384-bit | 384-bit |
| Mem. BW | 933 GB/s | 696 GB/s | 864 GB/s | 936 GB/s |
| CUDA Cores | 3,584 | 10,752 | 18,176 | 10,496 |
| Tensor Cores | 224 (3rd Gen) | 336 (3rd Gen) | 568 (4th Gen) | 328 (3rd Gen) |
| RT Cores | N/A (GA100) | 84 (2nd Gen) | 142 (3rd Gen) | 82 (2nd Gen) |
| Max Power | 165W | 300W | 300W | 350W |
| MIG Support | Yes ≤ 4 | No | No | No |

Table 5.2 NVIDIA GPUs Specifications Comparison

Key operational considerations were addressed to ensure the system’s practicality

and ease of use. Designed for on-premises deployment, it is vital for archives with sensitive or restricted collections. While standard CPU hardware suffices for inference, using a GPU is advisable for fine-tuning with user-annotated datasets and for improving inference speed on large datasets.

For best performance with CUDA GPU acceleration, an NVIDIA graphics card is required. The specifications of the GPUs we tested are listed in Table 5.2. Users must also allocate significant disk space (up to 30 GB) to accommodate Python dependencies, pretrained model weights, and the PDF-to-page conversion outputs typical of large archival collections.

On a modern office desktop computer, the system can process hundreds of thousands of pages within a week, with throughput over 48 hours potentially exceeding 1,000,000 pages on higher-end hardware.

| Model size | A30 | A40 | L40 | RTX 3090 |
|------------|-------------|-------------|-------------|-------------|
| 0–70M | 1.58 / 5.21 | 1.15 / 3.24 | | 1.30 / 4.53 |
| 70–100M | 1.50 / 4.68 | 1.20 / 3.42 | 1.58 / 5.19 | |
| 100–200M | 1.48 / 4.60 | 1.04 / 2.83 | | 1.32 / 4.07 |
| 200–350M | 1.27 / 3.63 | 1.07 / 2.85 | | |

Table 5.3 Average training/evaluation throughput (batches of 11-16 samples per second) across NVIDIA GPU types and model size (parameters) ranges. Values are reported as *train* / *eval* pairs of the processing speed measurements.

| Model size | A30 | A40 | L40 | RTX 3090 |
|------------|------|------|------|----------|
| 0–70M | 4.81 | 3.42 | | 3.98 |
| 70–100M | 4.58 | 3.67 | 4.87 | |
| 100–200M | 5.19 | 3.21 | | 4.00 |
| 200–350M | 3.82 | 3.29 | | |

Table 5.4 Average efficiency (accuracy increase per hour) across NVIDIA GPU types and model size (parameters) ranges.

Tables 5.3 and 5.4 report training-time measurements on the NVIDIA GPUs listed in Table 5.2. Inference (evaluation) is about 2–3 × faster. While throughput depends slightly on model size, it is primarily determined by GPU characteristics.

Comprehensive installation and usage instructions are provided in the project’s documentation, separately for image-only (ViT, DiT, CNNs) and hybrid (CLIP) models. The core functionality is exposed via the CLI and is designed to work on both Unix and Windows systems.

In practice, the classifier can be integrated into a digitization pipeline: scanned images are processed automatically, and each page receives a category label. This label enables routing to downstream steps (e.g., sending plain text pages to OCR, sending tables to structured data extraction, and routing pages with illustrations to segmentation or human review). Automating this routing reduces manual sorting effort and improves throughput and consistency.

5.2.2 Agreement with field experts

We refined the classification logic based on criteria established in collaboration with archival experts (Section 1.3). These requirements ensure that automated labels match practical archival needs for retrieval and downstream processing:

- Photographs or drawings of significant size (at least postage-stamp sized) must be classified as `PHOTO` or `DRAW`, enabling targeted extraction of graphical content.
- Tables and forms must be detected even when borders are faint or missing; these are classified as `LINE_T`, `LINE_P`, or `LINE_HW`.
- Only pages containing clean, uniform text should be classified as `TEXT_P`, `TEXT_T`, or `TEXT_HW`. Such pages should be free of significant annotations or non-text elements; minor peripheral notes (e.g., handwritten page numbers) may be ignored.
- Pages with mixed text styles (`TEXT`) may include minor graphical elements (e.g., newspaper logos) that do not require separate extraction.
- Graphical elements embedded in tabular layouts or accompanied by table-like legends must be classified as `PHOTO_L` or `DRAW_L`, signaling the need to extract both graphics and structured data.

Given offline, batch-oriented workflows, the modest additional inference cost of transformer-based models is acceptable. To balance accuracy and model complexity, we selected **RegNetY 16GF (224)** for deployment. As an alternative for higher-memory GPU systems, **vit-large-patch16-384** can be used.

5.3 Similarity of predictions in different models

In Figure 3.3, both smaller and larger CLIP models, after only seven epochs of fine-tuning with standard preprocessing, achieve accuracy comparable to the image-only models discussed in Sections 3.2.1 to 3.2.2. In other words, with targeted

fine-tuning, CLIP (especially ViT-B/16) can achieve high accuracy on annotated page images (Figure 3.5).

However, when we applied the best image-only and hybrid models to unlabeled pages, we observed a clear difference in prediction agreement. As shown in Figure 5.2, CLIP models diverge markedly from image-only models and even from other CLIP variants. Image-only models share over 90% agreement in their predictions, whereas hybrid models show under 65% similarity with any other model.

The data providers confirmed that this lack of agreement makes hybrid predictions harder to trust in practice. Consequently, image-only models were preferred for archival sorting because they assign consistent labels to most pages. In contrast, the hybrid models produced erratic predictions and failed to identify a common category for over 80% of the unlabeled pages.

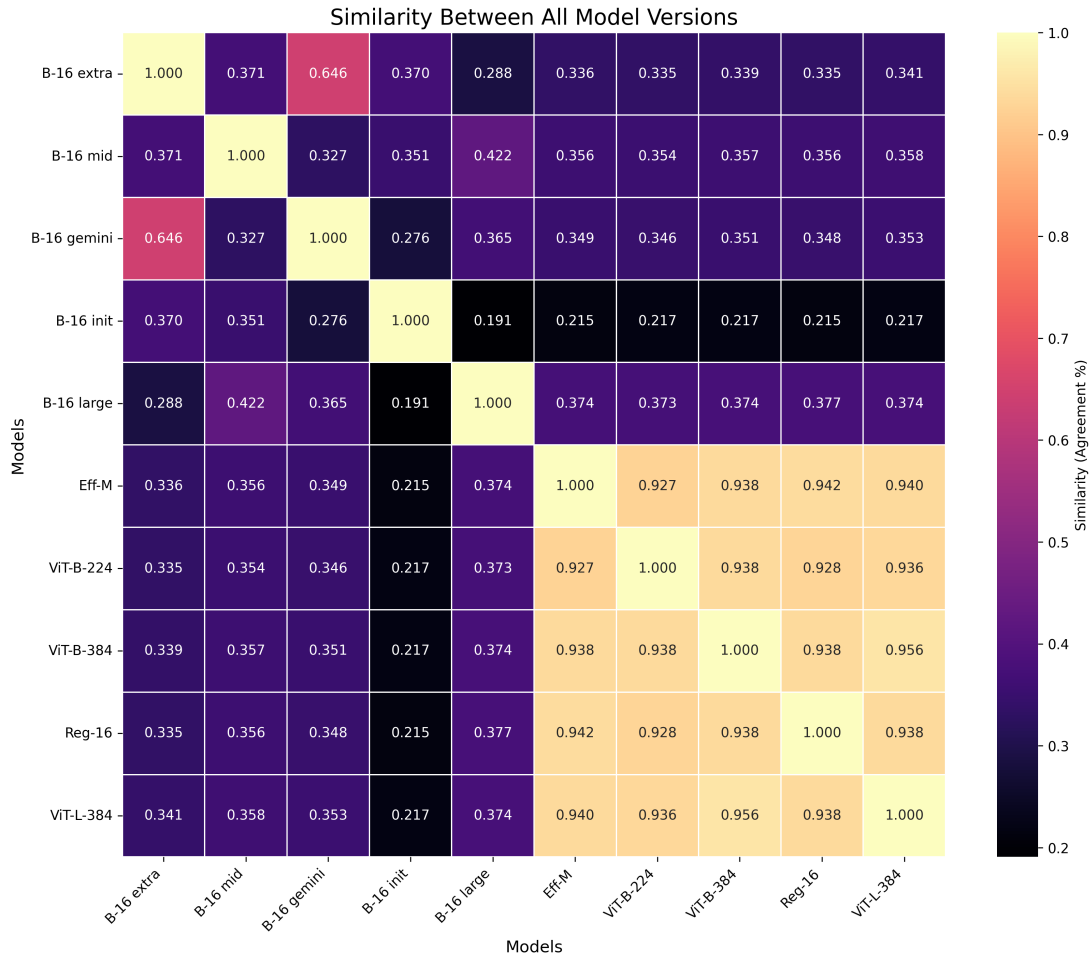


Figure 5.2 Similarity of predictions for CLIP (first five) and image-based (last five) models on the unlabeled collection (649,508 pages).

The low agreement on unlabeled pages contrasts with the high scores obtained by CLIP on annotated samples. One hypothesis is that hybrid models need more fine-grained category descriptions; for example, `DRAW` currently merges maps, illustrations, and sketches and could benefit from more specific descriptions within the same label. Another possible explanation is overfitting to previously seen pages, which would inflate test-set estimates.

Overall, hybrid models require substantially more dataset preparation to compete with image-only approaches in practice. We therefore released fine-tuned CLIP variants mainly for illustrative purposes; they were generally less useful for archival management than the image-only architectures.

5.3.1 Analysis of Common Mistakes

Across all models, errors are concentrated in a small number of confusions rather than being uniformly distributed. The dominant error source is the distinction between generic `TEXT` and typeset/transcribed text (`TEXT_T`). A secondary confusion involves separating drawings (`DRAW`) from drawings embedded in tabular layouts (`DRAW_L`) and other line-dominated categories.

The smallest CNN baseline (EfficientNet-V2-S) struggles most with the `TEXT` ambiguity: it correctly classifies 85% of `TEXT` samples and misclassifies 13% as `TEXT_T`. Scaling up reduces this confusion; EfficientNet-V2-L improves `TEXT` accuracy to 93% and reduces the error to 5.6%.

RegNetY-16GF performs best among the efficient models, reaching 94% accuracy on `TEXT` with only 5.1% confusion. It also reaches 99% accuracy on `DRAW` (EfficientNet-V2-S reaches 97%), suggesting that CNNs are sharper at edge- and structure-driven distinctions such as `DRAW` vs. `DRAW_L`.

Among Transformers, DiT-Large (pretrained for documents) still struggles more with `TEXT` vs. `TEXT_T` than the best CNNs, achieving 91% accuracy on `TEXT`. More generally, Transformer variants appear slightly “fuzzier” on purely visual structural distinctions: DiT-Base-RVL reaches 95% on `DRAW` and confuses 3.4% with other line/drawing classes; DiT-Large-RVL similarly reaches 95%.

CNNs (RegNetY / EfficientNet):

- **Strength and efficiency:** Strong edge/structure detection (high `DRAW` accuracy). RegNetY-16GF is a practical “sweet spot,” matching or beating much larger models.
- **Scaling behavior:** Increasing input resolution from 300 to 384 pixels per side (S→M) substantially improves fine-grained text distinctions (85%→92% accuracy on `TEXT`).

Transformers (DiT / ViT):

- **Strength:** Strong, consistent performance, but high parameter counts (300M+) are typically needed to compete with medium-sized CNNs (approximately 80M parameters).
- **Weakness:** Slightly weaker separation of visually similar structural categories (e.g., DRAW vs. DRAW_L) and less efficient resolution of the TEXT ambiguity.

Overall, if deployment efficiency is a priority, RegNetY-16GF is the strongest choice: it offers the highest accuracy (99.16%) with a fraction of the parameters of large Transformer models and performs best on the hardest distinction in our dataset (TEXT vs. TEXT_T).

5.4 Labeled collections from Prague and Brno

When we defined the five best image-only models, inference runs were performed for the whole Brno and Prague collections of page scans. After Top-3 predictions from all five models (EffN2-M, ViT-B224, ViT-B384, RegNY-16GF, ViT-L384) were obtained, an average of class scores from all models was computed for each category to derive Top-3 labels per input image file. Thus, Table 5.5 and Figure 5.3 show statistics for the Top-1 guess of the averaged predictions.

| Category | Brno IAB | Ambiguous | Prague IAP | Ambiguous |
|--------------------|-----------|-----------------|------------|----------------|
| DRAW | 138,643 | 15,147 (10.9%) | 128,364 | 15,504 (12.1%) |
| DRAW_L | 7,782 | 3,978 (51.1%) | 50,067 | 9,032 (18.0%) |
| LINE_HW | 7,696 | 4,347 (56.5%) | 15,285 | 5,375 (35.2%) |
| LINE_P | 156,836 | 25,055 (16.0%) | 73,457 | 5,828 (7.9%) |
| LINE_T | 19,220 | 8,688 (45.2%) | 44,167 | 8,987 (20.3%) |
| PHOTO | 112,704 | 8,913 (7.9%) | 119,767 | 4,788 (4.0%) |
| PHOTO_L | 1,163 | 500 (43.0%) | 7,239 | 1,790 (24.7%) |
| TEXT | 24,249 | 8,091 (33.4%) | 37,254 | 11,409 (30.6%) |
| TEXT_HW | 9,287 | 4,024 (43.3%) | 9,406 | 2,219 (23.6%) |
| TEXT_P | 96,155 | 15,815 (16.4%) | 87,938 | 9,455 (10.8%) |
| TEXT_T | 56,243 | 13,841 (24.6%) | 78,215 | 16,819 (21.5%) |
| Year range | 1937–2024 | — | 1920–2018 | — |
| Total pages | 629,978 | 108,399 (17.2%) | 651,159 | 91,206 (14.0%) |

Table 5.5 Labeled page counts by category in the Prague and Brno archives (whole collection’s best guess of 5 fine-tuned models’ averaged Top-3 predictions). “Ambiguous” denotes pages with a Top-1 averaged class score < 0.9.

Table 5.5 summarizes the resulting labeled page counts in both collections, where the volume is concentrated in a small number of high-level document types: printed tables, drawings, photos, and text categories (printed and typewritten). IAB is dominated by printed tables, whereas IAP contains substantially more tabulated drawings (schemes) and typewritten texts.

The highest ambiguity rates appear in visually “borderline” sub-classes with weak cues or frequent overlap with neighboring categories: handwritten tables and tabulated drawings (schemes) exceed 50% ambiguity in IAB, and typewritten tables, mixed texts, handwritten texts, and tabulated photos remain consistently ambiguous in both archives. Practically, this suggests that some portion of the “uncertainty” is likely due to true multi-label structure rather than pure model error.

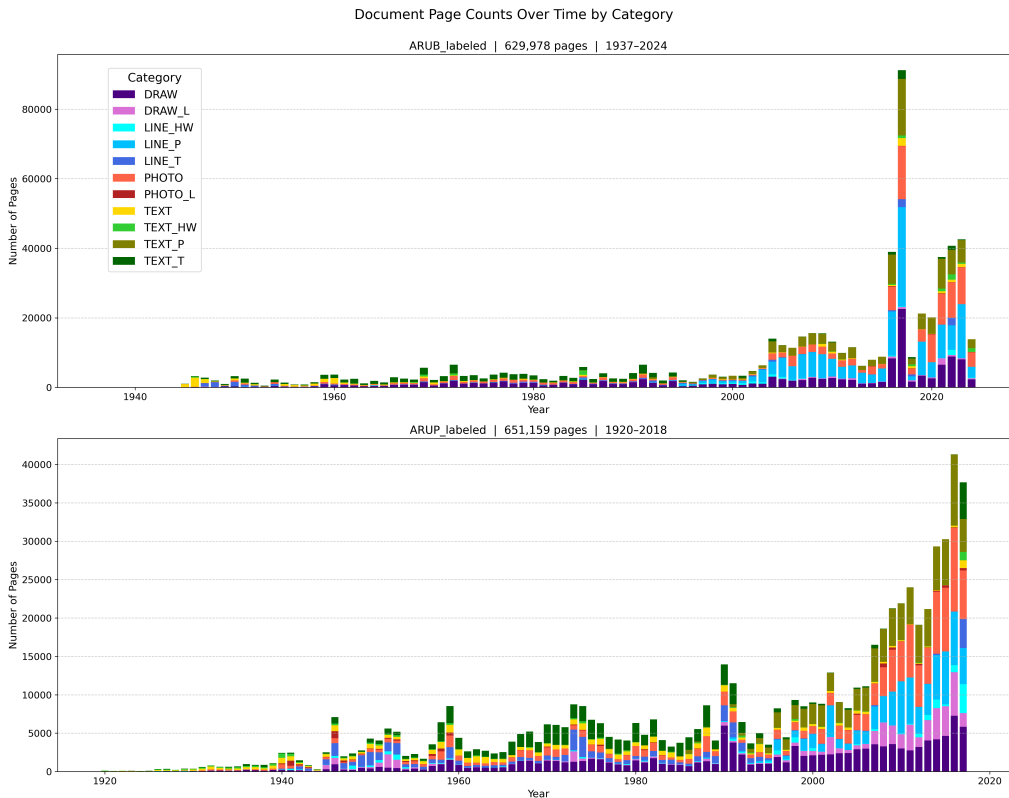


Figure 5.3 Stacked annual counts for Prague and Brno data from IAP and IAB: Categorized page-scan counts over time in the archives of scanned documents (best guess of 5 fine-tuned models’ averaged Top-3 predictions)

Both archives in Figure 5.3 show relatively low and stable activity, followed by a broad increase from the 1990s onward and a sharp expansion since the 2000s, where printed tables, photos, and printed texts drive most of the growth.

Conclusion

This thesis addressed the need for automated page-image classification in heterogeneous historical archives. A reliable page classifier enables content-specific downstream processing—including OCR, table extraction, and graphic analysis—without applying every processing pipeline to every page.

After characterizing the challenges of our dataset—visual defects, skew, and mixed content types (Introduction and Chapter 1)—we developed a subset-selection algorithm based on randomized periodic indexing (Chapter 2). We then demonstrated the limitations of existing document layout analysis tools (Chapter 3) and evaluated a lightweight RFC baseline, which achieved only $\approx 75\%$ accuracy (Section 3.1.2). This result is consistent with surveys reporting the limitations of hand-crafted features for document understanding [Liu+21]. Following these low-compute experiments, we defined and annotated eleven categories (Section 2.1), reaching nearly 50,000 labeled pages in the final dataset version.

Fine-tuning modern CNNs (RegNetY [Rad+20] and EfficientNetV2 [TL21] families) markedly improved performance to $\approx 97.9\text{--}99.1\%$ accuracy. Fine-tuned Vision Transformer (ViT) [Dos+20] and Document Image Transformer (DiT) [Li+22] models consistently matched the CNNs, achieving $\approx 98.5\text{--}99.1\%$ Top-1 accuracy (Table 5.1). We also showed that CLIP models [Rad+21] can reach $\approx 99\%$ classification accuracy after fine-tuning, although their inter-model agreement remained low.

Based on this empirical evaluation, **RegNetY-16GF (224px)** was selected for deployment due to its balance of accuracy, generalization, and computational cost in an offline archival setting. In addition, **ViT-Large (384px)** was selected as a more resource-demanding alternative among ViT models. Other ViT variants, **CLIP-ViT-B/16 (224px)**, and **EfficientNetV2-M (384px)** were released as examples of models that perform above the accuracy–model-size trendline.

The final system is implemented in PyTorch and HuggingFace Transformers (Chapter 4). It provides modular configuration, a CLI, and cross-platform scripts to support integration into existing archival pipelines (Chapter 5).

The released tool set directly addresses the previously identified gap: an open-source, content-based page-classification tool suitable for standard desktop hardware, cross-platform deployment, and practical use by archivists.

Contributions

- Analyzed archival page-image characteristics and documented failure modes of existing DLA tools (e.g., DeepDoctection) on the historical-archives data.

- Designed, annotated, and published the dataset of labeled pages [LK25]; and developed and released the accompanying software solution [Lut+25] in accordance with the FAIR principles.
- Released eight fine-tuned CLIP model-weight variants in the HuggingFace repository, accompanied by category-description sets in a separate GitHub folder.
- Published three medium-sized fine-tuned ViT models, two variants of EfficientNetV2-M, and one RegNetY-16GF model—all exceeding $\approx 98.79\%$ accuracy—in a separate HuggingFace repository.
- Identified RegNetY-16GF as the most effective model for this task by rigorously fine-tuning and comparing deep CNNs and transformer architectures. All image-only model versions above the accuracy–model-size trendline were released in the same repository.
- Provided deployment guidance for large-scale, on-premises archival processing, including a configurable pipeline and an extensible category taxonomy [Lut+25].
- Showed that a compact CNN (EfficientNetV2-M) can outperform its larger counterpart (EfficientNetV2-L), and that RegNetY-16GF outperforms the 12GF and 64GF variants, making it a practical and efficient model for deployment.

Future work

- Explore architectural optimizations to further improve efficiency and performance.
- Integrate the classifier into broader digital-archive management frameworks; although developed for archaeological archives, our data characteristics overlap with many archival and library collections.
- Expand the category taxonomy to cover additional document types (e.g., Table 2.3).
- Investigate advanced fine-tuning using predicted and user-refined annotations to improve utility and adaptability.

By delivering near-perfect classification accuracy and a practical deployment framework, this thesis reduces manual effort in historical-document workflows and supports digital humanities research and mass digitization initiatives [Nik+22; Liu+21].

LLM assisted copy editing

This thesis was written with assistance from LLMs. Early drafts (factual bullet points and rough paragraphs) were provided to Gemini 2.5 and GPT-4 to generate a more fluent narrative.

These AI-assisted edits primarily affected wording, structure, and formatting. I reviewed and revised the resulting text to ensure that it accurately reflects our work and that no incorrect assumptions remained.

In particular, Chapter 4 was initially generated and then manually post-edited based on the GitHub project materials (README, configuration file, Python code, and OS-specific data-processing scripts). Because the code base and documentation already contained user-oriented system descriptions, the generated text served as a solid starting point for the system overview.

Chapter 1 was written manually from the beginning and only then stylized into a scientific-article format. Chapters 3 and 5 were generated from concise paragraph outlines and then manually post-edited to remove inaccuracies.

The Introduction was based on a Deep Research run using a section skeleton and short bullet points. When most chapters were complete and the technical details had been added to the LLMs-generated drafts, the Conclusion was composed from narrative bullet points and the preceding thesis content. Some sources suggested by LLMs were then manually verified and cited in the introduction or conclusion.

In later stages, the models were asked to produce a coherent overview of the thesis and the relevant materials; therefore, the requests focused on language and narrative composition rather than technical content.

Finally, during manual writing and post-editing, I used the free version of Grammarly for grammar and spelling checks. In addition, Writefull (integrated in Overleaf) was used to align the text with a scientific writing style. Similarly, Overleaf's AI Assistant was used for light, medium, and heavy refinements of text (e.g., removing repetitions, fixing sentence structures, aligning hyphen formats, shortening of paragraphs), and searching for several relevant works to include and cite in the thesis manuscript.

Although many edits were made during the initial drafting, additional refinements were applied throughout the thesis after incorporating the LLM outputs.

Bibliography

- [BZK22] BEYER, L.; ZHAI, X.; KOLESNIKOV, A. Better plain vit baselines for imagenet-1k. *arXiv preprint arXiv:2205.01580*. 2022.
- [BBC23] BISWAS, B.; BHATTACHARYA, U.; CHAUDHURI, B. B. Document image skew detection and correction: A survey. 2023.
- [Bre01] BREIMAN, L. Random forests. *Machine learning*. 2001, vol. 45, pp. 5–32.
- [Dos+20] DOSOVITSKIY, A.; BEYER, L.; KOLESNIKOV, A.; WEISSENBORN, D.; ZHAI, X.; UNTERTHINER, T.; DEHGHANI, M.; MINDERER, M.; HEIGOLD, G.; GELLY, S., et al. An image is worth 16x16 words: Transformers for image recognition at scale. *arXiv preprint arXiv:2010.11929*. 2020.
- [HSD73] HARALICK, R. M.; SHANMUGAM, K.; DINSTEN, I. H. Textural features for image classification. *IEEE Transactions on systems, man, and cybernetics*. 1973, no. 6, pp. 610–621.
- [HUD15] HARLEY, A. W.; UFKES, A.; DERPANIS, K. G. Evaluation of Deep Convolutional Nets for Document Image Classification and Retrieval. In: *International Conference on Document Analysis and Recognition (ICDAR)*. 2015.
- [HD19] HENDRYCKS, D.; DIETTERICH, T. Benchmarking neural network robustness to common corruptions and perturbations. In: *International Conference on Learning Representations*. 2019.
- [Hu62] HU, M.-K. Visual pattern recognition by moment invariants. *IRE transactions on information theory*. 1962, vol. 8, no. 2, pp. 179–187.
- [Lew+06] LEWIS, D.; AGAM, G.; ARGAMON, S.; FRIEDER, O.; GROSSMAN, D.; HEARD, J. Building a test collection for complex document information processing. In: *Proceedings of the 29th annual international ACM SIGIR conference on Research and development in information retrieval*. 2006, pp. 665–666.
- [Li+22] LI, J.; XU, Y.; LV, T.; CUI, L.; ZHANG, C.; WEI, F. Dit: Self-supervised pre-training for document image transformer. In: *Proceedings of the 30th ACM international conference on multimedia*. 2022, pp. 3530–3539.
- [Liu+21] LIU, L.; WANG, Z.; QIU, T.; CHEN, Q.; LU, Y.; SUEN, C. Y. Document image classification: Progress over two decades. *Neurocomputing*. 2021, vol. 453, pp. 223–240.
- [LK25] LUTSAI, K.; KRIVANKOVA, D. *Annotated page images from the (archaeological) historical archive*. 2025. Version 1.0.0. Available also from: <http://hdl.handle.net/20.500.12800/1-5959>.

- [Lut+25] LUTSAI, K.; STRANAK, P.; NOVAK, D.; KRIVANKOVA, D. *ATRIUM's page classifier: Classification of historical page images using fine-tuned ViT*. 2025. Version 1.0.0. Available also from: <https://github.com/ufal/atrium-page-classification>.
- [Nik+22] NIKOLAIDOU, K.; SEURET, M.; MOKAYED, H.; LIWICKI, M. A survey of historical document image datasets. *International Journal on Document Analysis and Recognition (IJDAR)*. 2022, vol. 25, no. 4, pp. 305–338.
- [Pas19] PASZKE, A. Pytorch: An imperative style, high-performance deep learning library. *arXiv preprint arXiv:1912.01703*. 2019.
- [Rad+21] RADFORD, A.; KIM, J. W.; HALLACY, C.; RAMESH, A.; GOH, G.; AGARWAL, S.; SASTRY, G.; ASKELL, A.; MISHKIN, P.; CLARK, J., et al. Learning transferable visual models from natural language supervision. In: *International conference on machine learning*. Pmlr, 2021, pp. 8748–8763.
- [Rad+20] RADOSAVOVIC, I.; KOSARAJU, R. P.; GIRSHICK, R.; HE, K.; DOLLÁR, P. Designing network design spaces. In: *Proceedings of the IEEE/CVF conference on computer vision and pattern recognition*. 2020, pp. 10428–10436.
- [Rid+21] RIDNIK, T.; BEN-BARUCH, E.; NOY, A.; ZELNIK-MANOR, L. Imagenet-21k pretraining for the masses. *arXiv preprint arXiv:2104.10972*. 2021.
- [Smi07a] SMITH, R. An Overview of the Tesseract OCR Engine. In: *ICDAR '07: Proceedings of the Ninth International Conference on Document Analysis and Recognition*. Washington, DC, USA: IEEE Computer Society, 2007, pp. 629–633. ISBN 0-7695-2822-8. Available also from: <https://storage.googleapis.com/pub-tools-public-publication-data/pdf/33418.pdf>.
- [Smi07b] SMITH, R. An overview of the Tesseract OCR engine. In: *Ninth international conference on document analysis and recognition (ICDAR 2007)*. IEEE, 2007, vol. 2, pp. 629–633.
- [TL19] TAN, M.; LE, Q. Efficientnet: Rethinking model scaling for convolutional neural networks. In: *International conference on machine learning*. PMLR, 2019, pp. 6105–6114.
- [TL21] TAN, M.; LE, Q. EfficientNetV2: Smaller Models and Faster Training. In: *International Conference on Machine Learning*. PMLR, 2021.
- [Tou+21] TOUVRON, H.; CORD, M.; DOUZE, M.; MASSA, F.; SABLAYROLLES, A.; JÉGOU, H. Training data-efficient image transformers & distillation through attention. In: *International Conference on Machine Learning*. PMLR, 2021.

- [Wol+19] WOLF, T.; DEBUT, L.; SANH, V.; CHAUMOND, J.; DELANGUE, C.; MOI, A.; CISTAC, P.; RAULT, T.; LOUF, R.; FUNTOWICZ, M., et al. Huggingface’s transformers: State-of-the-art natural language processing. *arXiv preprint arXiv:1910.03771*. 2019.
- [Xu+23] XU, H.; XIE, S.; TAN, X. E.; HUANG, P.-Y.; HOWES, R.; SHARMA, V.; LI, S.-W.; GHOSH, G.; ZETTLEMOYER, L.; FEICHTENHOFER, C. Demystifying clip data. *arXiv preprint arXiv:2309.16671*. 2023.
- [Xu+20] XU, Y.; LI, M.; CUI, L.; HUANG, S.; WEI, F.; ZHOU, M. Layoutlm: Pre-training of text and layout for document image understanding. In: *Proceedings of the 26th ACM SIGKDD international conference on knowledge discovery & data mining*. 2020, pp. 1192–1200.
- [You11] YOUSEFI, J. Image binarization using Otsu thresholding algorithm. *Ontario, Canada: University of Guelph*. 2011, vol. 10, p. 9.
- [ZTY19] ZHONG, X.; TANG, J.; YEPES, A. J. PubLayNet: Largest Dataset Ever for Document Layout Analysis. In: *International Conference on Document Analysis and Recognition (ICDAR)*. 2019.

List of Figures

| | | |
|-----|---|----|
| 1 | One of the oldest and one of the newest pages in our collection. Both contain graphical objects of interest, but the modern page is annotated with a structured data format (table). | 8 |
| 2 | Prague and Brno data from IAP and IAB (unlabeled): Page-scan counts over time in the archives of scanned documents | 9 |
| 3 | Page examples derived from the same collection that differ substantially in size, content, and paper condition. | 10 |
| 4 | Examples of scans with different physical sizes from our annotated subset | 11 |
| 5 | Pages with background artifacts that degrade OCR performance . . | 12 |
| 1.1 | Examples of content defects that reduce readability. | 16 |
| 1.2 | Defects and physical page features transferred to digitized scans as transparent or black fragments. | 17 |
| 1.3 | Variability of handwritten font sizes based on the format of physical pages | 18 |
| 1.4 | DLA application samples | 21 |
| 1.5 | DD mistakes on pages with tables and figures | 22 |
| 1.6 | DD mistakes on pages with maps and drawings | 23 |
| 2.1 | RFC (Section 3.1.2) confusion matrices of early annotation schemes (fewer than 3,000 samples in total) | 26 |
| 2.2 | Proportions of categories in train, development, and test subsets (columns) across five folds (rows) on a timescale of document creation dates. | 31 |
| 2.3 | Distribution of categories in the final annotated dataset (Dataset 3) based on the document creation year | 33 |
| 2.4 | Distribution of categories in the performance test subset (samples not included in training subsets of the five cross-validation folds), based on the document creation year. | 34 |
| 2.5 | Temporal distributions of categories across annotation versions (Datasets 0, 2, and 3), based on the document creation year | 35 |
| 2.6 | Confusion matrices of Top-1 predictions for ViT-Base at 224×224 resolution, fine-tuned on successive dataset versions and evaluated on the refined test set (before the final test set was created). Accuracy scores are not included. Dataset numbers refer to the versions in Table 2.4. | 36 |

| | | |
|-----|--|----|
| 3.1 | Low-compute models compared on the same data in cross-fold validation. Left: data-provider annotation. Right: our proposed annotation scheme. | 38 |
| 3.2 | Zero-shot CLIP models comparison of classification accuracy per category descriptions set plus averaged text features variants of all four base models | 45 |
| 3.3 | Comparison of fine-tuned CLIP models by classification accuracy across category description sets (label set names in alphabetical order). “Average” denotes averaged text features. | 45 |
| 3.4 | CLIP zero-shot confusion matrices (averaged text features) | 46 |
| 3.5 | CLIP best models (ViT-B/16 variations) confusion matrices, seven epochs | 47 |
| 3.6 | Category distribution in the expanded test dataset (all non-training samples from the first-fold split, random seed 420; 14,162 pages). | 48 |
| 3.7 | Combined zero-shot and fine-tuned CLIP models: comparison of classification accuracy across category description sets on the standard test dataset (5,449 pages). | 49 |
| 3.8 | Combined zero-shot and fine-tuned CLIP models: comparison of classification accuracy across category description sets on an expanded test dataset (all non-training samples from the first-fold split, random seed 420; 14,162 pages). | 49 |
| 4.1 | System overview for the image-only (CNNs and Transformer) variants | 50 |
| 4.2 | Model overview for the hybrid CLIP variant | 51 |
| 4.3 | Example JSON response from the /predict endpoint (model v5.3, Top-3 predictions) | 54 |
| 4.4 | Model inference use-case: input PDF is parsed into a folder of pages, then sorted into category-specific subdirectories | 56 |
| 5.1 | Accuracy vs. parameter count across evaluated models. Models above the trendline deliver superior efficiency. | 58 |
| 5.2 | Similarity of predictions for CLIP (first five) and image-based (last five) models on the unlabeled collection (649,508 pages). | 63 |
| 5.3 | Stacked annual counts for Prague and Brno data from IAP and IAB: Categorized page-scan counts over time in the archives of scanned documents (best guess of 5 fine-tuned models’ averaged Top-3 predictions) | 66 |
| A.1 | Water damage resulting in blur and overlapping ink | 81 |
| A.2 | Corner-hole damage exposing paper fibers & mixed content (yellowish paper texture) | 82 |

| | | |
|------|--|-----|
| A.3 | Gray-background artifacts and table/drawing elements | 83 |
| A.4 | Stamp annotations and faded ink impressions | 84 |
| A.5 | Bleed-through artifacts on thin paper | 84 |
| A.6 | Skewed table prints and alignment issues | 85 |
| A.7 | Edgehole damage and paper tearing | 86 |
| A.8 | Large drawn tables and grained-paper scans | 87 |
| A.9 | Scans from thick volumes and journals | 88 |
| A.10 | Typewritten text corrections | 88 |
| A.11 | Tables with color artifacts (e.g., scanning noise, pen stains, and paper discoloration) | 89 |
| A.12 | Mixed-text pages and scribbles | 89 |
| | | |
| B.1 | DD attempt on a newspaper page with drawings | 90 |
| B.2 | DD attempt on a table | 91 |
| B.3 | DD attempt on a plain text | 91 |
| B.4 | DD attempt on a photo with text | 92 |
| B.5 | DD mistakes on pages with photos | 92 |
| B.6 | DD mistakes on pages with drawings | 93 |
| B.7 | DD mistakes on pages with tables | 93 |
| B.8 | DD mistakes on pages with plain texts | 94 |
| | | |
| C.1 | Label DRAW examples | 96 |
| C.2 | Label DRAW_L examples | 97 |
| C.3 | Label LINE_HW examples | 98 |
| C.4 | Label LINE_P examples | 99 |
| C.5 | Label LINE_T examples | 100 |
| C.6 | Label PHOTO examples | 101 |
| C.7 | Label PHOTO_L examples | 102 |
| C.8 | Label TEXT examples | 103 |
| C.9 | Label TEXT_HW examples | 104 |
| C.10 | Label TEXT_P examples | 105 |
| C.11 | Label TEXT_T examples | 106 |
| | | |
| G.1 | EfficientNetV2 confusion matrices, three epochs | 123 |
| G.2 | RegNetY confusion matrices, three epochs | 123 |
| G.3 | DiT confusion matrices, three epochs | 124 |
| G.4 | ViT confusion matrices, three epochs | 124 |
| G.5 | Finetuned CLIP best models in each base model group confusion matrices, seven epochs | 125 |

List of Tables

| | | |
|-----|---|----|
| 1.1 | Classification categories based on detected content features and line complexity. No ground-truth labels existed for this scheme. | 20 |
| 1.2 | Category definitions initially designed by the data provider, inspired by the previously observed DLA attempts | 24 |
| 1.3 | Overview of the revised intermediate category definitions derived from the initial provider’s proposal | 25 |
| 2.1 | Overview of categories used in the fine-tuned models; unless otherwise specified, each category includes pages primarily dominated by the described content type. | 27 |
| 2.2 | Coverage of data feature variability, summarizing the mapping between content type and writing mode. | 29 |
| 2.3 | Expanded label scheme illustrating coverage of data variability (analytical only). | 29 |
| 2.4 | Category distribution across the models’ dataset partitions. The set of eleven categories tabulated here refers to the final labels scheme described in Section 2.1 | 33 |
| 3.1 | Specifications of EfficientNetV2 and RegNetY Models | 40 |
| 3.2 | Specifications of DiT and ViT models | 41 |
| 3.3 | Consolidated model performance ranking (Top-1 accuracy) | 42 |
| 3.4 | Specifications of OpenAI’s CLIP-ViT models | 43 |
| 3.5 | Summary of CLIP category description sets. “Rev.” denotes the revision (model version) fine-tuned to a specific label set of text features. | 44 |
| 4.1 | Summary of configuration settings in <code>config.txt</code> sections | 52 |
| 4.2 | Selected CLI options in <code>run.py</code> (representative subset) | 53 |
| 4.3 | REST API endpoints exposed by the web service | 54 |
| 5.1 | Top-1 accuracy and model complexity for all evaluated architectures. <i>Italic</i> : most efficient; bold : most accurate (and most efficient) per model type. | 59 |
| 5.2 | NVIDIA GPUs Specifications Comparison | 60 |
| 5.3 | Average training/evaluation throughput (batches of 11-16 samples per second) across NVIDIA GPU types and model size (parameters) ranges. Values are reported as <i>train / eval</i> pairs of the processing speed measurements. | 61 |

| | | |
|-----|--|-----|
| 5.4 | Average efficiency (accuracy increase per hour) across NVIDIA GPU types and model size (parameters) ranges. | 61 |
| 5.5 | Labeled page counts by category in the Prague and Brno archives (whole collection’s best guess of 5 fine-tuned models’ averaged Top-3 predictions). “Ambiguous” denotes pages with a Top-1 averaged class score < 0.9. | 65 |
| D.1 | Initial Document Classification Labels | 107 |
| D.2 | Short Document Classification Labels | 107 |
| D.3 | Minimal Document Classification Labels | 108 |
| D.4 | Page-based Document Classification Labels (Proposed by GPT Deep Research based on Chapter 1 content) | 108 |
| D.5 | Cropped out word “page” from Table D.4 — Document Classification Labels | 109 |
| D.6 | Long Document Classification Labels (Proposed by Gemini Deep Research based on Chapter 1 content) | 110 |
| D.7 | Comprehensive Document Classification Labels with Examples . . . | 111 |
| D.8 | Enhanced Document Classification Labels with Detailed Annotations | 112 |
| D.9 | Extended Document Classification Labels | 113 |
| F.1 | CLI options for <code>run.py</code> | 122 |

List of Abbreviations

AI Artificial Intelligence

API Application Programming Interface

CLI Command-line Interface

CLIP Contrastive Language-Image Pretraining (CLIP — is designed to understand the connection between images and text. The models achieve this by mapping image and text embeddings into the same vector space, allowing for comparison and similarity assessment between the two modalities.)

CNN Convolutional Neural Network (CNN — is a type of deep learning model particularly well-suited for analyzing visual data like images and videos. It excels at identifying patterns and features within these images, making it a cornerstone for computer vision tasks such as image recognition and object detection.)

CPU Central Processing Unit

CSV Comma-separated Values

CUDA Compute Unified Device Architecture (CUDA — is a parallel computing platform and programming model developed by NVIDIA. It allows software developers to use NVIDIA GPUs for general-purpose processing, rather than just graphics rendering.)

DD DeepDoctection (DeepDoctection — is a Python library that orchestrates Scan and PDF document layout analysis and extraction for RAG (Retrieval-Augmented Generation)

DiT Document Image Transformer (DiT — is an image transformer pretrained on large-scale unlabeled document images. It learns to predict the missing visual tokens from a corrupted input image. The pretrained DiT model can be used as a backbone in other models for visual document tasks like document image classification and table detection.)

DLA Document Layout Analysis (DLA — is a field focused on automatically identifying and categorizing different elements within a document's visual structure using computer vision and machine learning.)

e.g., for example (exempli gratia)

GPU Graphics Processing Unit

HTML HyperText Markup Language (HTML — is the standard markup language for structuring content on the Web.)

HTTP Hypertext Transfer Protocol (HTTP — is the application-layer protocol used for communication on the Web.)

IAB Institute of Archaeology of the Czech Academy of Sciences in Brno (Archeologický ústav AV ČR Brno v. v. i. (ARÚB), IAB — is comprised of Czech and foreign researchers, technicians and service employees who are connected by a professional interest in investigating the history of humankind from the Paleolithic to the Middle Ages.)

IAP Institute of Archaeology of the Czech Academy of Sciences in Prague (Archeologický ústav AV ČR Praha v. v. i. (ARÚP), IAP — is a leading research institution dedicated to the study of the human past in its entirety, focusing on the Czech Republic and abroad. It is part of the Czech Academy of Sciences and is known for its comprehensive approach to archaeological research, encompassing fieldwork, analysis of material remains, and the development of general models of past societies)

IFAL Institute of Formal and Applied Linguistics (Ústav formální a aplikované lingvistiky (ÚFAL), IFAL — is a research department at Charles University in Prague, Czech Republic. It focuses on language technologies, computational linguistics, and machine learning.)

JPEG Joint Photographic Experts Group

JSON JavaScript Object Notation (JSON — is a lightweight data-interchange format, commonly used for APIs and configuration.)

k-NN k-nearest neighbors (model type)

LDA Latent Dirichlet Analysis (model type)

LLM Large Language Model (LLM — is a type of artificial intelligence (AI) program, deep learning model trained on massive amounts of text data. LLMs excel at understanding, generating, and manipulating human language, enabling them to perform various tasks like text generation, translation, question answering, etc.)

MIT Licensing policy created in Massachusetts Institute of Technology (MIT license — is a permissive free software license, widely used in the open-source

community. It allows for the use, modification, and distribution of software, including commercial use, with minimal restrictions.)

OCR Optical Character Recognition (OCR — is a technology that converts images of text into machine-readable text.)

PDF Portable Document File

PNG Portable Network Graphics

REST Representational State Transfer (REST — is an architectural style for designing networked applications; a API that follows these constraints is often called a REST API.)

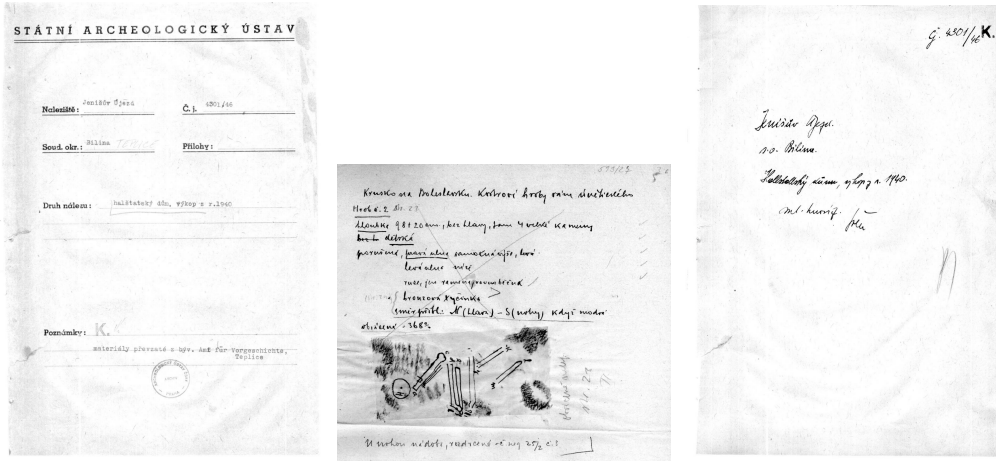
RFC Random Forest Classifier (RFC — is a powerful ensemble learning method that combines multiple decision trees to make predictions. It's a versatile tool used for both classification and regression tasks, known for its accuracy, robustness, and ability to handle large datasets with many features.)

SVM Support Vector Machine (model type)

TIFF Tagged Image File Format

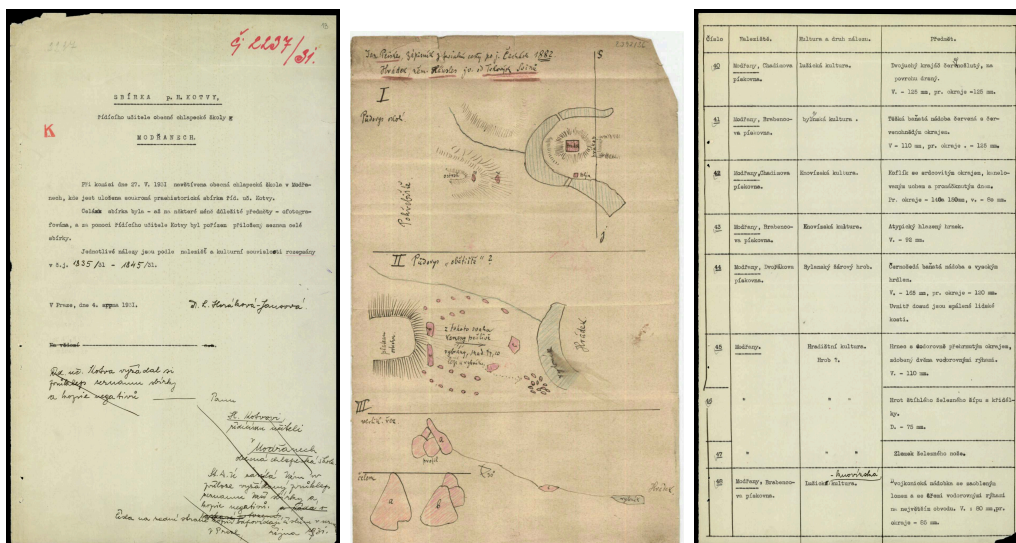
ViT Vision Transformer (ViT — is a type of neural network architecture that applies the Transformer model, originally designed for natural language processing (NLP), to computer vision tasks, particularly image classification. The models break down an image into patches, treat them as a sequence of tokens, and process them using a Transformer encoder.)

A Source data pages



(a) Mixed text with round stamp, water-blurred
 (b) Handwritten text, water-damaged
 (c) Typewritten text blurred by water stains

Figure A.1 Water damage resulting in blur and overlapping ink



(a) Major text correction (b) Handwritten drawing (c) Typewritten table layout with a corner-hole tear next to a corner-hole with a torn corner-hole

Figure A.2 Corner-hole damage exposing paper fibers & mixed content (yellowish paper texture)

| | | | |
|-----------------|--------------|--------------------------------|-------|
| Průběh: | PRĚRUBENICE | SiO ₂ | 19,93 |
| Úroveň: | Země: | Fe ₂ O ₃ | 10,88 |
| Číslo vzorku: | C. číslo: 13 | FeO | 54,8 |
| Množství oxidů: | skuzky | Fe | 2,78 |
| | | MnO | 4,04 |
| | | CaO | 2,8 |
| | | MgO | 0,40 |
| | | CuO | |
| | | P ₂ O ₅ | 0,04 |
| | | Al ₂ O ₃ | 3,45 |
| Tabulka v %: | Zapomená: | | |

SPRIN 38

| | | | |
|-----------------|-------------|--------------------------------|-------|
| Průběh: | PRĚRUBENICE | SiO ₂ | 19,93 |
| Úroveň: | Země: | Fe ₂ O ₃ | 10,88 |
| Číslo vzorku: | C. číslo: 1 | FeO | 54,8 |
| Množství oxidů: | Muska | Fe | 2,78 |
| | | MnO | 4,04 |
| | | CaO | 2,8 |
| | | MgO | 0,40 |
| | | CuO | |
| | | P ₂ O ₅ | 0,04 |
| | | Al ₂ O ₃ | 3,45 |
| Tabulka v %: | Zapomená: | | |

SPRIN 12

| | | | |
|-----------------|-----------|--------------------------------|--|
| Průběh: | | SiO ₂ | |
| Úroveň: | Země: | Fe ₂ O ₃ | |
| Číslo vzorku: | C. číslo: | FeO | |
| Množství oxidů: | | Fe | |
| | | MnO | |
| | | CaO | |
| | | MgO | |
| | | CuO | |
| | | P ₂ O ₅ | |
| | | Al ₂ O ₃ | |
| Tabulka v %: | Zapomená: | | |

| | | | |
|-----------------|-------------|--------------------------------|-------|
| Průběh: | PRĚRUBENICE | SiO ₂ | 19,93 |
| Úroveň: | Země: | Fe ₂ O ₃ | 10,88 |
| Číslo vzorku: | C. číslo: 1 | FeO | 54,8 |
| Množství oxidů: | Muska | Fe | 2,78 |
| | | MnO | 4,04 |
| | | CaO | 2,8 |
| | | MgO | 0,40 |
| | | CuO | |
| | | P ₂ O ₅ | 0,04 |
| | | Al ₂ O ₃ | 3,45 |
| Tabulka v %: | Zapomená: | | |

(a) Handwritten comment on skewed color table

(b) Color-printed table, slight skew

OBĚDOVICE - "Na Požárce", výzkum 1997

Objekt: 089 Tabulka: 1

Čtverec: 267 Přesah do:

Rozměry: 1,74 x 1,5 m Hloubka: 0,14 m

Výplň: černohnědá, písčito-hlinitá

Datace: neolit

Keramika: A Mazanice: A Kov:

BN/drtidla: Š: Kameny:

Zv.kosti: Uhliky: Jiné:

Č.sáčků: 001, 038, 039

Poznámka:

OBĚDOVICE - "Na Požárce", výzkum 1997

Objekt: 090 Tabulka: 1

Čtverec: 267 Přesah do:

Rozměry: 3,38 x 1,96 m Hloubka: 0,16 m

Výplň: černohnědá, písčito-hlinitá

Datace: k. slezskoplatěnická, neolit

Keramika: A Mazanice: A Kov:

BN/drtidla: Š: Kameny:

Zv.kosti: Uhliky: A Jiné:

Č.sáčků: 002, 003, 004, 006, 007, 035, 036, 037,

Poznámka: v objektu příměs neolitické keramiky

(c) Typewritten table with visible skew

- 91 - 9. Seznam nálezů: sonda 2a-2d
Sezona 1974 - str. 31

| Průř. | Šířka | Sonda | Obj. | Detov. | torza | O b s a h |
|---------|-------|-------|---------|--------|-----------------|-----------------|
| šáček | | | KJ, | | | střepy |
| | | | v, | | | |
| | | | sděsti | | | |
| /74-72 | 72 | 2b | v.3, | 10.st. | 1 torzo (sle- | 0 |
| | | | povrch | | pené se 2 st- | |
| | | | plochy | | řepí) horní | |
| | | | šedinká | | části hrnce | |
| | | | | | "ker.slavník, | |
| | | | | | šáse" | |
| | | | | | (obr. 34:1) | |
| /74-117 | 117 | 2c | DWHZ, | r.995 | 0 | 1 okraj tuhová- |
| | | | 90/100- | | | ho hrnce Stř-MH |
| | | | -120cm | | | DH |
| /74-103 | 103 | 2d | v.3,50/ | 10.st. | 1 torzo (sle- | 0 |
| | | | /šed- | | peno se 2 st- | |
| | | | -osa 70 | | řepí) horní | |
| | | | cm | | části hrnce | |
| | | | | | Stř-MH | |
| | | | | | (obr. 32:1a, b) | |
| /74-139 | 139 | 2c | DWHZ, | r.995 | 1 torzo (sle- | 0 |
| | | | po pō- | | peno se 2 st- | |
| | | | trah | | řepí) horní | |
| | | | v.3 | | části hrnce | |
| | | | | | "ker.slavník, | |
| | | | | | šáse" | |
| | | | | | (obr. 35:1) | |
| /74-141 | 141 | 2c | v.3, | 10.st. | 0 | 1 velký střep |
| | | | prvních | | | s horní částí |
| | | | 20 cm | | | hrnce Stř-MH |
| | | | | | | (obr. 32:2) |

(d) Arrow marking on a skewed table page

Figure A.6 Skewed table prints and alignment issues

| číslo | popis | kultura | Velikost | číslo |
|-------|------------------------------|---------|------------|-------|
| 1 | Kopřivnáč, křem. | pařk. | Formica | 2445 |
| 2 | Plachý křem. (sp. křem.) | pařk. | " | 2446 |
| 3 | Křem. | noř. | " | 2444 |
| 4 | Návnatý mlát | noř. | " | |
| 5 | Plachý křem. | pařk. | Mozky | 2824 |
| 6 | Křem. křem. | noř. | " | 335 |
| 7 | Mlat | pařk. | " | 335 |
| 8 | Plachý křem. | noř. | " | 335 |
| 9 | Polovina plach. křem. | pařk. | " | 335 |
| 10 | Kopřivnáč, křem. | " | " | 335 |
| 11 | Sekernolák | šm. | Lučivá | 2910 |
| 12 | Plachý mlát | pařk. | Váňka | 2784 |
| 13 | Křem. | noř. | Váňka | 2787 |
| 14 | Křem. | " | Váňka | 2785 |
| 15 | " | " | St. Pávek | 2787 |
| 16 | Křem. kopřivnáč | pařk. | Peričan | 997 |
| 17 | Křem. z želez. želez. želez. | noř. | St. Pávek | 1819 |
| 18 | Křem. mlát | pařk. | Peričan | 996 |
| 19 | Plachý křem. | noř. | E. Hladec | 1133 |
| 20 | Mlat křem. | pařk. | " | " |
| 21 | Křem. pírka | noř. | Konopice | 1682 |
| 22 | Křem. | noř. | Váňka | " |
| 23 | Křem. | " | z d. domce | 1201 |
| 24 | " | " | " | 1201 |
| 25 | " malý | noř. | " | 1201 |
| 26 | " | noř. | " | " |
| 27 | " | " | " | 1201 |
| 28 | Křem. plachý | pařk. | " | " |
| 29 | " | " | " | " |
| 30 | glomok mlát | " | " | " |
| 31 | " | " | " | " |
| 32 | Plachý sekernolák | šm. | " | 4 |

(a) Table print with edgehole stains

Záznam o konání na Kouřimí ze dne 13. září 1957.

Pohřebiště na Kouřimí, objevené pomocí fosforové analýzy, vneslo do výzkumu novou problematiku. Pohřebiště leží v terénu s velmi složitou geologickou strukturou, neboť někde vystupuje skála až na povrch v přírodních lavách, jiné zase jsou ložky hlinité nebo štěrkové a situace komplikuje ještě středověký lom, jehož hranice byla zachycena na okraji pohřebiště. Hroby jsou vesměs normální situovány, při čemž některé z nich mají zřetelně ochráněná z místního kamene, někdy také jsou kamenné postavené kolem jako stěly buď v hlavě nebo v nohách. Některé hroby pak jsou přímo vytesány ve skále, jiné zase leží v těžkém terénu, v němž není možno dobře zachytit náhřeby jámy, který se jeví většinou až skoro u dna, poněvadž jsou v sasuťovém materiálu. Proto by se doporučovalo, aby si vedoucí výzkumu Dr. Šolle vyřídil podrobně ohledání terénu geologem /Dr. Želva, Dr. Prantl/, aby bylo zejména ve složitých případech jasno, co je přirozené a co je druhotné.

Hroby jsou na několika místech zjištěny ve zřetelné superpozici, a to buďto dva jedinci jsou dána do hroby, při čemž spodní pohřeb je poražen, jindy zase horní pohřeb bezohledně leže spodní starší, že jedná těžké je to v případech, kdy pohřebiště leží doslova v sasuťovém terénu a kdy jeho podloží netvoří ani rostlá skála ani původní hlína.

Nejzajímavější je, že byly objeveny prostorné jámové hroby, které zřetelně i superpozici jsou starší. Do této skupiny patří i hrob bojovníka /s. 25/ i bohatý šenkýř hrob /s. 106/ a hrob š. 96 a 110, které jsou v různých místech pohřebiště a zatím se zdá, že nejsou prostorově na sebe vázány. U všech těchto jmenovaných hrobů leží pohřby na dně těmž na skále, takže je obtížná situace jak pro zachování kostí, tak pro zachování a svednutí hrobového inventáře. Zvláště zřetelná, ale zároveň také problematická je situace u hrobu 110, kde hroby 79 a 80 jsou v superpozici nad velkým jámovým hrobem 110. Vědro ponechané na špalce sápuového materiálu patří hrobu 80, kdežto vědro na dně jámy patří k hrobu 110. Ze zachovaného profilu hranice mezi sektory i z charakteru okolního terénu je vidět, že původní zasypání jámového hrobu 110 bylo z velké části sasuťové. Při tom však u dna jámy na severní straně a na západní straně je několik kamenů, které se zdají tvořit vlastní hranici jámy a buď dojez, že snad

(b) Typewritten text adjacent to edgeholes

| | | | | |
|-------|-------------------|-------|-----------|------|
| 188 | Křem. | noř. | Utkanice | 2241 |
| 189 | glomok hroby | šm. | Lučivá | |
| 190 | hřib | hřib | Lučivá | |
| X 191 | " | noř. | Lučivá | |
| X 192 | hřib z domce | šm.? | Lučivá | |
| 193 | " | " | neznámá | |
| 200 | Sekernolák | noř. | Velanka | 2183 |
| 201 | glomok sekernolák | " | Velanka | 2270 |
| 202 | " | pařk. | Velanka | |
| 203 | glomok hroby | šm. | neznámá | |
| 204 | Sekernolák | pařk. | Lučivá | |
| 205 | Křem. | noř. | Lučivá | |
| 206 | glomok sekernolák | pařk. | Lučivá | |
| 207 | " | " | Lučivá | 4012 |
| 208 | Křem. plachý | pařk. | " | |
| 209 | Křem. | noř. | " | |
| 210 | glomok sekernolák | " | Lučivá | |
| 211 | glomok hřib | " | Lučivá | |
| 212 | glomok hřib | šm. | Chomutice | |
| 213 | glomok hřib | šm. | Velanka | |
| 214 | glomok hřib | šm. | neznámá | |
| 215 | glomok hřib | šm. | Chomutice | |

(c) Hole through table on yellowed paper

- 117 - 8J-2662/55

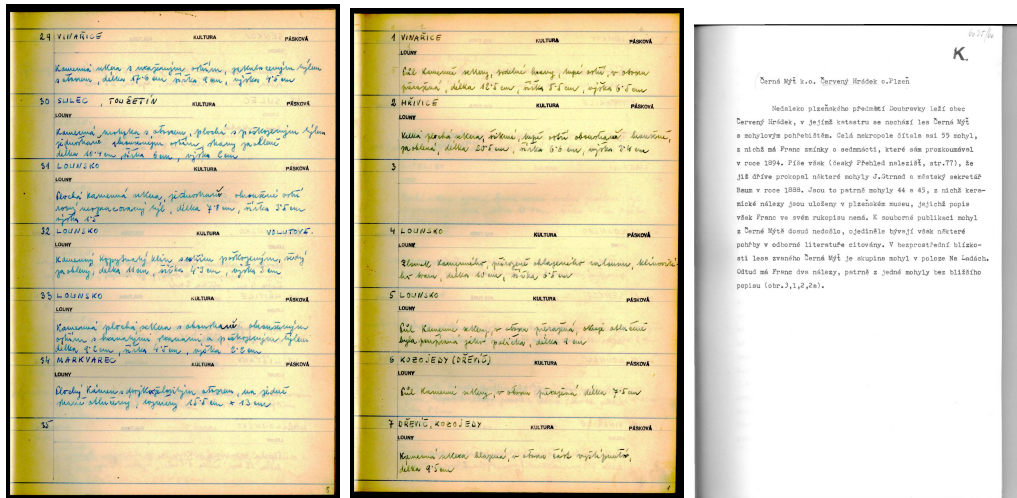
na akropoli, z nichž zůstaly vyhloubené základy pro poulnové polštáře, jež zůstávají zatím kouřimskou zvláštností, i když výzkum na hrudišti přívoreckém přinesl již doklady obdobné. V té době byl velkolepe upraven i prostor mezi akropoli a o. evněnou nářaží, vycvrcení cíle prostoty a rovnoměrně zložena nových sídlišť. Sídlištní a/1 vyúsit též prostor za jižní a jihozápadní stranou vašem okrajovým.

Pohřbívalo se nejen na výsunním pohřebišti u líbaše, určeném pro vrstvy společensky nejvyšší, ale současně i pro vnější hradbami, odkud zřejmě esovitou zřetelní pokrčilejšího charakteru. U/1 však dokonce zložen nový hruťov uvnitř vnitřního hrudištního areálu v místech, kde lze vřevěti jak z horizontální stratiografie, tak faktickými sídlištními doklady spodních vrstev, nejstarší původní centrum osídlení hradiska, které v průběhu vývoje bylo opuštěno ve prospěch střediska na akropoli. Toto pohřebiště, ohrané zčásti v r. 1937 E. Přeslovou, poskylo zatím 59 hrobů, jež se svým tvarem a rozměry i způsobem obložení nejvíce podobají nejmladší skupině pohřebišť u líbaše. Je nápadné, že žádný z hrobů neobohoval jedině milodaru nebo šperku, kromě stěpů v zášupě, což je samo dostatečným svědectvím pozdějšího datování. Příčinou chudosti vybavení těchto pohřbů může být jižte postupující proces christianisace, zdá se však, že mohlo jít i o zřetel společenského rozvrstvení, které neodvratilo, aby všichni obyvatelé hradiska byli pochováni na tomto pohřebišti.

V tom případě by chudoba pohřbů vnitřního hrudiště souhlasila s nižším postavením společenským. Druhý výklad, že do těchto míst bylo pochováno od románského hradiska na Kouřimí, od sv. Jiří, postřada pokladu, jednak pro velkou vzdálenost místa, i proto, že románské obyvatelstvo, sídlící u sv. Jiří, bylo pochováno na výspě meandru říčky Kouřimky, obtěžající hradisko u sv. Vojtěcha. netřeba tedy předpokládat na Staré Kouřimí další pohřebiště románské epochy, jež ostat-

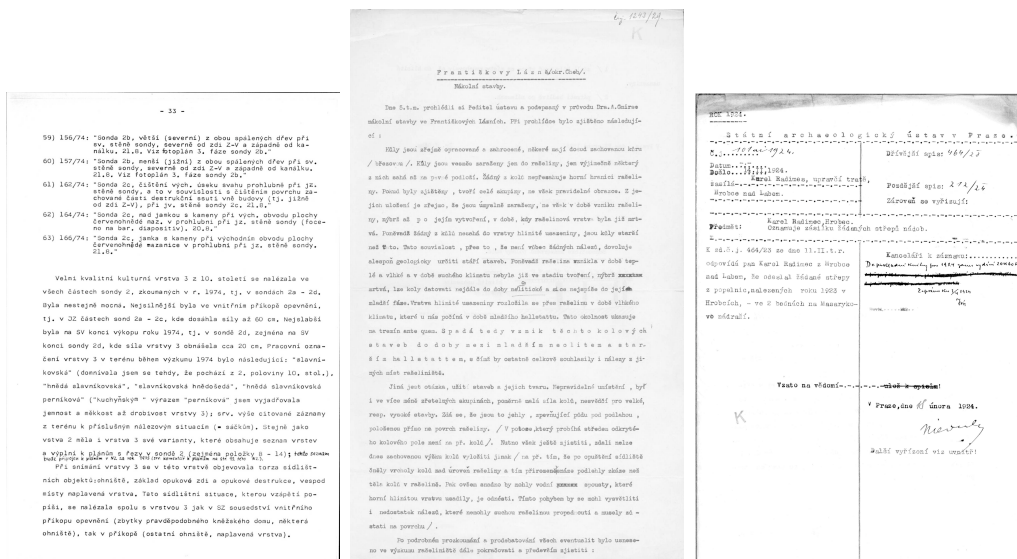
(d) Cornerhole & skewed text print

Figure A.7 Edgehole damage and paper tearing



(a) Color table in thick journal scan (b) Black-and-white journal page with table (c) Text from a thick book scan

Figure A.9 Scans from thick volumes and journals



(a) Corrected typewritten text (b) Minor typewritten correction (c) Crossed-out lines & gray corners

Figure A.10 Typewritten text corrections

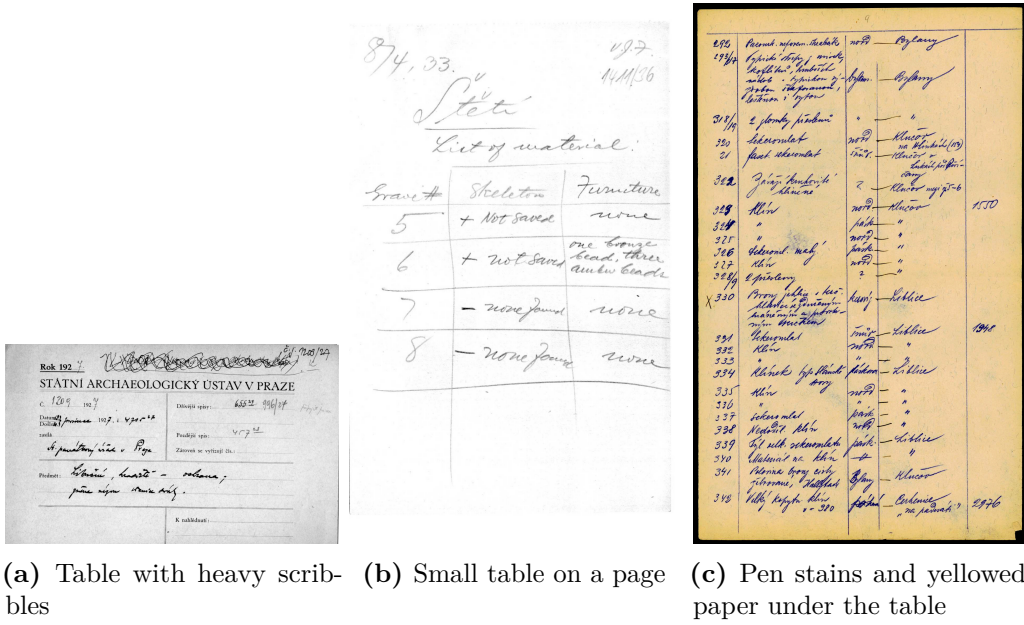


Figure A.11 Tables with color artifacts (e.g., scanning noise, pen stains, and paper discoloration)

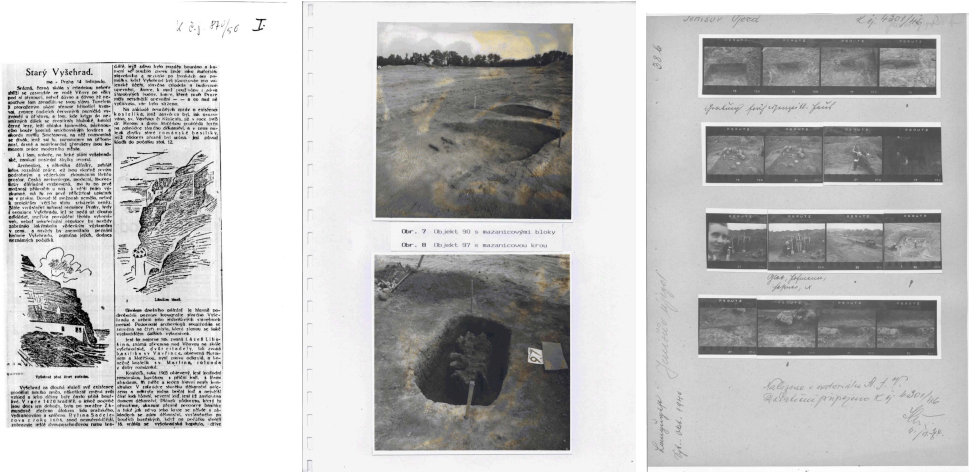


Figure A.12 Mixed-text pages and scribbles

B Parsing attempts

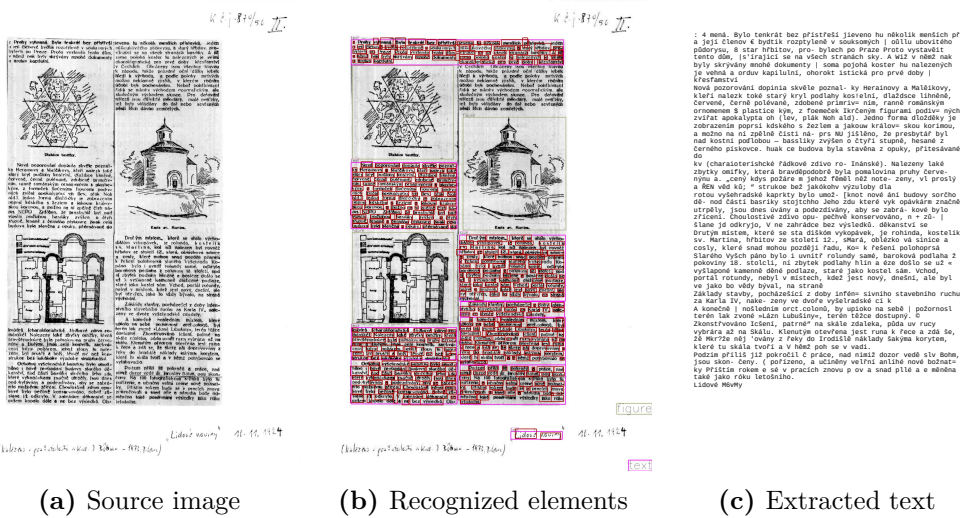


Figure B.1 DD attempt on a newspaper page with drawings

- 101 -
Tabulka obrábění a náklady
Šedá 2a = 2d (1374) = str. 2

Na následujících obráběních 8, 6 - 26 předvádím ukázky
charakteristických keramických náleží a některých signifikant-
ních celků. Zprva se shrnují náleží obrábě 8, 6 - 26 v tabulce:

| vrstva, objekt | měřivá situace | obr. č. |
|--|--|--|
| objekt I (po r. 995) | 102/74 106/74 | 6 7 - 8 |
| objekt II (po r. 995) | 100/74 | 9 |
| DMZ U.8.9.995 | 56/74 60/74 64/74 69/74 | 10 204 13 12 - 13, 2613 |
| vrstva 3 (10.stol., doba exist. kůlna r. 995) | 62/74 | 2612 |
| vrstva 3 (10.stol., brzy po sčítání pravděpodobně kněžského domu) | 49/74 54/74 61/74 69/74 102/74 | 14 15 17 - 18 19 - 20 2611 |
| vrstva 3 (10.stol., doba exist. pravděpodobně kněžského domu) | 109/74 | 21 - 22 |
| vrstva 3 (10.stol., doba exist. terasy pravděpodobně kněžského domu) | 106/74 130/74 133/74 | 2611 23 24 - 25 |

(a) Source image

- 101 -
Tabulka obrábění a náklady
Šedá 2a = 2d (1374) = str. 2

| vrstva, objekt | měřivá situace | obr. č. |
|--|--|--|
| objekt I (po r. 995) | 102/74 106/74 | 6 7 - 8 |
| objekt II (po r. 995) | 100/74 | 9 |
| DMZ U.8.9.995 | 56/74 60/74 64/74 69/74 | 10 204 13 12 - 13, 2613 |
| vrstva 3 (10.stol., doba exist. kůlna r. 995) | 62/74 | 2612 |
| vrstva 3 (10.stol., brzy po sčítání pravděpodobně kněžského domu) | 49/74 54/74 61/74 69/74 102/74 | 14 15 17 - 18 19 - 20 2611 |
| vrstva 3 (10.stol., doba exist. pravděpodobně kněžského domu) | 109/74 | 21 - 22 |
| vrstva 3 (10.stol., doba exist. terasy pravděpodobně kněžského domu) | 106/74 130/74 133/74 | 2611 23 24 - 25 |

(b) Recognized table cells

--- TABLE 1 ---
obráběních 8, 6 - 26 předvádím ukázky
charakteristických keramických náleží z některých
signifikantních celků. Zprva zde shrnují náleží
obrábě 8, 6 - 26 v tabulce: vrstva, objekt
náleží situace obr. č.

5 m 5 5 5 0 0 0 m m 0 0 E S S o S S m S E S E m 0 v
S P S P S 0 n P S m S S R SP 0 m B 0 M 7 m E 0 S D m 0
m 0 m E m m m m S S S - 5 = 55 - E 55 - 555 - 554 - 5
- - = m E 0 0 0 0 0 m 0 0 S m S S = m m m m m 555
objekt I (po r. 995) 102/74
106/74 7-8
objekt II (po r. 995) 101/74
DMZ (28.9.995) 58/14
60/74 4
64/14 11
65/14 12 = 13,
vrstva 3 (10.stol., možná 26:3
kolem r. 995) 62/14 vrstva 3 (10.stol., brzy 49/14
po zániku pravdě- 618/74 podobného kněž-
domu 99/14 102/74 26:2 14
15
61/74 16
17 - 19 - 18 20
vrstva 3 (10.stol., doba zá- 109/74 21 = 22
naku pravdě-
něho kněžského
domu)
vrstva 3 (10.stol., doba exist- 126/74 26:1
tence 130/74 23
ho kněžského domu) 133/14 24 = 25

(c) Extracted table

Figure B.2 DD attempt on a table

odhaleno na západní straně této sondy. Vypalné váhy jemného zrna, přítomnost diabasů, železné strusky a železné rudy v jeho výplni nás nenechávají na pochybách, že se jedná o peci (pyrotechnologické) zařízení určené k výrobě a zpracování železa (nebo o vyřizovací pec). Přítomnost keramiky v záspěch objektivě umocňuje domněnu, že se jedná o peci (pyrotechnologické) zařízení určené k výrobě a zpracování železa (nebo o vyřizovací pec). Přítomnost keramiky v záspěch objektivě umocňuje domněnu, že se jedná o peci (pyrotechnologické) zařízení určené k výrobě a zpracování železa (nebo o vyřizovací pec). Přítomnost keramiky v záspěch objektivě umocňuje domněnu, že se jedná o peci (pyrotechnologické) zařízení určené k výrobě a zpracování železa (nebo o vyřizovací pec).

(a) Source image

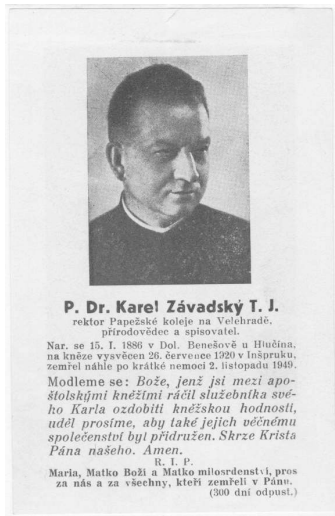
odhaleno na západní straně této sondy. Vypalné váhy jemného zrna, přítomnost diabasů, železné strusky a železné rudy v jeho výplni nás nenechávají na pochybách, že se jedná o peci (pyrotechnologické) zařízení určené k výrobě a zpracování železa (nebo o vyřizovací pec). Přítomnost keramiky v záspěch objektivě umocňuje domněnu, že se jedná o peci (pyrotechnologické) zařízení určené k výrobě a zpracování železa (nebo o vyřizovací pec). Přítomnost keramiky v záspěch objektivě umocňuje domněnu, že se jedná o peci (pyrotechnologické) zařízení určené k výrobě a zpracování železa (nebo o vyřizovací pec).

(b) Recognized lines

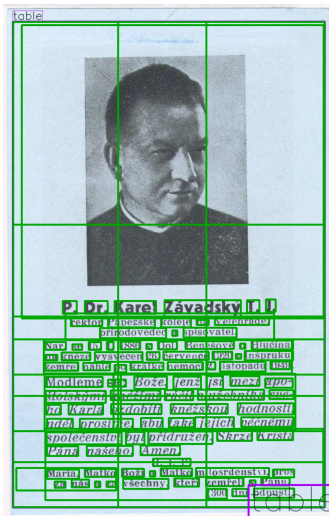
odhaleno na západní straně této sondy. Vypalné váhy jemného zrna, přítomnost diabasů, železné strusky a železné rudy v jeho výplni nás nenechávají na pochybách, že se jedná o peci (pyrotechnologické) zařízení určené k výrobě a zpracování železa (nebo o vyřizovací pec). Přítomnost keramiky v záspěch objektivě umocňuje domněnu, že se jedná o peci (pyrotechnologické) zařízení určené k výrobě a zpracování železa (nebo o vyřizovací pec). Přítomnost keramiky v záspěch objektivě umocňuje domněnu, že se jedná o peci (pyrotechnologické) zařízení určené k výrobě a zpracování železa (nebo o vyřizovací pec).

(c) Extracted lines

Figure B.3 DD attempt on a plain text



(a) Source image



(b) Recognized elements

--- TABLE 1 ---

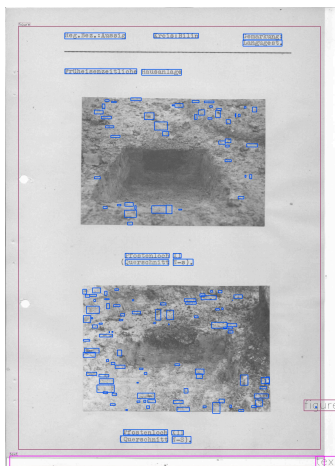
P. Dr. Karel Závadský T. J.

rektor Papežské koleje na
 Velehradě, přírodovědec a
 spisovatel.
 Nar. se 15. I. 1886 v Dol.
 Benešově u Hlučína, na kněze
 vysvěcen 26. července 1920 v
 Inšpruku, zemřel náhle po krátké
 nemoci 2. listopadu 1949
 Modleme se: štoláskými ho Karla
 uděl prosíme, Bože, jenž jsi mezi
 apo- kněžimi ráčil služebníka
 své- ozdobi kněžskou hodností,
 aby také jejich věčnému

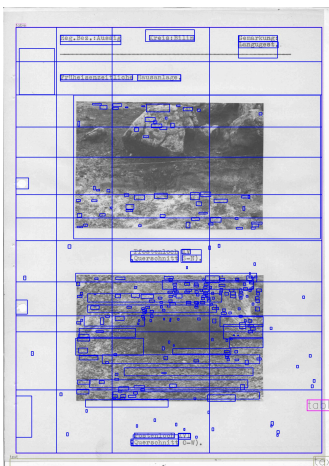
společenství byl přidružen. Skrze
 Krista Pána našeho. Amen. RA:
 Maria, Matko Boží a Matko
 milosrdnosti, pros za nás a za
 všechny, kteří zemřeli v Pánu.
 (300 dní odpust.)

(c) Extracted text

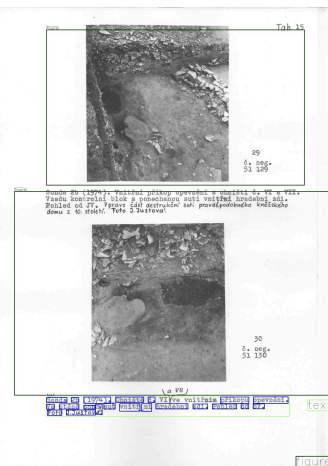
Figure B.4 DD attempt on a photo with text



(a) Imaginary characters

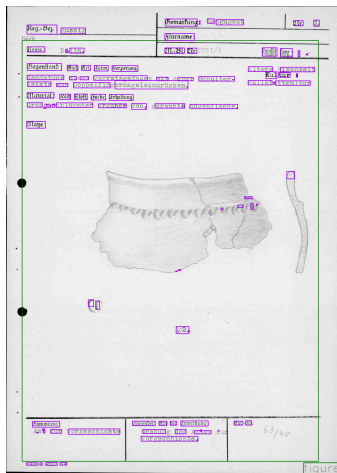


(b) Imaginary table

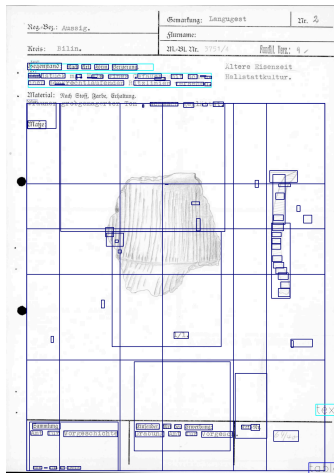


(c) Missed paragraph

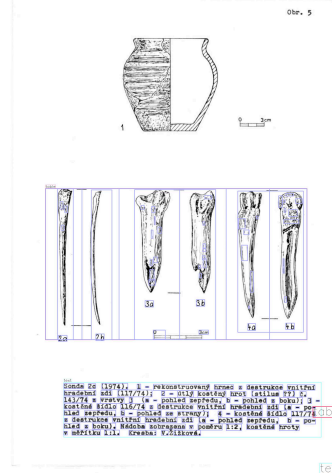
Figure B.5 DD mistakes on pages with photos



(a) Missed table & drawing

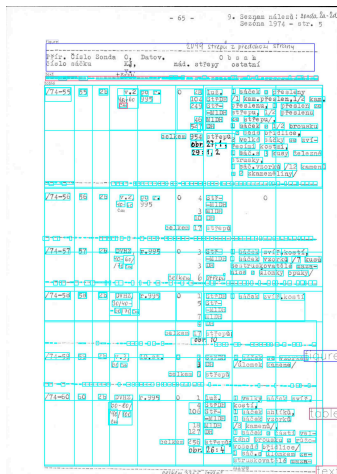


(b) Partial table

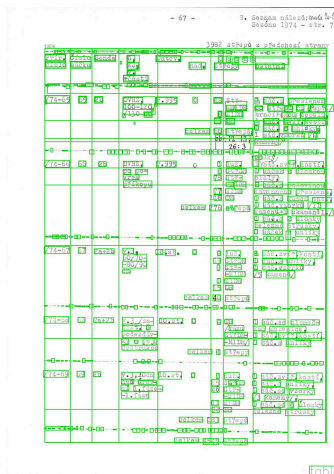


(c) Missed drawing

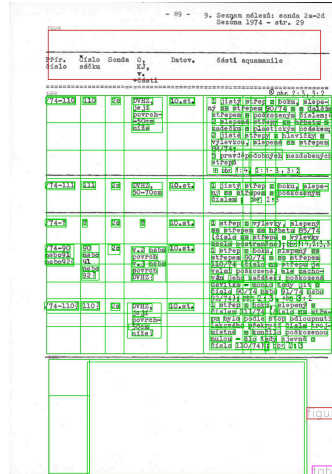
Figure B.6 DD mistakes on pages with drawings



(a) Text as a figure

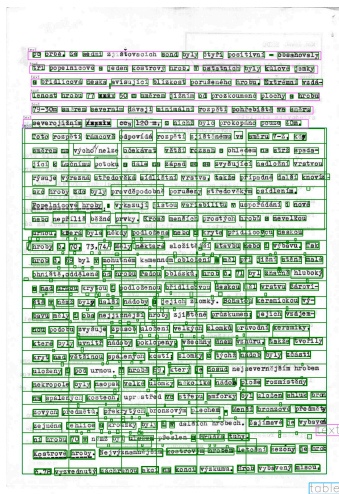


(b) Text as a row

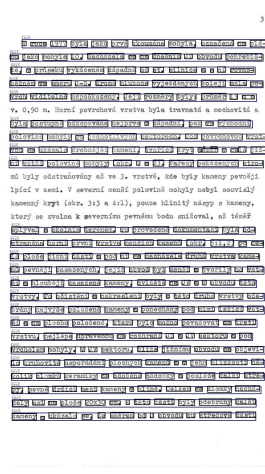


(c) Imaginary cells

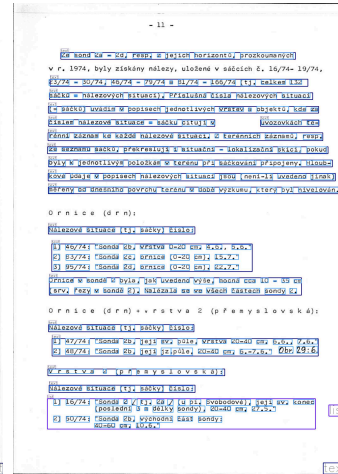
Figure B.7 DD mistakes on pages with tables



(a) Text as table



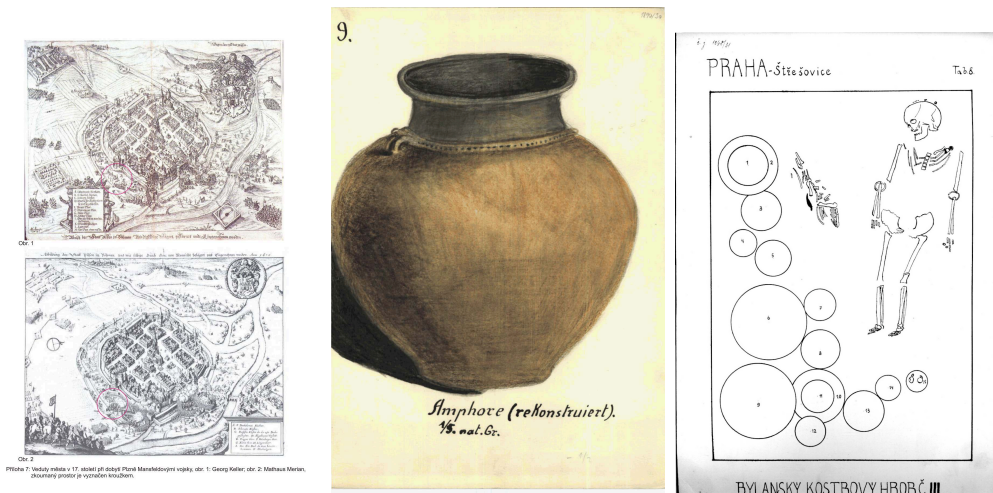
(b) Missed font



(c) Missed lines

Figure B.8 DD mistakes on pages with plain texts

C Label examples



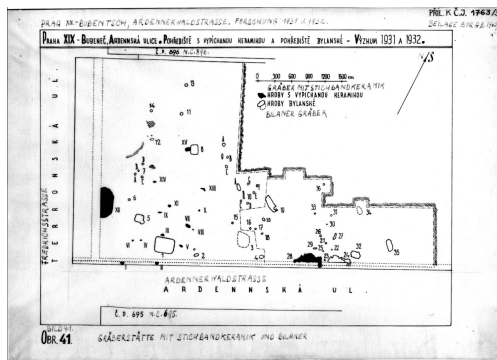
(a) City drawings

(b) Realistic painting

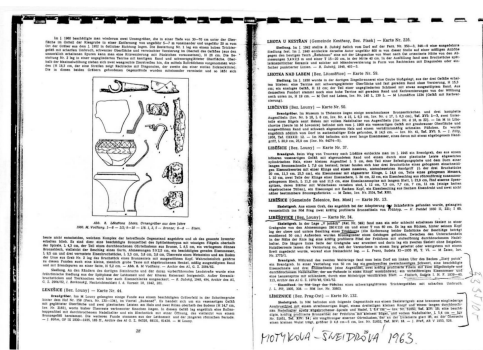
(c) Ground schematic



(d) Territory map



(e) Building plan

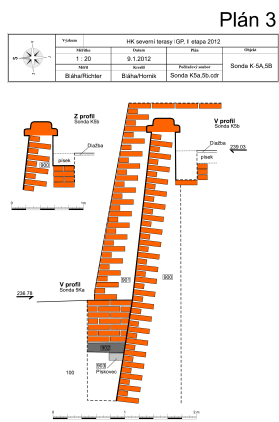


(f) Within book scan



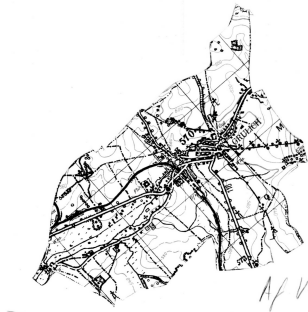
(g) Within written notes

Figure C.1 Label DRAW examples



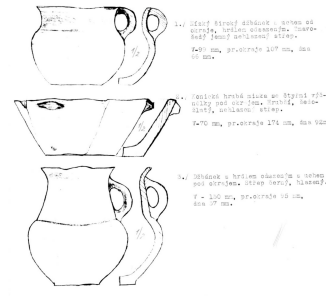
(a) Scheme with a legend

| | | | |
|-----------------|----------------|-------------------|----------|
| OBEC: Praha 2 | OKRES: Praha 2 | C. č.: 287/2012 | C. pol.: |
| Číslo parcely: | Název: HK | Průřez: | |
| Číslo mapy: | 325/14 | Kulturní památka: | |
| Uchovávatel: | Uchovávatel: | Uchovávatel: | |
| Číslo inženýra: | | | |

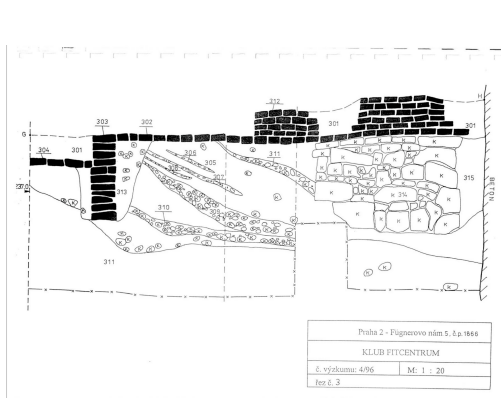


(b) Map inside a form

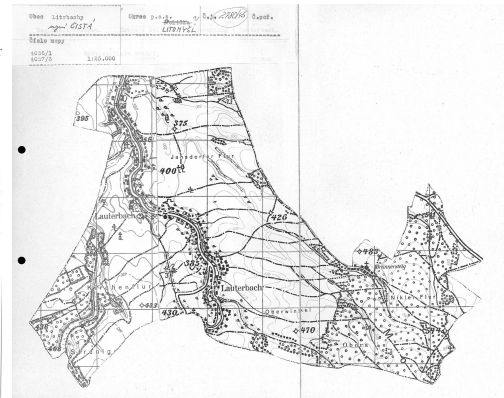
| | | | |
|-----------------|----------------|-------------------|----------|
| OBEC: Praha 2 | OKRES: Praha 2 | C. č.: 287/2012 | C. pol.: |
| Číslo parcely: | Název: HK | Průřez: | |
| Číslo mapy: | 325/14 | Kulturní památka: | |
| Uchovávatel: | Uchovávatel: | Uchovávatel: | |
| Číslo inženýra: | | | |



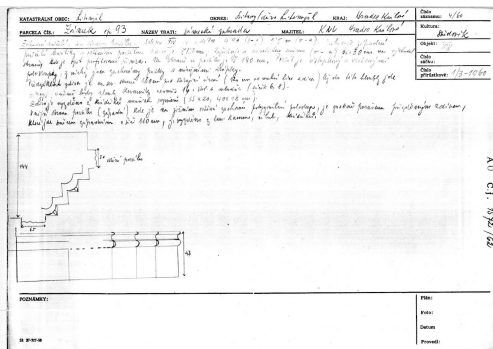
(c) Drawing inside a form



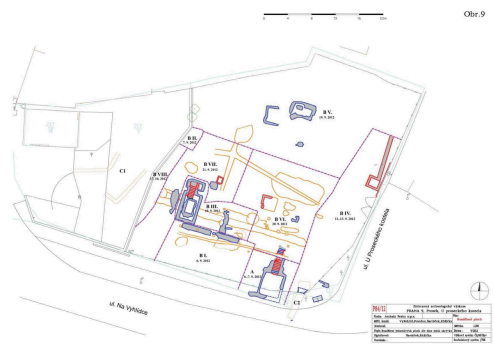
(d) Wall drawing



(e) Territory map

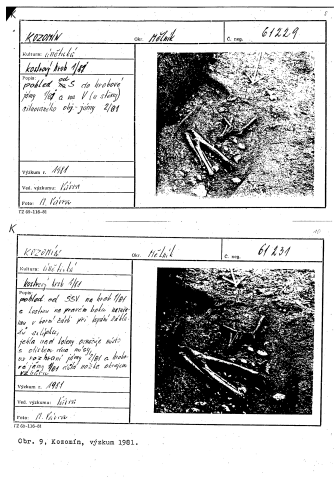


(f) Schema in a form



(g) Buildings top view

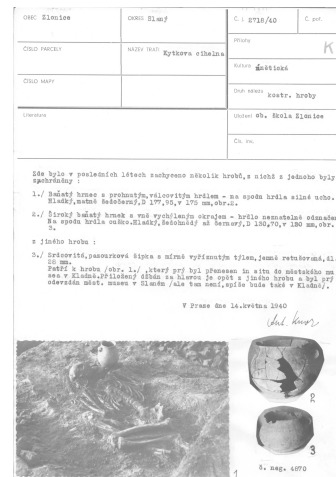
Figure C.2 Label DRAW_L examples



(a) Manual captions



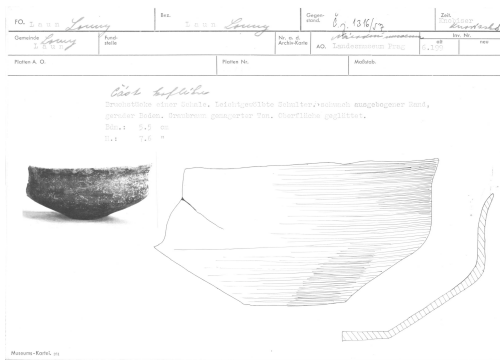
(b) Map with legend



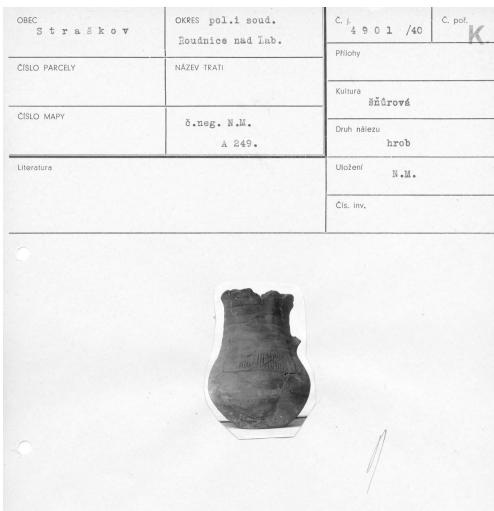
(c) Photo cutouts



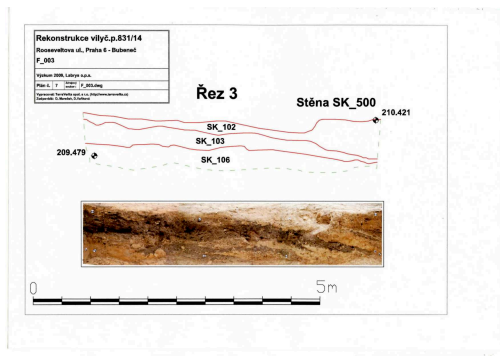
(d) Photo and legend



(e) Near drawing

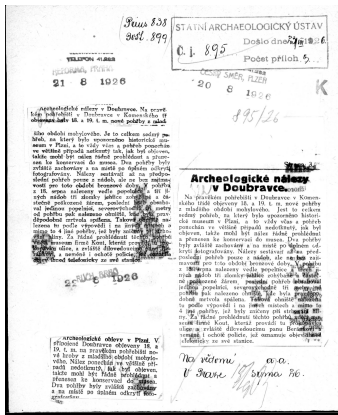


(f) Within filled form

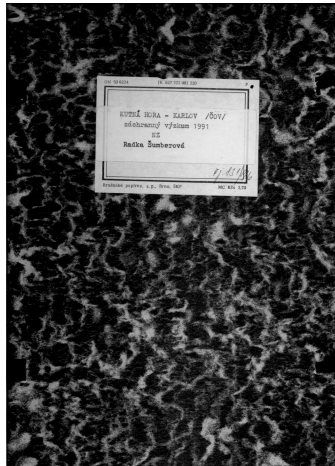


(g) Object and legend

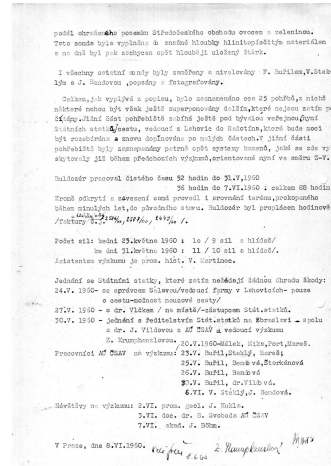
Figure C.7 Label PHOTO_L examples



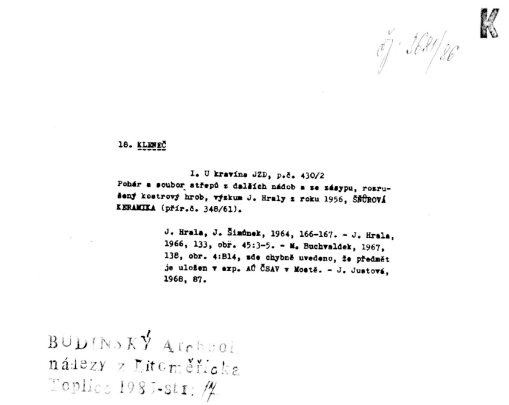
(a) Newspaper cutouts



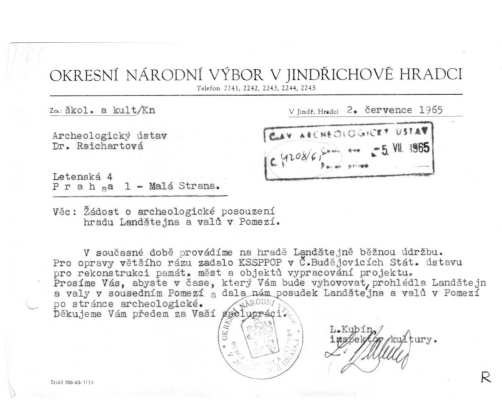
(b) Journal cover



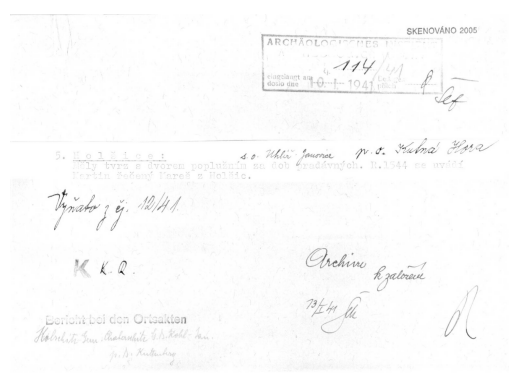
(c) Manual correction



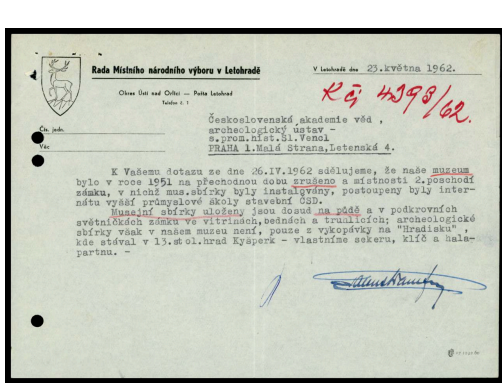
(d) Text comment



(e) Front page



(f) Whitespace



(g) Postcard scan

Figure C.8 Label TEXT examples

D CLIP category descriptions

| Label | Description |
|---------|---|
| DRAW | drawings, maps, paintings, schematics, graphics with labels |
| DRAW_L | drawings, maps, paintings, schematics, graphics with a table legend, inside a table or form |
| LINE_HW | handwritten text lines inside a table or form |
| LINE_P | printed text lines inside a table or form |
| LINE_T | typed text lines inside a table or form |
| PHOTO | photos or cutouts from photos with labels |
| PHOTO_L | photos with a table caption, inside a table or form |
| TEXT | mixed printed and handwritten texts |
| TEXT_HW | handwritten text page |
| TEXT_P | printed text page |
| TEXT_T | typed document page |

Table D.1 Initial Document Classification Labels

| Label | Description |
|---------|--|
| DRAW | a drawings or a map or a diagram |
| DRAW_L | a table and drawings or a map or a diagram |
| LINE_HW | a table or a filled form of handwritten texts |
| LINE_P | a table or a filled form of printed texts |
| LINE_T | a table or a filled form of typed texts |
| PHOTO | photos or photo cutouts |
| PHOTO_L | a table and photos or photo cutouts |
| TEXT | printed and handwritten text styles on a page |
| TEXT_HW | a handwritten plain text page or handwritten text paragraphs |
| TEXT_P | a printed plain text page or printed text paragraphs |
| TEXT_T | a typed plain text document page or typed text paragraphs |

Table D.2 Short Document Classification Labels

| Label | Description |
|--------------|--------------------------------------|
| DRAW | a drawings or a map or a diagram |
| DRAW_L | a table and a drawings or a map |
| LINE_HW | a handwritten table or a filled form |
| LINE_P | a printed table or a filled form |
| LINE_T | a typed table or a filled form |
| PHOTO | photos on a page |
| PHOTO_L | a table and photos |
| TEXT | printed text and handwritten comment |
| TEXT_HW | a handwritten text |
| TEXT_P | a printed text |
| TEXT_T | a typed text |

Table D.3 Minimal Document Classification Labels

| Label | Description |
|--------------|--|
| DRAW | A page with a drawing, map, painting, or schematic |
| DRAW_L | A page with a drawing or map presented in a table layout |
| LINE_HW | A page with handwritten text in a table layout |
| LINE_P | A page with printed text in a table layout |
| LINE_T | A page with typed text in a table layout |
| PHOTO | A page with a photograph or photographic image |
| PHOTO_L | A page with a photograph presented in a table layout |
| TEXT | A page with mixed handwritten, printed, or typed text |
| TEXT_HW | A page with only handwritten text in paragraphs |
| TEXT_P | A page with only printed text in paragraphs |
| TEXT_T | A page with only typed text in paragraphs |

Table D.4 Page-based Document Classification Labels (Proposed by GPT Deep Research based on Chapter 1 content)

| Label | Description |
|--------------|---|
| DRAW | a drawings or a map or a diagram |
| DRAW_L | a drawings or a map or a diagram and a table |
| LINE_HW | a table or a filled form of handwritten cells |
| LINE_P | a table or a filled form of printed cells |
| LINE_T | a table or a filled form of typed cells |
| PHOTO | photos or photo cutouts |
| PHOTO_L | photos or photo cutouts and a table |
| TEXT | mixed text styles |
| TEXT_HW | a handwritten text page |
| TEXT_P | a printed text page |
| TEXT_T | a typed document page |

Table D.5 Cropped out word “page” from Table D.4 — Document Classification Labels

| Label | Description |
|--------------|---|
| DRAW | A drawing, a map, a painting, a schematic, or a graphic with labels on a document page. |
| DRAW_L | A drawing, a map, a painting, a schematic, or a graphic with an accompanying table or tabular legend on a document page. |
| LINE_HW | A table or a filled form containing handwritten text lines on a document page. |
| LINE_P | A table or a filled form containing printed text lines on a document page. |
| LINE_T | A table or a filled form containing typed text lines on a document page. |
| PHOTO | A photo or a photo cutout attached to a document page. |
| PHOTO_L | A photo or a photo cutout with an accompanying table or tabular legend on a document page. |
| TEXT | A document page with mixed printed and handwritten text styles, such as a newspaper or book cutout with handwritten comments. |
| TEXT_HW | A handwritten plain text, handwritten text paragraphs, or handwritten list items on a document page. |
| TEXT_P | A printed plain text, printed text paragraphs, or printed list items on a document page. |
| TEXT_T | A typed plain text, typed text paragraphs, or typed list items on a document page. |

Table D.6 Long Document Classification Labels (Proposed by Gemini Deep Research based on Chapter 1 content)

| Label | Description |
|--------------|--|
| DRAW | A drawing, a map, a painting, a sketch, a diagram, a schematic, or a graphic with labels on a document page. |
| DRAW_L | A drawing, a map, a painting, a sketch, a diagram, a schematic, or a graphic with an accompanying table or tabular legend on a document page. |
| LINE_HW | A table or a filled form with handwritten text lines on a document page. Such as a filled report |
| LINE_P | A table or a filled form with printed text lines on a document page. |
| LINE_T | A table or a filled form with typed text lines on a document page. Such as a filled report |
| PHOTO | A photo or a photo cutout with labels attached to a document page. |
| PHOTO_L | A photo or a photo cutout labeled with an accompanying table or tabular legend on a document page. |
| TEXT | A document page with mixed printed and handwritten text styles, such as a newspaper or book cutout with handwritten comments. |
| TEXT_HW | A handwritten plain text, handwritten text paragraphs, or handwritten list items on a document page. Such as a field diary scans and notebook notes. |
| TEXT_P | A printed plain text, printed text paragraphs, or printed list items on a document page. Such as a clean book page scan or an article page scan. |
| TEXT_T | A typed plain text, typed text paragraphs, or typed list items on a document page. Such as an old style field report scans |

Table D.7 Comprehensive Document Classification Labels with Examples

| Label | Description |
|--------------|---|
| DRAW | A page with a drawing, map, painting, or schematic with text annotation |
| DRAW_L | A page with a drawing or map presented in a table layout or with a legend table |
| LINE_HW | A page with handwritten text in a table layout or a manually filled form |
| LINE_P | A page with printed text in a table layout or a large printed table that takes a whole page |
| LINE_T | A page with typed text in a table layout or a filled with typed text form |
| PHOTO | A page with a photograph or photographic image with text annotation |
| PHOTO_L | A page with a photograph presented in a table layout or with a legend table |
| TEXT | A page with mixed handwritten, printed, or typed text such as a previously printed and then manually commented page from a book, a newspaper, or an article |
| TEXT_HW | A page with only handwritten text in paragraphs such as a page from field journals |
| TEXT_P | A page with only printed text in paragraphs, lists, and plain text layouts such as a page from an article or a thesis |
| TEXT_T | A page with only typed text in paragraphs, lists, and plain text layouts such as a page from an article or a thesis |

Table D.8 Enhanced Document Classification Labels with Detailed Annotations

| Label | Description |
|--------------|---|
| DRAW | a drawings or a map or a diagram |
| DRAW_L | a table or a tabular legend and drawings or a map or a diagram |
| LINE_HW | a table or a filled form of handwritten texts on a page |
| LINE_P | a table or a filled form of printed texts on a document page |
| LINE_T | a table or a filled form of typed texts on a document page |
| PHOTO | photos or photo cutouts attached to the document page |
| PHOTO_L | a table or a tabular legend and photos or photo cutouts on a document page |
| TEXT | printed and handwritten text styles on a page like a newspaper cutout or a book cutout commented in another way |
| TEXT_HW | a handwritten plain text or handwritten text paragraphs on a page |
| TEXT_P | a printed plain text or printed text paragraphs or printed list items on a document page |
| TEXT_T | a typed plain text or typed text paragraphs or typed list items on a document page |

Table D.9 Extended Document Classification Labels

E LLM prompts

This appendix includes prompts for generation of category text embeddings used in CLIP models, specifically Tables D.4 & D.6, referred to as **gpt** & **gemini** category descriptions sets.

GPT research prompt:

```
<table short>
or
<table init>
or
<table min>

based on the provided tables you must compose descriptions
  for the defined categories

these descriptions will be used in few-shot finetuning of
  clip (ViT-L/14@336px and ViT-B/32)

find best practices in defining such text embedding and
  return a single refined table

a table from the related article should help you as well:
<table 11-labels>

and also a list with data expert opinions
<final expert feedback criteria list>

To tailor the refined descriptions optimally for CLIP fine-
tuning, could you please confirm:

1. Should the language be concise and technical, or is a
   more descriptive tone preferred?
2. Are the descriptions going to be shown to annotators, or
   are they strictly for model training?
3. Should we keep compatibility with the LaTeX formatting
   you showed (e.g., escaping underscores like \_)?
4. Do you have a maximum character length per description?
5. Once I have this, I can finalize the optimal descriptions
   for each label.
```

1. chose based on the found info
2. only model training
3. latex format is only for my own convenience, use raw text
4. depends on the model input size, find it as well
5. and importantly provide a refined table with label - description, not only found info

where <table *> lines refer to Tables D.2 D.1 D.3 and 2.2.

Gemini research prompt:

```
<table short>  
or  
<table init>  
or  
<table min>
```

based on the provided tables you must compose descriptions for the defined categories

these descriptions will be used in few-shot finetuning of clip (ViT-L/14@336px and ViT-B/32)

find best practices in defining such text embedding and return a single refined table

I've put together a research plan. If you need to update it in any way, let me know.

CLIP Text Embedding Refinement:

-Research Websites:

- (1) Analyze the three provided sets of label descriptions to identify the core concept and common elements associated with each category (e.g., DRAW, LINE_HW, TEXT_P).
- (2) Research best practices for crafting effective text descriptions or prompts for vision-language models like CLIP, specifically for few-shot fine-tuning in classification tasks.
- (3) Evaluate how factors such as conciseness, specificity, the inclusion of key visual attributes, and the overall

clarity of descriptions influence the quality of text embeddings for distinguishing document layout elements.

- (4) Compare and contrast the strengths and weaknesses of the existing descriptions for each label, considering their potential impact on CLIP's ability to learn and generalize from limited examples.
- (5) Synthesize a refined, concise, and highly discriminative description for each category, ensuring it accurately represents the visual content and is optimized for generating robust text embeddings for CLIP.
- (6) Compile the refined descriptions into a single, clear table format, presenting the 'label' and its corresponding 'description'.

-Analyze Results

-Create Report

Start research

Notably, the same prompt as used for Gemini was tested with GPT as well. The generated table of category descriptions' text embeddings contained multiple complex for tokenization phrasings, thus an expanded version of the prompt including labels definition Table 2.2 and a list of expert-defined criteria from Section 1.3.

F System architecture

F.1 Finetuning to downstream task functionality

The system implements finetuning of pretrained models on domain-specific historical document scans. This transfer learning approach adapts general-purpose vision and hybrid models to the specialized task of document page classification.

To address class imbalance during finetuning, the system uses a custom **BalancedBatchSampler** that extends PyTorch’s **BatchSampler**. The objective is to ensure each training batch contains a fixed number of classes and a fixed number of samples per class, thereby improving training stability. The sampler operates as follows:

- For a given tensor of labels (subset of the whole dataset), the sampler first builds an index list for each class and shuffles it.
- On each iteration, it randomly selects a specified number of distinct classes (`n_classes`).
- It then takes a specified number of indices (`n_samples`) for each selected class. When a class’s index list is exhausted, it is reset and reshuffled.

This process generates class-balanced mini-batches of size $n_classes \times n_samples$ whose implementation logic is adapted from the CLIP finetuning repository. Although the balanced-batch requirement is CLIP-specific, the same algorithm was used in other models’ finetuning.

Moreover, the cross-validation technique was used to finetune five folds (data subset selections) of different pretrained models, which were then averaged to get the generalized model weights. The averaging was performed for fold checkpoints matching a given pattern of the common base model. State dictionary of each model was loaded and added element-wise to other models’ weights, which was then divided by the number of located folds. This procedure implements a simple, unweighted arithmetic average of all state-dict entries (including buffers such as batch-norm statistics), thus, this approach, which can be memory-intensive for large models, assumes that the parameterization is broadly compatible across folds.

F.1.1 Transformation into model-friendly inputs

Before being processed by a model, input images undergo several transformations:

1. Image loading and validation for corrupted files (if safety load is enabled).

2. Resizing to the model’s input resolution (e.g., 224×224 , 336×336 or 384×384 pixels)
3. Normalization of pixel values according to the model’s preprocessor requirements, optionally, during finetuning, applying the image preprocessing transformations (detailed in Section F.1.3).
4. Organization into batches for efficient processing, optionally, during finetuning, use a balanced batch sampler (mentioned in Section F.1).

The inference batch size is configurable based on available hardware resources. For prediction tasks, only transformations provided by the model’s preprocessor are applied to preserve the original image content, whereas finetuning always employs additional data augmentation techniques to improve model robustness.

F.1.2 Hyper-parameters

The finetuning process is controlled by several hyperparameters:

- **Learning rate:** Default $1e-5$ or $5e-5$, configurable in the code
- **Epochs:** Default 3 or 7, adjustable in configuration
- **Batch size:** Variable based on memory constraints, set in configuration (e.g., 12 or 16)
- **Warmup ratio:** 0.1 (10% of training steps)
- **Evaluation strategy:** Per-epoch evaluation
- **Saving strategy:** Best model checkpoint saving
- **Best model selection:** Based on accuracy metric

These default parameters are optimized for datasets containing 10,000-50,000 page samples. The documentation recommends adjusting the number of epochs according to evaluation loss to prevent overfitting and modifying the learning rate if the training loss does not converge to values lower than 0.001 as expected.

F.1.3 Preprocessing of images

During finetuning, images undergo data augmentation to improve model robustness. The system applies the following transformations:

- Brightness adjustment (probability factor: 0.5)
- Contrast modification (probability factor: 0.5)
- Saturation changes (probability factor: 0.5)
- Hue variation (probability factor: 0.5)
- Sharpness enhancement (random factor between 0.5-1.5)
- Gaussian blur (random radius between 0-2)

Notably, geometric transformations like rotation or flipping are avoided due to the orientation-sensitive nature of document pages and the importance of preserving structural layouts.

F.1.4 Data split by category proportions

To ensure robust evaluation, the system automatically splits the dataset into training (80%) and evaluation (10%), and test (10%) sets while maintaining a proportional representation of all categories. This stratified approach ensures that evaluation results accurately reflect performance across all document types, even in the presence of class-imbalanced datasets.

The exact logic of the dataset split procedure was described in Section 2.2.1, where the rejection of a standard randomized shuffling approach was justified. The specialized subset selection based on a randomized periodic step in the time-sorted dataset was developed to support the variability of each category representation in the evaluation and test subsets. The data distributions in Figure 2.3 illustrate the category-specific variability obtained in the chronologically ordered samples after applying the developed split procedure.

F.2 Output

The system generates outputs in multiple formats, designed for both direct user inspection and integration into downstream document processing pipelines. The output results are organized in standardized formats for further analysis.

F.2.1 Directory level parsing

When processing directories of images, the system is optimized for efficiency and usability:

- A list of image files to be processed can be divided into chunks of specified size if requested by the user (recommended for directories containing thousands of pages)
- Page files (of a chunk) are loaded in batches of scaled and preprocessed vectorized images to ensure memory efficiency; thus `batch_size` controls how many images are loaded into memory when a single model prediction attempt is performed.
- Progress information (e.g., `{current_iteration}-th batch - Processed {already_predicted} images in {minutes_from_start} min` or directory evaluation `Testing: {processed}% |{dynamic_progress_bar}| {cur_iter}/{total} [{time:spent}<{time:left}, {mean_time}s/it]`) is registered in the console output.
- Results are organized by file and page number, and consolidated into CSV tables (processed chunk's results are recorded, proceeding to the next chunk) with columns for predicted category labels and their scores.

This approach to processing directories in chunked lists of images and loading them into memory in small batches balances memory usage with throughput, enabling the efficient handling of large document collections.

F.2.2 Confusion matrix plot generation

The evaluation process automatically generates confusion matrices to visualize category-specific classification performance. These plots help users identify systematic classification errors and understand model limitations. Key features include:

- A clear representation of the relationship between predicted and true categories.
- Diagonal elements representing correct classifications, and off-diagonal elements highlighting error patterns.
- Separate matrices generated for different top-N configurations (e.g., Top-1, Top-3).

In practice, confusion matrices across models reveal the most problematic category pairs. If such mistakes repeatedly occur in various models, then the annotated data should be examined for interchangeable samples in the most problematic cases (e.g., category precision is constantly lower by 1-2% compared to other categories). If the size of the category allows for reduction, samples exhibiting a higher amount of mixed features common to multiple categories must be removed entirely.

| Group | Flag | Alias | Description |
|--------------------------------|------------------|-------|---|
| General | | | |
| | -help | -h | Displays available command options. |
| | -hf | | Retrieve or publish model to HuggingFace. |
| | -revision | -rev | Specifies the global model version. |
| | -model/-base | -m/-b | Sets the base architecture (CLIP / image-only). |
| | -file | -f | Provides a single image file to process. |
| | -file_format | -ff | Files format of interest |
| Prediction | | | |
| | -file | -f | Provides a single image file path to process. |
| | -directory | -d | Path to folder with pages to be processed. |
| | -dir | | Run a whole directory processing. |
| | -inner | | Include files from nested directories. |
| | -chunk | | Process input files and save results in chunks. |
| | -topn | -tn | Sets N in Top-N for all predictions. |
| | -raw | | Output raw scores for all categories. |
| | -best | | Output Top-1 predictions for every best model. |
| | -safe | | Safely load images, skipping corrupted ones. |
| Training and Evaluation | | | |
| | -train | | Run model finetuning (training). |
| | -lr | | Learning rate for the optimizer. |
| | -epochs | | Number of training epochs. |
| | -max_categ | -mc | Maximum number of samples per category. |
| | -folds | | Number of folds for cross-validation. |
| | -average | | Run averaging of finetuned fold models. |
| | -average_pattern | -ap | Prefix of finetuned models' filenames. |
| | -eval | | Evaluate a saved model. |
| CLIP-specific | | | |
| | -avg | | Average features of category description files. |
| | -cat_prefix | | Prefix for category description TSV files. |
| | -cat_csv | -cc | Prefix for category description TSV files. |
| | -cat_dir | | Directory with category description files. |
| | -model_path | | Path to model .pt checkpoint or folder. |
| | -eval_dir | | Evaluate a directory of saved models. |
| | -model_dir | | Path to the model checkpoints directory. |
| | -zero_shot | | Run off-the-shelf CLIP models. |
| | -vis | | Visualize model accuracy statistics. |

Table F.1 CLI options for `run.py`

G Confusion matrices of all models

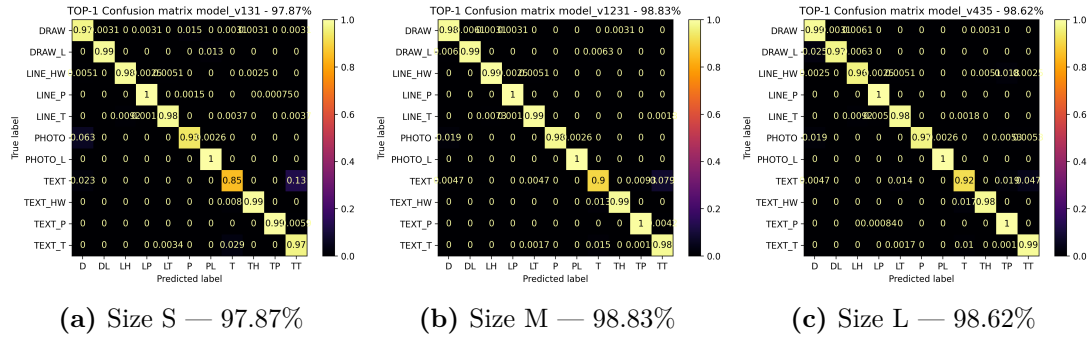


Figure G.1 EfficientNetV2 confusion matrices, three epochs

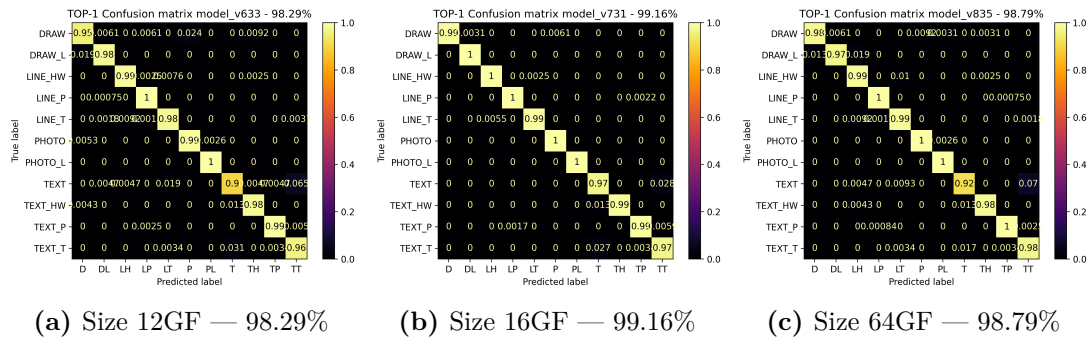


Figure G.2 RegNetY confusion matrices, three epochs

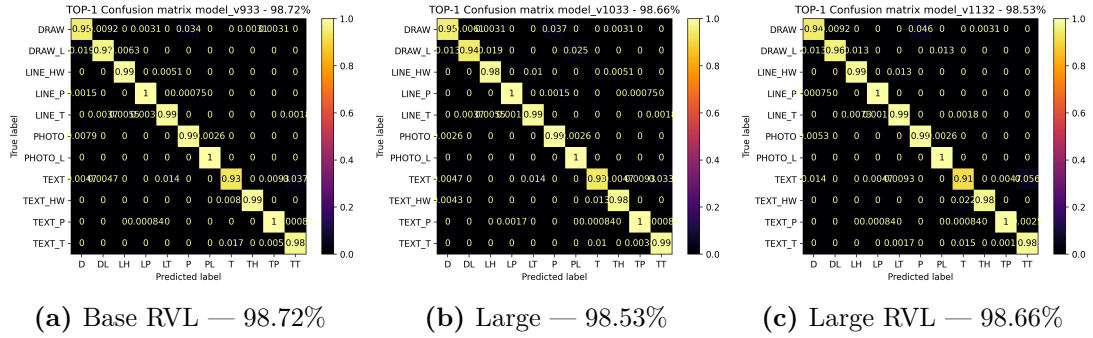


Figure G.3 DiT confusion matrices, three epochs

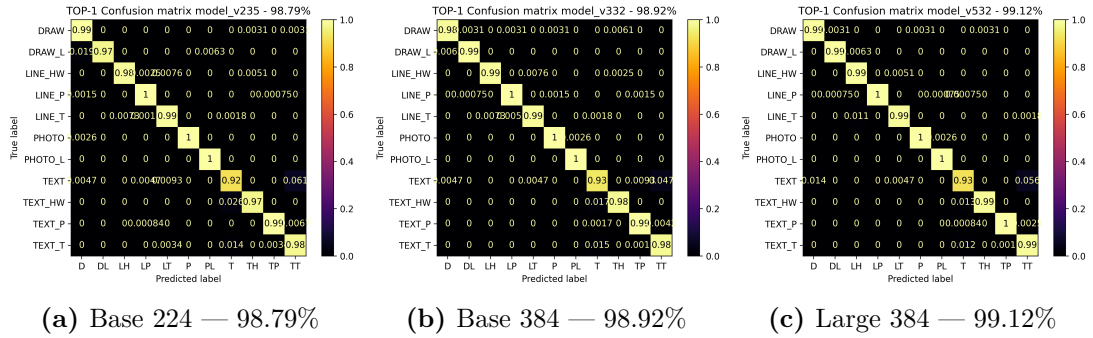
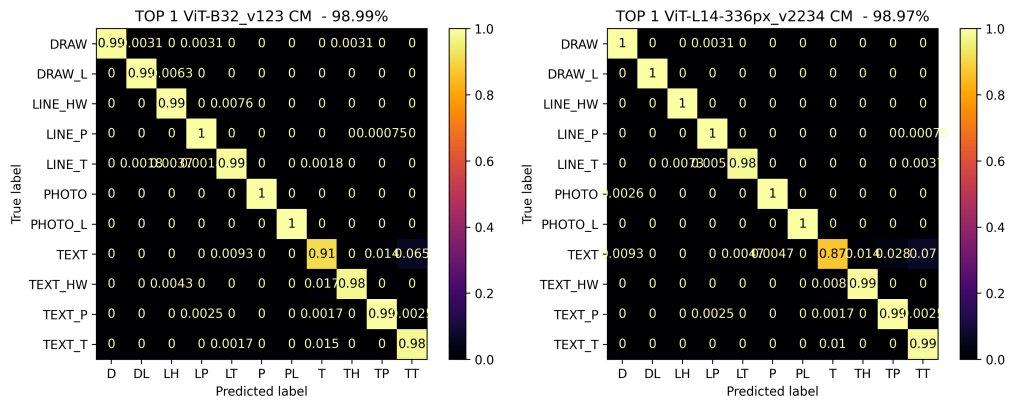
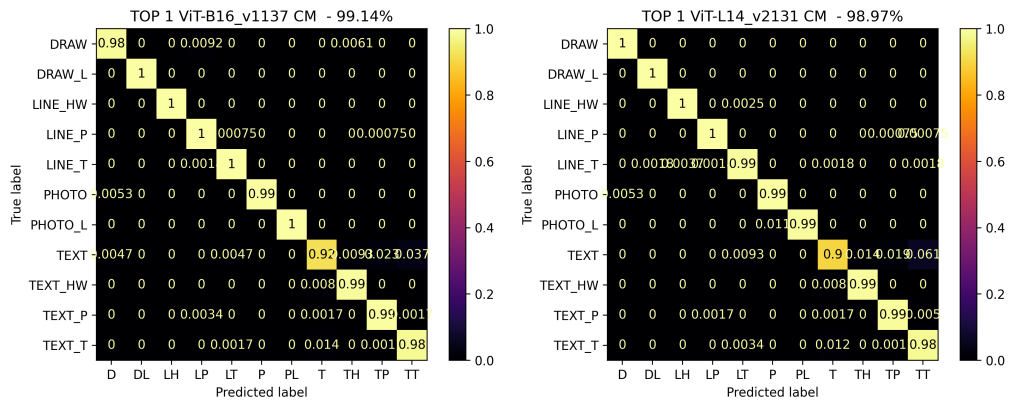


Figure G.4 ViT confusion matrices, three epochs



(a) ViT-B/32 averaged — 98.99%

(b) ViT-L/14-336 gemini D.6 — 98.97%



(c) ViT-B/16 mid Table D.2 — 99.14%

(d) ViT-L/14 init Table D.1 — 98.97%

Figure G.5 Finetuned CLIP best models in each base model group confusion matrices, seven epochs